About the recognition of rotationally induced chemical homogeneity in massive main sequence stars

Bachelor thesis in physics
by
Denise Keller

conducted at the
Argelander-Institute for Astronomy

submitted to the
Faculty of Mathematics and Natural Sciences of the University of Bonn

July 2010

1. Assessor: Prof. Dr. Norbert Langer
2. Assessor: Prof. Dr. Pavel Kroupa

Contents

1 Motivation

1.1 Introduction

The most important and the best observable objects in the Universe are stars. A lot of them can be admired in the night sky with the naked eye, which has been performed for millennia. Over the centuries, there have consistently been milestones for astronomy, be it in scientific understanding or in practical implementation. Even today we have not reached the end of possibilities and there continually arise new exciting questions, which need to be answered by better and better technology.

Thus there are numerous powerful telescopes on the Earth today, which demand and advance international cooperation. As a result of the expansive new knowledge generated, there are more specialized and new astronomical fields of research and the progress in some areas is enormously accelerated. Theoretical considerations, which are performed by more and more powerful processors, can actually be verified by improved telescope technique. And relations and intersections between the subareas are found consistently, since all explored objects and phenomena are located in one, our, Universe.

One of these fields of research deals with the life and death of stars. To understand how, when and why the life of a star ends, one firstly has to understand how this life has appeared. This is explored in the first steps with theoretical considerations and numerical calculations. Afterwards observational data is used to try to support the ideas that have been developed. This approach retrieves in this paper. First of all, some paragraphs about the things that are already known and on which one can build further considerations.

By now it is known that massive stars, stars with more than about ten solar masses are extremely important for the evolution, structure and appearance of the Universe. They reliably provide energy during their time on the main sequence in the form of winds and ionizing radiation. This can lead to, for example, creation of new star formation areas due to heating of the interstellar medium. An even bigger energy supply is created at the end of a massive star's life by a supernova. In a supernova, in one second an energy is released which is equivalent to the energy produced by all stars in the whole Universe in that time. This also releases all heavy elements generated in the core until then by nucleosythesis. In further reactions, for example due to neutrinos, even more elements are formed. Without such explosions in the cosmos, the creation of most of the elements would not be possible. As a result of supernovae, the chemical composition of the Universe evolves towards higher metallicities with time, which means the enrichment of elements heavier than helium. This development would never have happened without massive stars. This means, we would not have had the genesis of carbon and water based creatures, like us humans.

The exact evolution of massive stars is still very unsure. In particular, the stars of the early Universe with very low metallicity still ask riddles, especially because the possibilities of proof in terms of direct observations are very difficult. On the one hand, such stars possess a very high redshift, which is equivalent to a large distance to Earth. On the other hand, most of these stars already have disappeared by supernovae or other stellar remnants and cannot be observed anymore. So these objects are even more interesting and important, since they give indication about the evolution of the Universe itself and the further development of new stars and all the other objects like star clusters, galaxies and the structure of the interstellar medium.

We want to obtain precise knowledge about the chemical constitution of the Universe and its objects. This is quite easily possible through observations of stars, since, as mentioned before, most of the elements originate from stellar objects. They therefore provide a good profile of the abundances of each element. The easiest way to understand that is to consider the relative abundance of hydrogen and helium, which is about 75% and 25% according to the standard model. Exactly these ratios are found in the interior of stars, which are located at the main sequence, hence in the phase of hydrogen burning in the core. By the way, this is the longest phase in the course of the star's life and thus it is most likely to observe a star in the main sequence stage. Because of this, the hydrogen burning is best understood. However, it is not possible to directly observe the interior, where the nucleosynthesis takes place. Therefore, usually spectroscopic measurements of the stellar surface are performed and the products of nuclear fusion due to physical, chemical and thermodynamic considerations are calculated. [Burbidge et al. (1957)], [Kippenhahn, Weigert (1991)]

The elements at the star's surface normally have no direct time relation to the processes in the stellar interior, which means that they do not reflect recent processes in the core. The elements, which have been created in the interior of the star, are transported to the surface, for instance by convection streams, over the period of a lifetime of a star, hence several millions of years. Hence, by spectroscopy of the star's surface one is only able to reconstruct what happened in the stellar interior millions of years ago. This is different if the star is rotating around its own axis with a certain velocity. It is assumed, that from a certain velocity on the rotational effect is strong enough to change the evolution of the star significantly, so that all elements created in the core become visible at the surface very quickly.
This effect, which is very important for this thesis, is further explained in chapter 1.3. At first, it is important to understand the nucleosynthesis in the interior of a massive star.

1.2 Nucleosynthesis in massive main sequence stars

Nucleosynthesis means nuclear reactions in which new atomic nuclei are created from already existing ones. Out of one element a new one is created and additionally a certain amount of energy is released or absorbed to preserve energy conservation. The easiest example of nucleosynthesis is the fusion of hydrogen to helium, which is called hydrogen burning. To provide a simple description of the process: four hydrogen nuclei, thus four protons, and two electrons are transformed into a helium nucleus, which consists of two protons and two neutrons.

Since these reactions happen millions of times in the star's interior, one speaks of a reaction chain. Reaction chains are very temperature dependent, this means that they only take place in a small area of temperature. In stars with low or intermediate mass the so-called proton-proton chain (pp-chain) is dominant. For higher stellar masses, the massive stars examined in this paper, the temperature and pressure in the core is remarkably higher. Thus another reaction chain occurs, the so-called CNO-cycle, which then dominates the hydrogen burning in the core. In this chain a helium nucleus is created out of four protons and two electrons as well, but here isotopes of the elements carbon, nitrogen and oxygen act as catalysts. There are among other reactions:

$$^{12}\mathrm{C} + {}^{1}\mathrm{H} \rightarrow {}^{13}\mathrm{N} + \gamma \ , \tag{1.1}$$

$$^{13}\mathrm{C} + {}^{1}\mathrm{H} \rightarrow {}^{14}\mathrm{N} + \gamma \ , \tag{1.2}$$

$$^{14}\mathrm{N} + {}^{1}\mathrm{H} \rightarrow {}^{15}\mathrm{O} + \gamma \ , \tag{1.3}$$

$$^{15}\mathrm{N} + {}^{1}\mathrm{H} \rightarrow {}^{12}\mathrm{C} + {}^{4}\mathrm{He} \ , \tag{1.4}$$

$$^{15}\mathrm{N} + {}^{1}\mathrm{H} \rightarrow {}^{16}\mathrm{O} + \gamma \ , \tag{1.5}$$

$$^{16}\mathrm{O} + {}^{1}\mathrm{H} \rightarrow {}^{17}\mathrm{F} + \gamma \ . \tag{1.6}$$

$$^{13}\mathrm{N} \rightarrow {}^{13}\mathrm{C} + e^{+} + \nu_e \ , \tag{1.7}$$

$$^{15}\mathrm{O} \rightarrow {}^{15}\mathrm{N} + e^{+} + \nu_e \ . \tag{1.8}$$

The fusion of carbon, nitrogen and oxygen with a hydrogen atom (reaction 1.1-1.6) is called proton capture and reactions 1.7 and 1.8 are called β^{+}-decay. Reactions 1.1-1.4 group the CN-cycle, in which the abundance of the stable oxygen isotope ^{16}O is conserved. If oxygen is involved in the reaction, then it is the CNO-cycle. [Bethe (1939)], [Langer (2009)]

Over time a large amount of carbon and oxygen is transformed into nitrogen until the abundance of the involved isotopes, except ^{1}H and ^{4}He, remains stable for a long time. There is a state in which the carbon, nitrogen and oxygen isotopes recreate each other by the further reactions shown above. The number of carbon, nitrogen and oxygen isotopes is conserved in this state and it is called equilibrium.

The distribution of the number of isotopes in the stellar interior changes from the presumed initial values

$$^{12}\mathrm{C} : {}^{14}\mathrm{N} : {}^{16}\mathrm{O} \qquad 1 : 0.3 : 3 \tag{1.9}$$

to approximately

$$^{12}\mathrm{C} : {}^{14}\mathrm{N} : {}^{16}\mathrm{O} \qquad 1 : 50 - 100 : 1 - 5 \tag{1.10}$$

for the resulting equilibrium. [Heger, Langer (2000)]

The processes of the CN-cycle can also be rephrased mathematically, which is shown in the following. The time of when the reaction chain begins is considered, therefore the number distribution of equation 1.9 can be used. Furthermore, it is assumed, that initially only carbon is present, out of which nitrogen is created by proton capture. Out of six carbon protons and one hydrogen proton seven nitrogen protons are created by nucleosynthesis. So the decrease of carbon atoms dC is directly related to the increase of nitrogen atoms dN and dC can be expressed by dN. Therefore one nitrogen atom is equivalent to $\frac{6}{7}$ carbon atoms and is noted as

$$dC = -\frac{6}{7} dN \ . \tag{1.11}$$

As long as there are already oxygen atoms, their fraction stays constant in the star's interior. The change of isotopes can be expressed as the following:

$$dO = 0 \ . \tag{1.12}$$

To compare the ratios of abundance, they are graphed and, out of the considerations above, an expectation value of the slope in the initial area can be determined. This means that these theoretical considerations are only valid at the beginning of the CN-cycle. As soon as the chain develops towards equilibrium, other assumptions have to be made.
The change of the fractions $\frac{N}{C}$ and $\frac{N}{O}$ are examined.

$$d\left(\frac{N}{C}\right) = \frac{dN}{C} - \frac{N}{C^2}\frac{dC}{dN} dN \tag{1.13}$$

$$= \frac{dN}{C}\left[1 + \frac{6}{7}\frac{N}{C}\right] \tag{1.14}$$

$$d\left(\frac{N}{O}\right) = \frac{dN}{O} \tag{1.15}$$

Out of that this slope results

$$\frac{d\left(\frac{N}{C}\right)}{d\left(\frac{N}{O}\right)} = \frac{\frac{N}{C}}{\frac{N}{O}}\left[1 + \frac{6}{7}\frac{N}{C}\right] \ . \tag{1.16}$$

Applying the assumption of the number distribution from equation 1.9, the following value results for the expected slope:

$$\frac{d\left(\frac{N}{C}\right)}{d\left(\frac{N}{O}\right)} = 3.92 \ . \tag{1.17}$$

[Przybilla et al. (2010)]
These theoretical considerations are also tested in this thesis, see chapter 4.1.3.

The CNO-cycle is also a very important instrument to examine the fusion reactions in stars. Furthermore, it is the most important source of energy in massive stars of the main sequence to keep the balance between gravitational and radiation pressure in the star. Lighter elements than carbon, which can be present in stars as well, also participate in nuclear reactions, but they are not able to fulfill the task of energy supply. These reactions occur in much shorter time scales and no cycles reproduce these elements. Light elements such as lithium, beryllium and boron are quickly burnt in the core and through their disappearance a long-term energy production cannot be ensured. Light elements can only be found in the outer layers, hence the envelope of the star, since the temperatures are too low for nuclear reactions there. Considering heavier elements than nitrogen, it can be seen that they have too slow reaction times to work against the gravitational pressure from outside. [Bethe (1939)]

There are further reaction chains, which occur during hydrogen burning in the core. They consist of reactions of neon and sodium as well as magnesium and aluminium. Thereby a similar buildup and reduction of the reaction partners as in the CNO-cycle happens. In the NeNa-cycle the number of the neon isotopes ^{21}Ne and ^{22}Ne is reduced by the creation of the sodium isotope ^{23}Na. The abundance of the isotope ^{20}Ne stays the same. In the MgAl-cycle the long-lasting radioactive isotope ^{26}Al is created by the isotope ^{25}Mg with proton capture. The aluminium isotope decays to ^{26}Mg through electron capture after short time. Through another proton capture the aluminium isotope ^{27}Al can be created by ^{26}Mg. In these reactions ^{24}Mg remains unaffected. [Heger, Langer (2000)]
Moreover, it is possible that the NeNa- and MgAl-cycles interact with each other. Thus ^{24}Mg can be created by ^{23}Na with proton capture.
Furthermore, the fluorine isotope ^{19}F is involved in the CNO-cycle by reactions with oxygen. It can be produced by proton capture with ^{18}O, but it preferentially is transformed to ^{16}O by another proton capture. The fluorine isotope therefore disappears quickly from the stellar interior due to nuclear reactions in the temperature area in which the CNO-cycle and the NeNa- and MgAl-cycles preferably take place and it is being “destroyed”. [Langer (2009)]

An important area in the context of nucleosynthesis in massive stars is the behaviour in dependence of the metal content. The metallicity Z of a star has two possible definitions.

For observations of stars, it is defined by the ratio of iron to hydrogen with the assumption that the elements have enriched equally in the star. Thus the fraction of the measured abundances N normalised to the sun is stated:

$$Z = \lg\left(\frac{N_{Fe}}{N_H}\right) - \lg\left(\frac{N_{Fe}}{N_H}\right)_{\odot} , \tag{1.18}$$

$$\text{with } \lg\left(\frac{N_{Fe}}{N_H}\right)_{\odot} \approx \lg\left(\frac{1}{31000}\right) \approx -4.49 . \tag{1.19}$$

[Frebel (2008)]

For theoretical model calculations, the metallicity is defined by the sum of all elements heavier than helium. The abundance of hydrogen X, of helium Y and metals Z are described as mass fractions. The sum of those results in the inverse mean molecular weight μ of the star:

$$\frac{1}{\mu} = 2X + \frac{3}{4}Y + \frac{1}{2}Z . \tag{1.20}$$

The mean molecular weight of an isotope is the fraction of the number of nucleons, hence protons and neutrons, to the number of electrons and nuclei. If there is a mixture of isotopes, the total mean molecular weight of a star is calculated by equation 1.20. [Pols (2009)]

In metal poor stars, the abundance of carbon or heavier elements is very low. The CNO-cycle would be not efficient enough at a certain temperature, which means that it would not produce enough energy to establish energy balance in the star. Thereby stars with low metallicity are much denser and hotter in the core to maintain a high enough energy rate. Moreover, stellar winds, resulting in mass loss of the outer layers of a massive star, are created less strongly by the low abundance of carbon, nitrogen and oxygen. The mass loss has a proportional relation to the metallicity of a star. [de Mink (2010)] We will examine this notion in greater detail later.

1.3 Effects of rotation of massive main sequence stars

In this section resultant effects from the rotation of a massive star, are described and explained.
In the rotation of a star, the resulting centrifugal forces, which predominantly act on the outer layers of the star, cause an overall increase of the stellar surface area. With very strong forces, the star can deform so heavily that the radius at the equator increases strongly compared to the one at the poles. In general, this deforming effect is negligibly small and it can be considered that the stellar radius increases symmetrically. Since a weaker gravitational force acts from the outside, the pressure, and therefore the temperature, in the stellar interior decreases. As a consequence, the given fuel in the core is burnt with a lower rate, such that all nuclear fusion processes proceed slower. Subsequently less radiation intensity is produced and the luminosity of the star at the beginning of the main sequence is smaller. Due to that, the effective temperature, that is the surface temperature, can also be lower. One minor effect is that a star with a certain rotational velocity has a longer life and, therefore, stays longer on the main sequence than a comparable star without rotation. However, the effects on the luminosity and effective temperature reverse after a short time and they reach much higher values for most of their time on the main sequence than a comparable not rotating star. The causes are further explained in the following.
A rotating star firstly shows a completely different behaviour in a luminosity-effective temperature plot, hence a Hertzsprung-Russel diagram, than a not rotating star. This is further explained in the following figure 1.1. [de Mink (2010)],[Heger, Langer (2000)]

The most important effect of rotation, which is the matter of this thesis, is the mixing. Mixing refers to the transport of material between the layers of the star, whereby elements can also cycle from the envelope up into the core. The mixing effect can be caused by Eddington-Sweet circulations or shear mixing. In the first effect, due to thermal instabilities between the pole and equator areas of the star, meridional material streams occur, which can range over a large area in the star. In the second effect, balancing streams, which carry material, occur between two layers that rotate with different angular velocities. If this happens with many layers spread all over the star, the star is completely mixed.

The mixing also results in effects within the star and on its evolution. Hence, the exchange of material between the envelope and the core is the main cause for the increase of the hydrogen burning duration, because unburnt hydrogen can reach from the envelope to the core and provide new fuel. Due to the mixing, elements become visible at the surface, which otherwise stayed in the core forever, or elements from the envelope are transported to the core where they might participate in nuclear reactions and thereby disappear. This regards light elements, which are only found left in the envelope, as described in section 1.2. Thereby through efficient mixing the chemical structure of a star changes thoroughly. [de Mink (2010)]

The rotational velocity of a star is described by the velocity at the stellar equator. The initial velocity v_{init} is given as the specific fraction of the Kepler velocity v_{Kepler} and is called the initial rotation rate:

$$f_K = \frac{v_{\text{init}}}{v_{\text{Kepler}}} \ . \tag{1.21}$$

v_{init} can be determined by observations, which is not further explained here. For further explanation see [Heger, Langer (2000)]. The Kepler velocity can be calculated out of the specific stellar parameters, the gravitational constant G, the initial stellar mass M and its radius R as the following:

$$v_{\text{Kepler}} = \sqrt{\frac{GM}{R}} \ . \tag{1.22}$$

The higher the rotation rate, the stronger the effects explained above are visible. Also present is a critical velocity v_{crit} which is defined by the Eddington factor Γ. This factor consists of the opacity κ and the luminosity L of the star. Furthermore Γ scales with the speed of light c, the gravitational constant G and the initial stellar mass M:

$$v_{\text{crit}} = \sqrt{\frac{GM}{R}(1-\Gamma)} \qquad \text{with } \Gamma = \frac{\kappa L}{4\pi c G M} \ . \tag{1.23}$$

[Yoon, Langer (2005)]

In this context, we come back to the effect of mass loss. This phenomenon predominantly occurs in very massive stars and is very important for the understanding of element abundances, but until now is not well understood. As soon as a star has lost most of its hydrogen-rich envelope it is considered a Wolf-Rayet star. The surface abundance of hydrogen then decreased to a mass fraction of 40% at most. It is assumed that a Wolf-Rayet star has lost its envelope almost completely due to strong winds leaving the naked core, where the nucleosynthesis is happening, visible. Moreover, high abundances of nitrogen, carbon and oxygen are observed. As explained in section 1.2, the mass loss behaves proportionally to the metallicity. Furthermore, the loss rate intensifies with increasing rotational velocity of the star, because the outer layers of a very fast rotating star are only bound weakly to the gravitation of the star. The relation to Wolf-Rayet stars will be important in the further analysis. [Pols (2009)], [Yoon, Langer (2005)]

1.4 Quasi-chemically homogeneous evolution

The effects of a fast rotating star, described in the last section, result in a new chemical structure and evolution of the star. Due to the rotationally induced mixing there is no, or only a very small, chemical gradient between envelope and core. For example, during hydrogen burning in the stellar interior, the produced helium is mixed through the star due to the rotation. That means there is a very small difference of the element abundances between two layers in the star. Ideally, the star now has the same number density of the existing elements in each place and therefore has a chemically homogeneous structure. This also means that the star, which at the beginning of the main sequence mainly consists of hydrogen, is transformed into a star with a constistent amount of helium at the end of the main sequence. In reality, the star usually still has a very thin hydrogen envelope. [Yoon, Langer (2005)]

With the assumption of a chemically homogeneous structure of the star one can use the general relation $L \propto \mu^{\alpha} M^{\beta}$, [Kippenhahn, Weigert (1991)], with which one can see, that with increasing mean molecular weight μ of the star the luminosity L increases with constant stellar mass M. The powers α and β differ depending on the stellar mass and structure, but here only the understanding of the proportionality of L and μ matter. With increasing atomic mass also the mean molecular weight increases, for example from ionised hydrogen with $\mu = \frac{1}{2}$ to helium with $\mu = \frac{4}{3}$, compare equation 1.20. If a rotating star on the main sequence is enriched with more helium than a star with the same mass without rotation, then the total mean molecular weight of the rotating star is greater and thus its luminosity as well. The effect, that the luminosity of a rotating star evolves only after some time on the main sequence to higher values, can be explained by the duration until an effective mixing in the star is reached.

To distinguish rotationally induced mixing from other mixing processes, we consider the example of a convective mixing process. In the interior of a massive star, there is a convective core, which is surrounded by a radiative envelope. In the convective core, there are so-called convective streams, which are understood as transport in terms of material bubbles with different densities. If there are material streams which overshoot the core, one speaks of “convective core overshooting”. [Pols (2009)] Thereby the boundary layers between the convective core and the radiative envelope are mixed, so that similar effects occur in the star as by rotationally induced mixing, as can also be seen in the Hertzsprung-Russel diagram. So, the convective core, for example, is being enlarged in both cases, whereby the star’s luminosity increases. However, the “convective core overshooting” can never mix that large-scaled as the rotationally induced mixing. Hence, the changes of the star’s chemical structure, which become visible at the surface, can be best explained by the theory of the rotationally induced quasi-chemically homogeneous evolution.
The term “quasi-chemically homogeneous” means, that a rotating star is mixed so far, that this can be approximated by a chemically homogeneous structure, but the ideal case of a completely homogeneous star is never reached. [Heger, Langer (2000)]

Now we will further consider the behaviour in the Hertzsprung-Russel diagram (HRD). For this we use figure 1.1, which has been generated with the help of the program Gnuplot out of data from [Yoon et al. (2006)], which is available for the whole thesis, as will be explained in chapter 2. The figure shows different evolutionary tracks of a star with a mass of $12M_{\odot}$ and a metallicity of $Z = 0.004$ with different rotational velocities from 0.1 to 0.7 v_{Kepler} shown as luminosity $\log(L/L_{\odot})$ against effective temperature $\log T_{\mathrm{eff}}$. The metallicity is equal to the metallicity of the stars in the Small Magellanic Cloud, which is abbreviated as "SMC" in the following. It has to be noted, that here one sees the total stellar evolution from hydrogen core burning to the exhaustion of the last fuel.

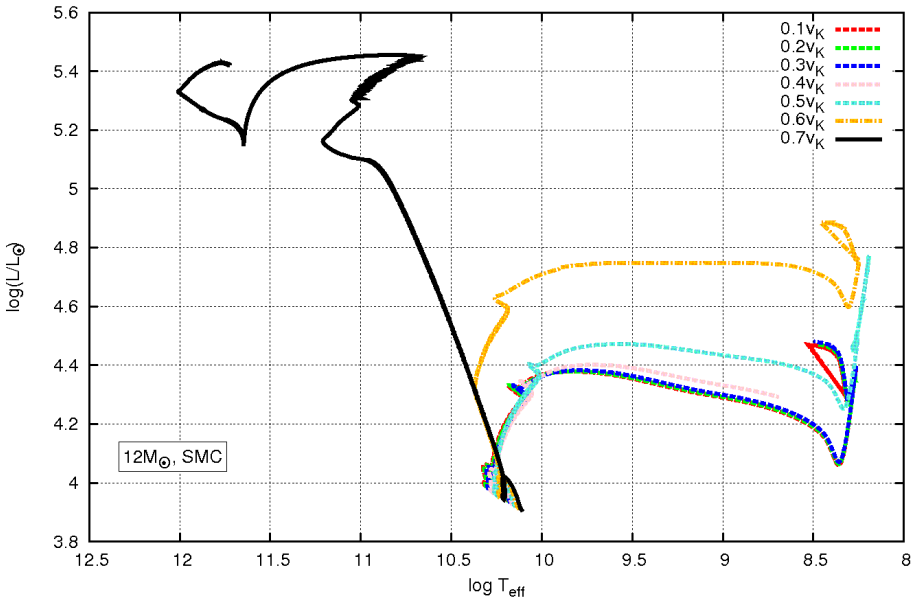

Figure 1.1: Example of a HRD with tracks of homogeneous evolution (continuous line) and non-homogeneous evolution (dashed lines), as well as partially homogeneous evolution (dashed-dotted line), for models with a mass of $12M_{\odot}$, metallicity of $Z = 0.004$ and different rotational velocities, see legend.

On examination of the main sequence, it can be seen that the curve with the continuous line ($f_K = 0.7$) proceeds from the bottom right to the top left, thus towards higher luminosity and effective temperature. The phase of the main sequence ends at an effective temperature of about 11 and a luminosity of approximately 5.1. The curve with the higher rotation rate, therefore, describes a chemically homogeneous evolution. Whereas the curve with the dashed lines proceeds from the bottom left to the top right, thereby showing a lower effective temperature with increasing luminosity. Here the hydrogen burning ends at an effective temperature of about 10 and a luminosity of 4.3 and 4.4. Therefore, the stars with low rotational rates evolve non-homogeneously. In addition, one identifies that there can be a mixed state, which is visible here at a rotational rate of 0.6. The star firstly evolves on the homogeneous track towards high temperatures, until, suddenly, a change to lower temperatures to the non-homogeneous area is visible. The main sequence ends at an effective temperature of about 10.2 and a luminosity of 4.6. This type of evolution is marked with dashed-dotted lines.

The different developing confirms that the evolutionary tracks of chemically homogeneous evolution and non-homogeneously evolving stars on the main sequence in theoretical models can be clearly distinguished. Furthermore, it can be seen, in comparison with other HR diagrams of different mass and rotational rates, that with higher stellar mass a lower rotation rate is necessary to mix the star thoroughly. [Heger, Langer (2000)], [Yoon, Langer (2005)]

It is not possible to map the evolutionary tracks of a star through observations, since the duration of the main sequence is far too long. In HR diagrams out of observational data, many different stars in different evolution stages with different luminosities and temperatures, as well as masses and metallicities, are found. The observed stars with homogeneous and non-homogeneous evolution overlap on the main sequence. This means that, in the observation of a star cluster or a section of the Milky Way, one is not able to perform a clear separation of the recorded stars in homogeneous and non-homogeneous evolution.
For better understanding to this figure 1.1 has been prepared. In figure 1.2 the evolutionary tracks of different stellar models are shown.

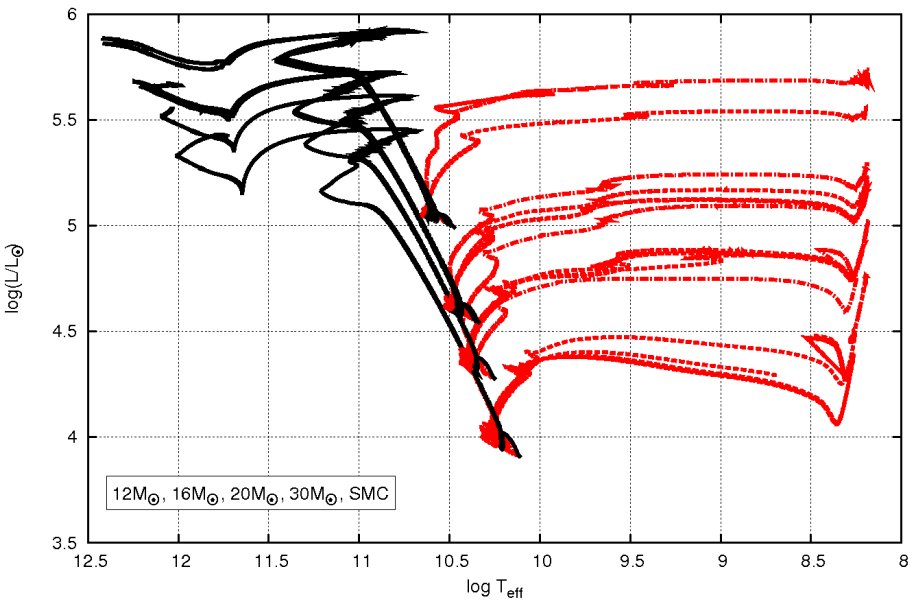

Figure 1.2: To the distinction of the evolutionary tracks of different stellar models with the masses 12, 16, 20 and 30$M_\odot$ and the SMC-metallicity for different rotation rates. The black solid lines represent fast rotation and the red dashed lines slow or no rotation. The overlap of the black and red lines on the main sequence makes clear, that in a HRD of observational data no distinction between homogeneous and non-homogeneous evolution is possible.

Since the evolutionary tracks of different stars now overlap on the main sequence, one cannot distinguish a well-defined separation between the rotation rates. To be able to identify and research chemically homogeneously evolving stars by direct observations, one needs a proper method of distinction. The method should provide clear and well-defined results, so that they can be easily used in observations. Thus, it is aspired to work out a distinction method, which is characterised by only one stellar parameter. In this thesis, a method is developed which is given by the stellar parameter of the element abundances at the star's surface.

1.5 Aim of this thesis

The aim of this thesis is, by the analysis of the element abundances at the stellar surface, to detect changes of the surface abundances of the elements with regard to the rotationally induced mixing during the main sequence. From that, a method will be worked out, which is able to distinguish homogeneously and non-homogeneously evolving stars, so that a direct and clear recognition of rotationally induced chemical homogeneity in massive main sequence stars is possible. Through observation of the element abundances at the surface, a star shall be identified clearly as chemically homogeneous opening possibilities for further research.

2 Used model calculations

In order to work on the questions mentioned above, data of numerical model calculations of different stellar models is used. The data originates [Yoon et al. (2006)] and is computed by a hydrodynamical stellar evolution code. In this the effects of rotation, transport of angular momentum, magnetic torques and hydrodynamical instabilities are considered as influences on the star's structure. In this thesis, the effects of rotation are most important. Stars with different metallicities between $Z = 0.004$ and $Z = 10^{-5}$ are examined. The range of the initial stellar mass is 12 to $60M_{\odot}$ and the calculations are done with rotational rates between 0.0 and 0.8.
The numerical calculations result in simulated data of the important stellar parameters: isotope abundances at the surface, time or age of the star, effective temperature, luminosity, mass, temperature in the stellar interior and many additional parameters secondary to this thesis.
The analysed abundances at the stellar surface involve the following isotopes:

Hydrogen	^{1}H	^{2}H	
Helium	^{3}He	^{4}He	
Lithium	^{6}Li	^{7}Li	
Beryllium	^{7}Be	^{9}Be	
Boron	^{8}B	^{10}B	^{11}B
Carbon	^{11}C	^{12}C	^{13}C
Nitrogen	^{12}N	^{14}N	^{15}N
Oxygen	^{16}O	^{17}O	^{18}O
Fluorine	^{19}F		
Neon	^{20}Ne	^{21}Ne	^{22}Ne
Sodium	^{23}Na		
Magnesium	^{24}Mg	^{25}Mg	^{26}Mg
Aluminium	^{26}Al	^{27}Al	
Silicon	^{28}Si	^{29}Si	^{30}Si
Iron	^{56}Fe		

The used work deals with finding out how gamma-ray bursts (GRBs) at the end of a star's life develop. This means, finding the cause of these highly energetic bursts of electromagnetic radiation. It is assumed that the predecessor stars of GRBs are related to the quasi-chemically homogeneous evolution. The bigger part of GRBs is predicted for the range of mass studied in this thesis and metallicities below $Z = 0.004$. Above this metallicity limit, a star's life usually ends by a supernova. As mentioned before, the metallicity $Z = 0.004$ equals the metal content in the Small Magellanic Cloud, as such, the results of this work can be compared with real objects out of observations.

3 Method of the analysis of the abundances

3.1 General approach

The data from the model calculations are analysed and handled graphically with the help of the program Gnuplot. Plots for element abundance at the stellar surface were graphed against time. We created plots for each stellar mass and metallicity per element with different rotation rates. The results are completely quoted in appendix A.1.

Firstly, it is essential to order the given star's data with different masses and rotation rates, which means to determine the difference between homogeneous and non-homogeneous evolution. For this, as described in section 1.3, a Hertzsprung-Russel diagram was created by graphing the different evolutionary tracks of a star with different rotational rates. If the evolutionary track equals the dashed lines of figure 1.1, it is a non-homogeneous evolution, but if it equals the dashed-dotted line, the star runs through a partially homogeneous evolution. If the developing proceeds as the solid line in fig. 1.1, the star evolves quasi-chemically homogeneous. The following curves in the figures are shown by this definition. The exact classifications of the evolutionary tracks are quoted in appendix A.2. The HRDs can be seen in figures A.1 to A.19 in appendix A.1.

Additionally, the existing data sets are adjusted to the needs described in the following. It is enough to consider the sum of the individual isotopes of each element, since usually one isotope of an element dominates in abundance and therefore remaining isotopes only create a very small change. This is practically implemented in the Gnuplot script. Furthermore, the element abundances shall be shown as fractions of the initial values, which is abbreviated with "initial". So each graph starts at the value "1" and it is possible to observe the percental change in progression. The initial abundance value of an element can be determined by consideration of the "zero-age main sequence", hence time zero displays the beginning of a star's life. It is assumed that the star initially has the same chemical composition as the interstellar medium from which it originated.

Furthermore, the data is only examined to the end of the main sequence. For this the value of the central temperature T_C is consulted. If it is greater than 10^8 K, one can act on the assumption, that hydrogen burning in the core ends and helium burning starts and, therefore, by definition, the main sequence is finalised in any case. In figure 3.1 the point in time of the end of the main sequence phase can be estimated, but practically this has been carried out with a C-program.

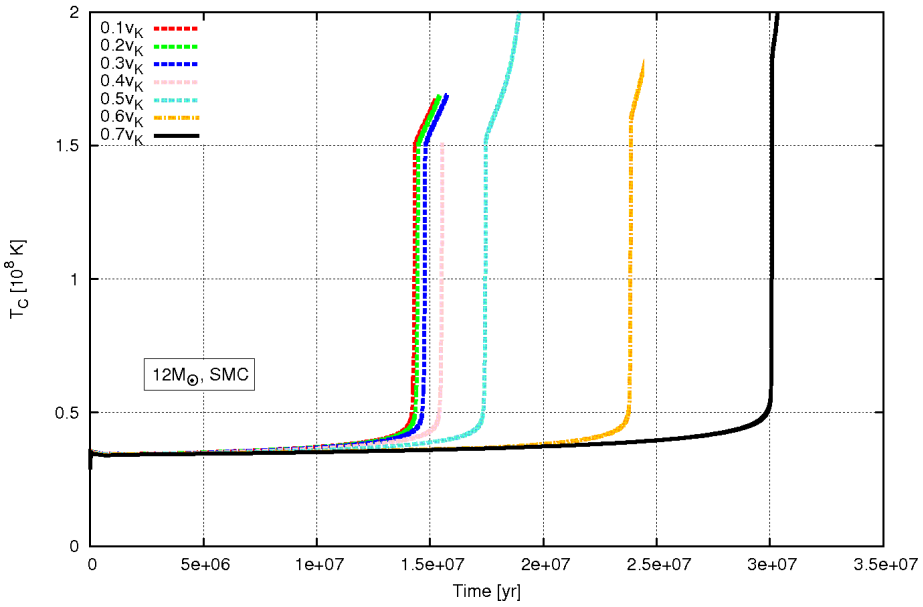

Figure 3.1: Developing of the central temperature with time for stars with M = $12M_{\odot}$, $Z = 0.004$ and different rotation rates, compare figure 1.1.

Now let's come to the actual method, with which homogeneously and non-homogeneously evolving stars can be distinguished from each other. The results of this analysis will give the possibility to also be used for observations. Thus, the curves of homogeneous and non-homogeneous evolution should be as far away from each other, that, also with measurement errors, they can be clearly separated. In most measurements of observations the uncertainty is about 0.2 dex. This means that the curves in the abundance-time plot have to be separated by at least 0.2 dex to provide clear results. These requirements are from now on shortly called "dex-criterion".

The so-called dex-value is mainly used in logarithmic plots, since the distance of 0.2 dex, usually on the y-axis, equals 0.2 scale divisions. The following conversion holds:

$$\Delta \log y = 0.2 \text{ dex} \tag{3.1}$$

$$\Leftrightarrow \log y_1 - \log y_2 = 0.2 \tag{3.2}$$

$$\Leftrightarrow \frac{y_1}{y_2} = 10^{0.2} \approx 1.585 \; . \tag{3.3}$$

The following figure clarifies how the distances in a diagram with logarithmic and linear plotted scales have to be read. As an example, a luminosity-effective temperature is used.

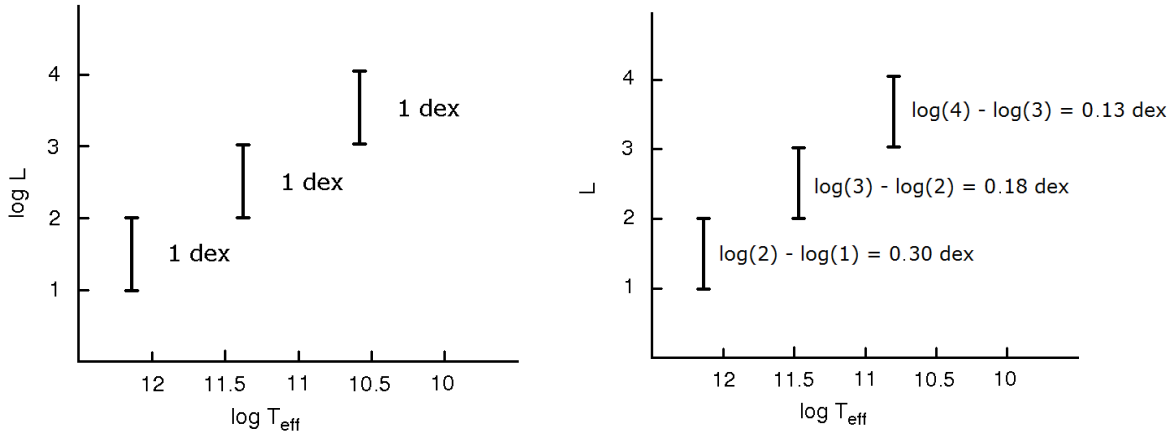

Figure 3.2: Explanation to the term of the dex-value, whereby the left diagram is plotted with a logarithmic scale and the right diagram with a linear scale.

If the maximal or minimal value of the element abundance of a non-homogeneously evolving star with rotational velocity a has a distance of not less than 0.2 dex to the curve of the element abundance of a homogeneously evolving star with rotational velocity b, whereby $b>a$, a clear distinction between both evolution types can be made. In figure 3.3 the "dex-criterion" is clarified with the help of the developing of the surface abundance of oxygen.

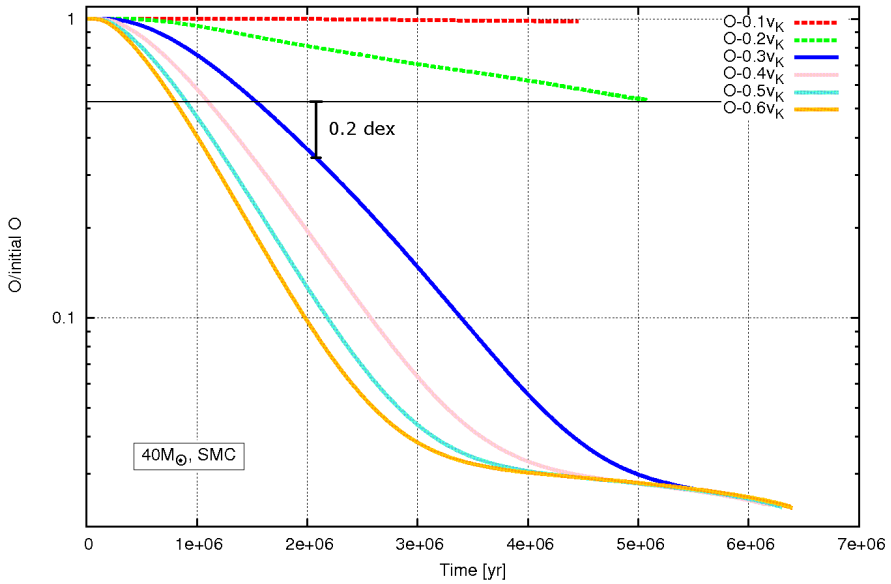

Figure 3.3: Example of an abundance-time diagram to explain the "dex-criterion" on the basis of the abundance change of oxygen at the surface of $40M_{\odot}$-stars with $Z = 0.004$ and different rotation rates. As soon as the abundance is below about 0.3-times the initial value, a $40M_{\odot}$-star can clearly be identified as chemically homogeneous.

The element, which fulfills the "dex-criterion", can serve in observations as a distinction characteristic between homogeneous and non-homogeneous evolution of massive main sequence stars.

3.2 Limiting

In the following, those elements which are not eligible for the demanded distinction of homogeneous and non-homogeneous evolution, due to several each specified reasons, are already excluded.

In all observed plots, it is quickly noticeable that the change in surface abundance of iron and silicon is negligibly small or nonexistent. This is because only the period of the main sequence is considered and these elements are created during later evolutionary stages of the star. Thus, these elements can be excluded directly from further analysis and omitted from the appendix.

By consideration of the elements lithium, beryllium and boron it is noticed that the non-homogeneously evolving models do not behave as expected. So at almost all stellar masses and metallicities the abundance of the three elements at the star's surface decreases to a lower value as in the homogeneously evolving models, compare fig. A.44 to A.79. Furthermore, one observes in all abundance-time diagrams at all evolution tracks that, at the beginning of the main sequence phase, the content of lithium, beryllium and boron decreases strongly. The higher the rotational velocity of the star, the more drastically the decrease proceeds. In the better part of the abundance-time diagrams, after a short-timed increase in abundance, the developing of most of the evolutionary tracks passes into saturation. In this, one can see that the higher the rotation rate, the higher the preserved mass fraction of the element. A particularly distinct example to this can be seen in figure 3.4, in which the progress of the lithium abundance of a $60M_{\odot}$-star model with $Z = 10^{-5}$ is visible.
The reasons for this unexpected developing of the abundances of lithium, beryllium and boron can only be conjectured at this point in time. Possible sources could be temperature dependent fusion processes in metal-poor stars or effects by mass loss. Further works will be necessary to understand the behaviour of these elements at low metallicities.

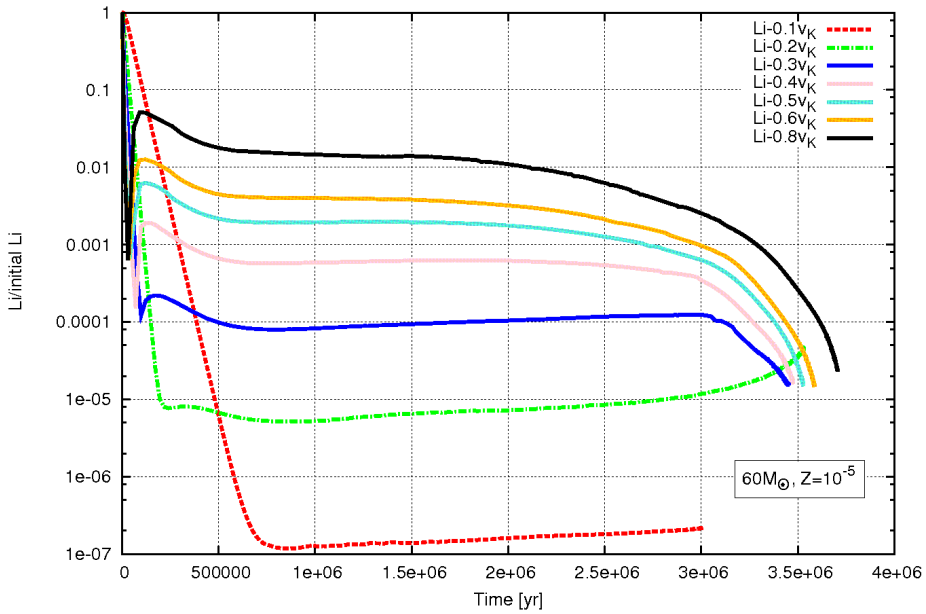

Figure 3.4: Example of an abundance-time plot of lithium in $60M_{\odot}$-stars with $Z = 10^{-5}$ and different rotation rates. It is not possible to thoroughly fathom the visible progression within the limits of this thesis.

In the further analysis with the help of the "dex-criterion" carbon, nitrogen, neon and magnesium can be clearly removed as well.

By consideration of carbon, the previously explained CNO-cycle becomes important. At first, the surface abundance of carbon clearly decreases in all evolution types, though it is stronger in the homogeneous curves. In those, one subsequently observes the state of equilibrium already towards the end of the main sequence, so that the abundance increases slightly after a saturation phase. Owing to this, the minimal values of the abundance curves of the non-homogeneous evolution and the maximal values of the curves with homogeneous evolution almost never have the necessary distance of 0.2 dex. Only in one model, namely $M = 40M_{\odot}$ and $Z = 0.004$, the "dex-criterion" is fulfilled, see appendix A.1 fig. A.85. In some cases, the curves of homogeneous and non-homogeneous evolution intersect. An example of this is visible in figure 3.5. Therefore, the element carbon is a poor choice for distinguishing chemically homogeneous evolution.

A similar behaviour shows nitrogen caused by the CNO-cycle. However, the nitrogen abundance of the homogeneous evolution continuously rises up to a saturation value. Here the "dex-criterion" is only fulfilled in one case. This example can be seen in figure 3.6. This means, that with the help of the nitrogen abundance at the stellar surface, it cannot be clearly distinguished between non-homogeneous and homogeneous evolution.

The behaviour of the mass fractions of carbon, nitrogen and oxygen to each other, which is shortly called CNO-abundances, will be analysed in detail in section 4.1.3.

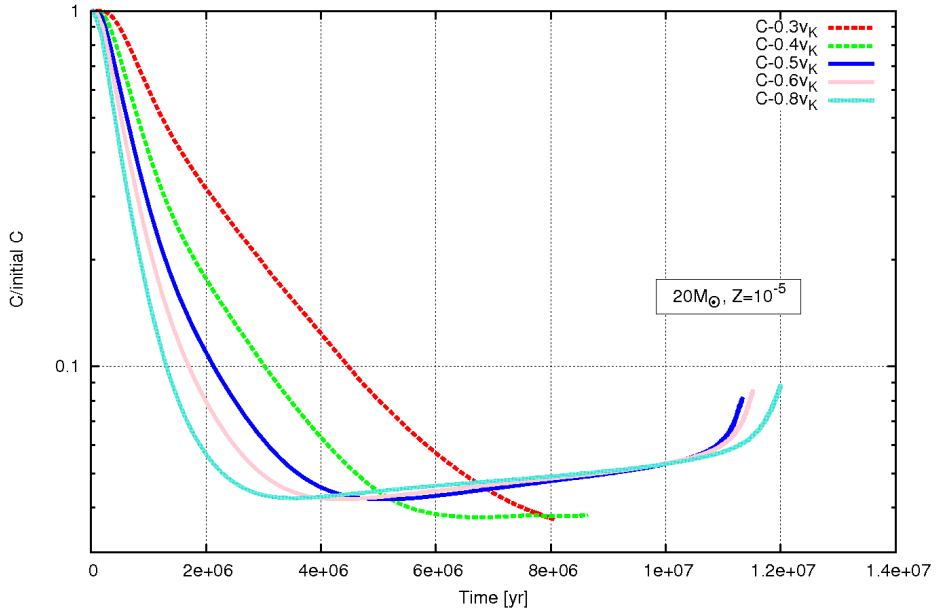

Figure 3.5: Example to the element abundance of carbon as a function of time for stars with $M = 20M_\odot$, $Z = 10^{-5}$ and different rotation rates, whereby the curves of homogeneous and non-homogeneous evolution intersect after about $5 \cdot 10^6$ years.

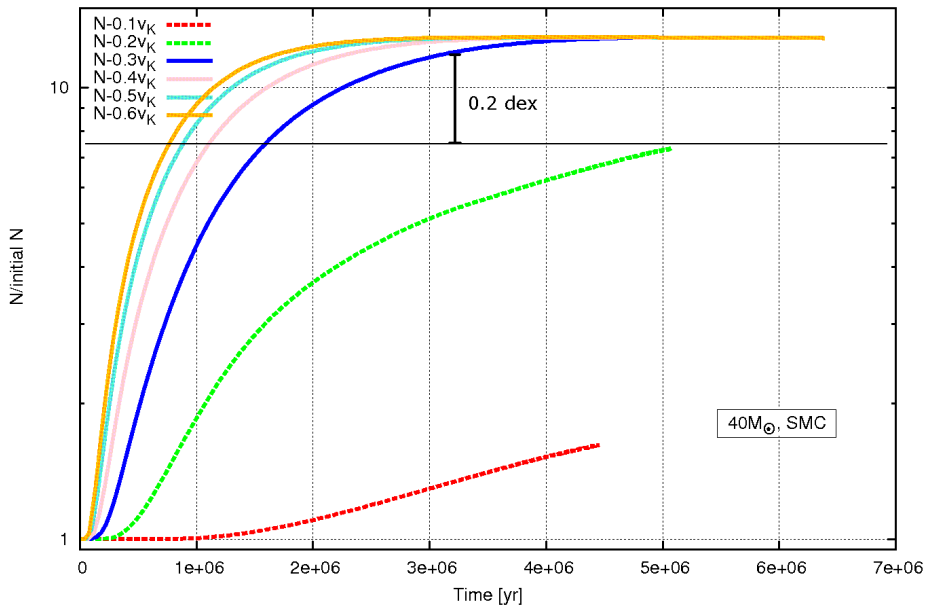

Figure 3.6: Example to the element abundance of nitrogen as a function of time in stars with $M = 40M_\odot$, $Z = 0.004$ and different rotation rates, whereby the evolutionary tracks with a rotation rate of 0.2 and 0.3 are just separated by 0.2 dex at about $3.2 \cdot 10^6$ years.

As can be checked in figures A.132 to A.143 in appendix A.1, the element neon is not eligible in any case for the recognition of chemically homogeneous stars. In the case of the SMC-metallicity the abundance of total neon changes too little. In the case of low metallicities, a similar behaviour to that of carbon can be observed. The necessary "dex-criterion" is never fulfilled by neon and the element can be excluded as a method of distinction for chemically homogeneous stars.

The element magnesium behaves similar to neon for the SMC-metallicity and therefore cannot be used, see appendix A.1 figures A.156 to A.162. For $Z = 10^{-5}$ one notices up to stellar models with $40M_{\odot}$ a totally different behaviour. An example can be seen in figure 3.7. After a short decrease in abundance in both homogeneous and non-homogeneous evolution, the abundance of magnesium increases. In the star models with homogeneous evolution the abundance increases up to 1.8 times the initial value and decreases quickly from the maximal value to almost zero. This is unexpected and cannot be explained immediately. The strong decrease of the magnesium abundance demands detailed consideration. The behaviour of the magnesium abundance at the surface in very metal-poor stars is particularly interesting, because a similar depletion of magnesium in metal-poor globular clusters has been observed and this cannot be explained yet. Thus, magnesium is further examined in section 4.2 regarding the dependence of the metallicity. However, magnesium does not fulfill the "dex-criterion" at this metallicity either.

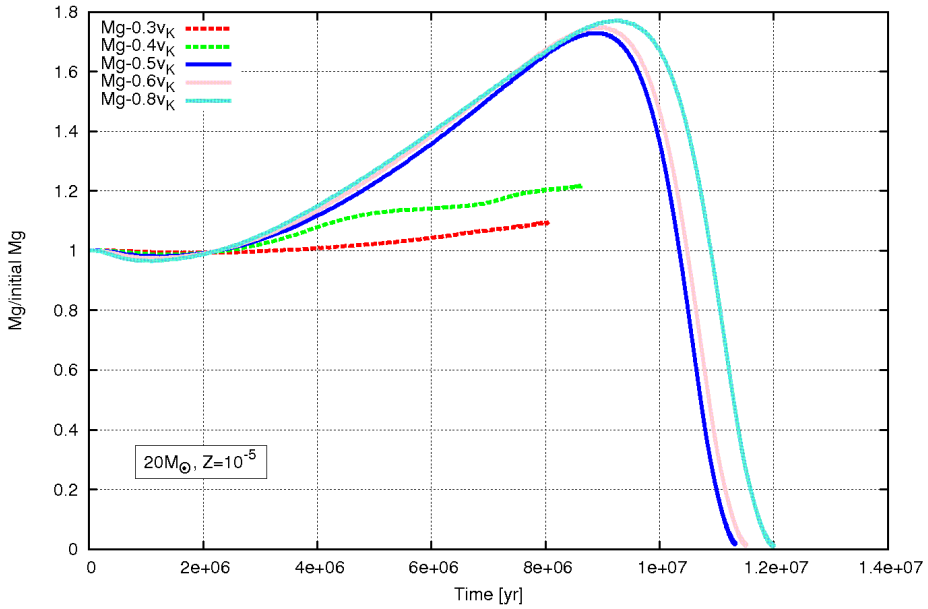

Figure 3.7: Example to the element abundance of magnesium as a function of time in stars with $M = 20M_{\odot}$, $Z = 10^{-5}$ and different rotation rates.

In the further analysis, the phenomenon of Wolf-Rayet stars needs special consideration. As previously explained in section 1.3, a Wolf-Rayet star has probably thrown away its hydrogen envelope completely and the naked helium core becomes visible. Once the hydrogen abundance at the surface is below a mass fraction of 40%, a homogeneously evolving star cannot clearly be distinguished from a Wolf-Rayet star. It cannot be identified, if the star has this element abundance by quasi-chemically homogeneous evolution or by strong mass loss. This means that an interpretation in the abundance-time diagrams from that point in time on, in which the hydrogen abundance has fallen below the threshold of 0.4, is not possible anymore. This threshold is referred to as "Wolf-Rayet threshold" throughout this paper. This also has consequent effects for the interpretation of the other elements. From the point in time of the "Wolf-Rayet threshold" on, for example, the mass fractions of helium and carbon, nitrogen or oxygen could have been caused by a Wolf-Rayet star. The products of the core burning, which is dominated by the CNO-cycle, can be directly observed at the surface. This means, that an element is only eligible for a distinction method of chemically homogeneous stars, if the "dex-criterion" is fulfilled before the point in time of the "Wolf-Rayet threshold".

To the analysis it should also be noted, that the stellar models with partially homogeneous evolution are temporarily mixed rotationally induced, meaning they show a changed chemical structure in comparison to non-homogeneously evolving stars. This means, that partially homogeneously evolving stars also feature enrichments at the surface in the abundance-time plot, but weaker than completely homogeneous stars. Out of the analysis in this work it should be possible to recognise completely homogeneous stars. Thus, only those elements are declared as eligible, with which partial and complete evolution can be distinguished. There is a more detailed analysis needed to obtain an exact figure of the behaviour of partially homogeneous in contrast to homogeneous evolution. This will not be done in this bachelor thesis.

4 Analysis of the abundances

4.1 Classification of the evolutionary type for $Z = 0.004$

In the following the remaining elements are tested in detail for the metallicity $Z = 0.004$ with the help of the "dex-criterion" on their eligibility of clear distinction between non-homogeneous and rotationally induced quasi-chemically homogeneous evolution in the abundance-time diagram. The considered metallicity is equal to the metal content in the Small Magellanic Cloud, so that the results, as already mentioned, can be directly verified and used in observations.

4.1.1 Hydrogen

In the analysis of the element hydrogen, its abundance-time diagrams are tested on the "dex-criterion" and the "Wolf-Rayet threshold" at the same time. Hydrogen is regarded as eligible, if the "dex-criterion" is fulfilled before the "Wolf-Rayet threshold". As can be examined in figures A.20 to A.26 in the appendix A.1, the hydrogen abundance at the star's surface sinks in all evolutionary tracks over the phase of the main sequence. In the non-homogeneous stellar models, the decrease in abundance is very small, because the hydrogen in the envelope is not participating in nuclear reactions and is mainly preserved. Instead, the slight decrease in the non-homogeneous models is caused by mass loss. In the homogeneously evolving evolution tracks the total hydrogen deposit in the star is "burnt" and the abundance decreases until the end of the main sequence to almost zero. To be eligible as a distinction method, the abundance in the homogeneously evolving star model above the value of 0.4 has to differ clearly from the non-homogeneously evolving models due to the described relation to Wolf-Rayet stars. This means, that if the abundance values of hydrogen in both evolution types differ just below the "Wolf-Rayet threshold", the star model is not eligible as a distinction method for chemically homogeneous evolution. Since the threshold of 0.4 is not an exact value, an uncertainty has to be taken into account for this value as well. In figure 4.1 an example is visible, in which the "dex-criterion" is just fulfilled between a relative abundance of 0.5 and 0.4. Such cases are called hardly eligible in the following.

It is demonstrated that the "dex-criterion" is fulfilled in the mass range $16M_\odot$ to $25M_\odot$ and $40M_\odot$. As a general threshold of abundance for the metallicity $Z = 0.004$, one can specify that a star can be identified as chemically homogeneous if the surface abundance of hydrogen lies between 0.56 and 0.4 times the initial value. Since this is a very small range, hydrogen cannot be recommended as a distinction method.

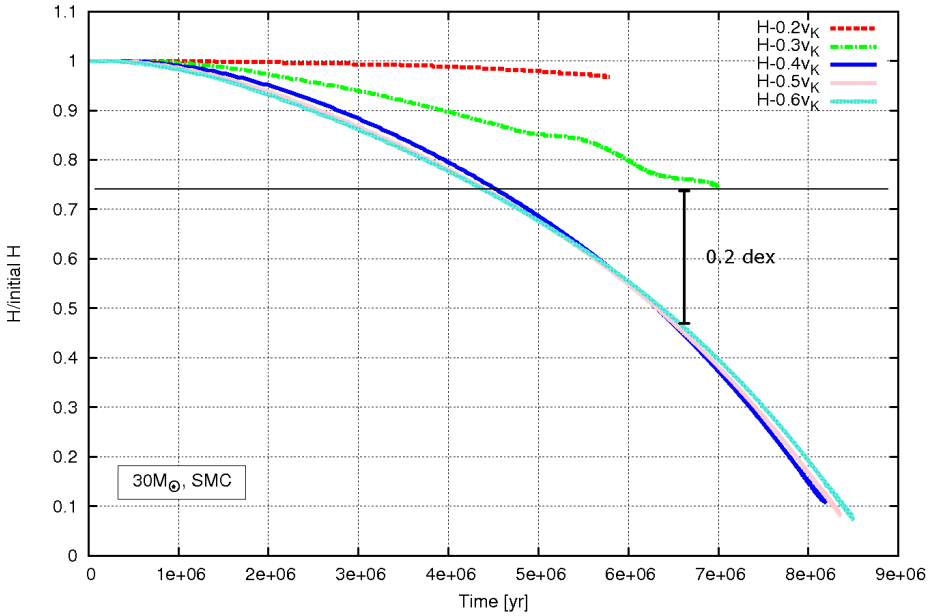

Figure 4.1: Example of an abundance-time diagram of hydrogen for stars with $30M_\odot$, $Z = 0.004$ and different rotation rates, in which the "dex-criterion" is fulfilled below a relative abundance of 0.5. The "Wolf-Rayet threshold" is at the point of $7 \cdot 10^6$ years.

4.1.2 Helium

For helium, the complementary behaviour of the surface abundance to the one of hydrogen is noticed, across all evolutionary tracks. During the main sequence phase, hydrogen is transformed into helium, so that a chemically homogeneous star is smoothly enriched with helium by the depletion of hydrogen and at the end of the main sequence, it approximately consists completely of helium. When the hydrogen abundance in the homogeneous star models has declined to almost zero, the helium abundance at the surface has its maximum value. However, again, the "Wolf-Rayet threshold" must be considered.

Generally, we are dealing with a homogeneous evolution if the abundance at the surface is at least 1.27 times the initial value. However, if the point in time of the "Wolf-Rayet threshold" in the abundance-time diagram of hydrogen in the diagram of helium is considered, it results in an upper limit, see figures 4.1 and4.2. The maximal value, up to which the "dex-criterion" is fulfilled, is 2.8 times the initial value, as can be checked in figure 4.2. This means, that the range in which helium can be used as a distinction method, is between a surface abundance of 1.27 and 2.8 times the initial value. The stellar models with $16M_\odot$ and $60M_\odot$ do not fulfill the "dex-criterion". The stellar models with $25M_\odot$ and $30M_\odot$ are not eligible as a distinction method due to the "Wolf-Rayet threshold". The figures A.33 to A.38 referring to helium and the metallicity $Z = 0.004$ can be found in the appendix A.1.

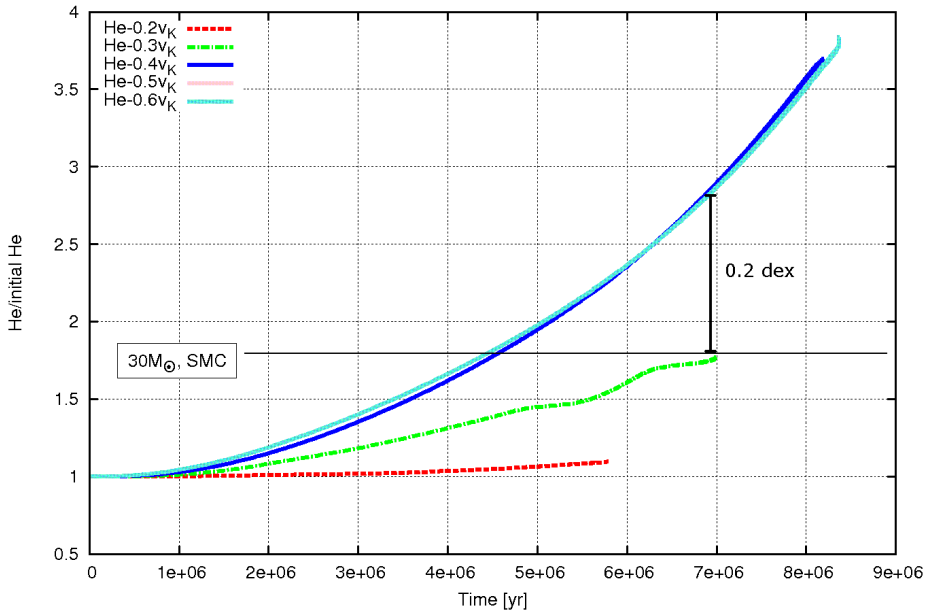

Figure 4.2: Example of an abundance-time diagram of helium for stars with $30M_\odot$, $Z = 0.004$ and different rotation rates, in which the "dex-criterion" is fulfilled from an abundance of 2.8 on. In comparison with fig. 4.1 one sees, that the criterion is fulfilled slightly before the point in time of the "Wolf-Rayet threshold", so that in this case helium is hardly eligible as a recognition feature.

4.1.3 Oxygen

In consideration of the behaviour of the surface abundance of oxygen in the abundance-time diagrams, one directly notices that the non-homogeneous and homogeneous evolution tracks show a very different behaviour, compare fig. A.104 to A.115 in appendix A.1. The oxygen abundance of the non-homogeneously evolving stars decreases slightly. The higher the rotation rate, the higher the decrease. The models of the homogeneously evolving stars show a strong decrease of the oxygen abundance until the end of the main sequence. In those stars the CNO-cycle causes oxygen to transform into other elements, predominantly nitrogen. The behaviour of partially homogeneously evolving stars can be observed easily in the diagrams of oxygen. As can be seen in figure 4.3, the partially homogeneous evolution track firstly proceeds parallel to the homogeneous one until the point of about $9 \cdot 10^6$ years, after which the surface abundance stays constant. The "dex-criterion" between partially and completely homogeneous evolution is fulfilled quite early. In testing the distinction between non-homogeneous and partially homogeneous evolution tracks, the "dex-criterion" would be already fulfilled after about $6 \cdot 10^6$ years and a surface abundance of circa 0.4 times the initial value, see fig. 4.3 as an example.

In general, for oxygen, the "dex-criterion" is fulfilled for all masses and metallicities. Considering the SMC-metallicity, an abundance threshold of 0.065 times the initial value is obtained, from which on a completely chemically homogeneous star can be clearly recognised. This low value is obtained by the stellar model with $12M_{\odot}$, compare fig. A.104, since the partially homogeneous evolution track behaves in a homogeneous manner for a long time and, therefore, a major part of the oxygen deposit is reduced. If the "dex-criterion" between the non-homogeneous and partially homogeneous track is tested, a higher value is obtained, from which on the star can be clearly identified as homogeneous. This is denoted with the dashed dex-bar in figure 4.3. As a global threshold for all masses of the SMC-metallicity, it results in 0.2 times the initial value. Below this value, a star can be recognised as chemically homogeneous with the help of its oxygen abundance at the surface. The "Wolf-Rayet threshold" becomes relevant from a surface abundance below 0.04 times the initial value.

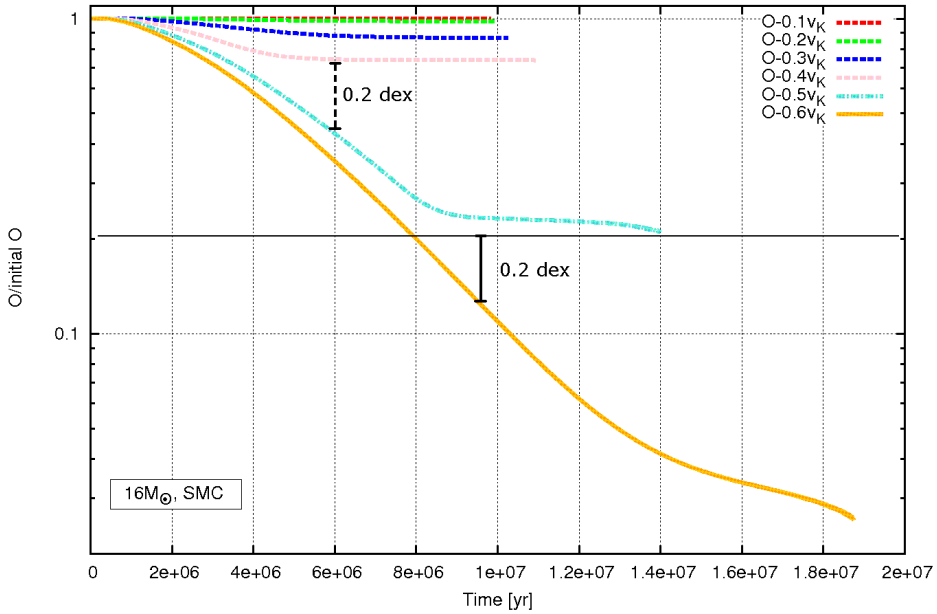

Figure 4.3: Example of an abundance-time diagram of oxygen for stars with $16M_{\odot}$, $Z = 0.004$ and different rotation rates, in which the "dex-criterion" is fulfilled for the curves with $f_K = 0.5$ and 0.6 from an abundance of 0.2 and from circa $9,5 \cdot 10^6$ years on (continuous dex-bar). If one tests the "dex-criterion" between non-homogeneous and partially homogeneous evolution tracks ($f_K = 0.4$ and 0.5), the dashed dex-bar results at the point of $6 \cdot 10^6$ years. This means, that the "dex-criterion" is fulfilled at an earlier point in time as in the testing between partially and completely homogeneous evolution tracks.

Detailed examination of the CNO-abundances

At this point, the mathematical formulation of the CN-cycle, described in section 1.2, is analysed. Thus, it is concretely tested if the ratios of the surface abundances of carbon, nitrogen and oxygen behave as expected as equation 1.17 with a slope of about 4. For this a $\frac{N}{C}$ - $\frac{N}{O}$ plot is created for each stellar model of the metallicity $Z = 0.004$ of different masses and rotational rates and a straight line with slope 4 is sketched in, which is denoted in the diagrams as $f(x)$. The plots are created within the main sequence and consist of the sums of the isotopes. Since the assumptions made in section 1.2 are only valid at the beginning of the CN-cycle, only the initial area is considered in the plots depicted here. For the curves of the homogeneous evolution it is expected that its developing corresponds well to the straight line $f(x)$. By the rotationally induced homogeneity, the development of the CN-cycle in the core and the envelope should develop equally. In the following, some diagrams are presented for clarification. All diagrams of the metallicity $Z = 0.004$ not shown, are visible in fig. A.116 to A.119 in the appendix A.1.

In the stellar models with $12M_{\odot}$ in figure 4.4 it can be seen that the abundances in all evolution tracks develop only in the area between 0.1 and 0.3 of the mass fraction of nitrogen and oxygen ($\frac{N}{O}$) and between 0 and 1 of the fractions of nitrogen and carbon ($\frac{N}{C}$) with a slope of about 4. The non-homogeneous evolution tracks ascend with a much higher slope afterwards, which means that the ratio of the abundances of nitrogen and carbon increase faster than the abundances of nitrogen and oxygen. In this, the evolutionary tracks with a higher rotation rate reach a higher nitrogen-carbon abundance fraction.

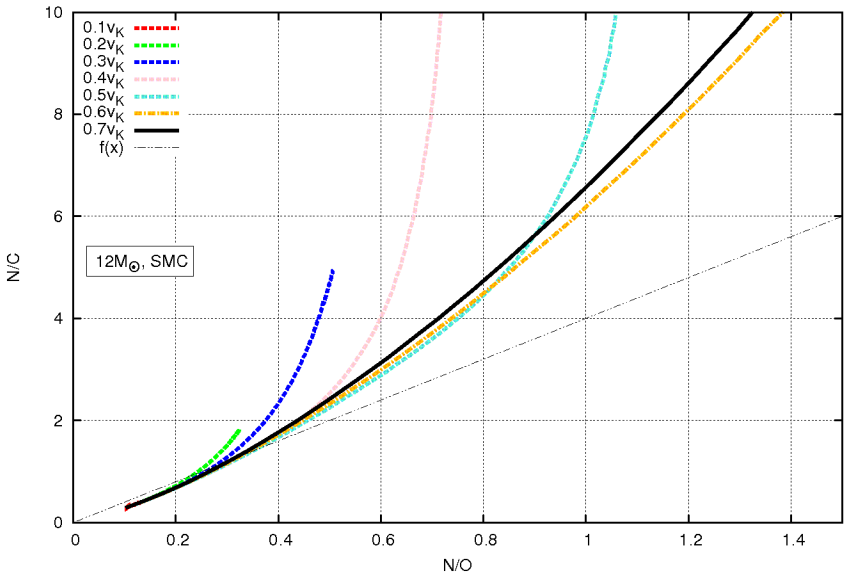

Figure 4.4: Example to the examination of the CNO-abundances in stars with $12M_{\odot}$, $Z = 0.004$ and different f_K as the ratios $\frac{N}{C}$ against $\frac{N}{O}$. The function $f(x)$ is a straight line with slope 4.

In stellar models with higher masses the range in which the curves in the $\frac{N}{C}$ - $\frac{N}{O}$ plot proceed with the expected slope becomes larger. The curves of the non-homogeneous evolution show a shallower developing with higher masses, compare fig. A.116 to A.119. In figure 4.5 an example of a stellar model with $25M_{\odot}$ can be seen, in which the homogeneously evolving models adapt very well to the straight line $f(x)$, now in the initial area. From about 0.1 to 0.6 of the mass fractions of $\frac{N}{O}$ and from 0 to about 2 of the mass fractions of $\frac{N}{C}$ the homogeneous evolution tracks proceed with a slope of 4. With higher mass, the homogeneously evolving stars consequently correspond better to the theoretical considerations of section 1.2. Moreover one notes that the homogeneous evolution tracks with low rotation rates from a

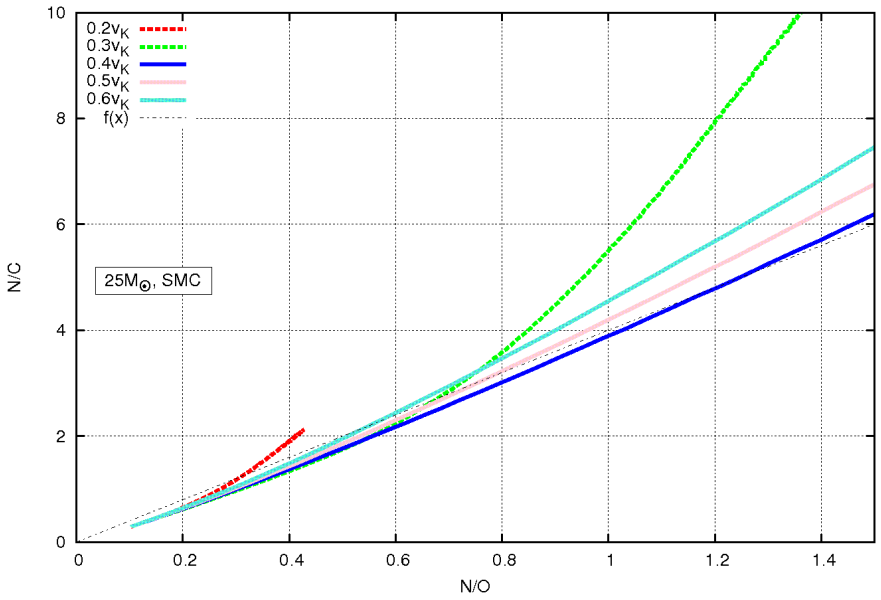

Figure 4.5: Example to the examination of the CNO-abundances in stars with $25M_{\odot}$, $Z = 0.004$ and different f_K as the ratios $\frac{N}{C}$ against $\frac{N}{O}$. The function $f(x)$ is a straight line with slope 4.

certain abundance ratio always have a smaller slope and those with high rotation rates have a slope greater than 4. During the proceeding CN-cycle faster rotating homogeneous stars, therefore, show a higher ratio $\frac{N}{C}$ and $\frac{N}{O}$. A clear example of this is visible in figure 4.6.

Overall, it can be stated that the chemically homogeneously evolving stars with a low nitrogen enrichment at the surface, as expected, behave in the manner of the CN-cycle. The higher the fractions of $\frac{N}{C}$ and $\frac{N}{O}$, the higher the deviation from the straight line $f(x)$. This is mainly caused by the fact that the relative abundance of oxygen stays constant only in a small span of time. The considerations from section 1.2 and, consequently, the equation 1.17 are not valid for $dO \neq 0$ anymore.

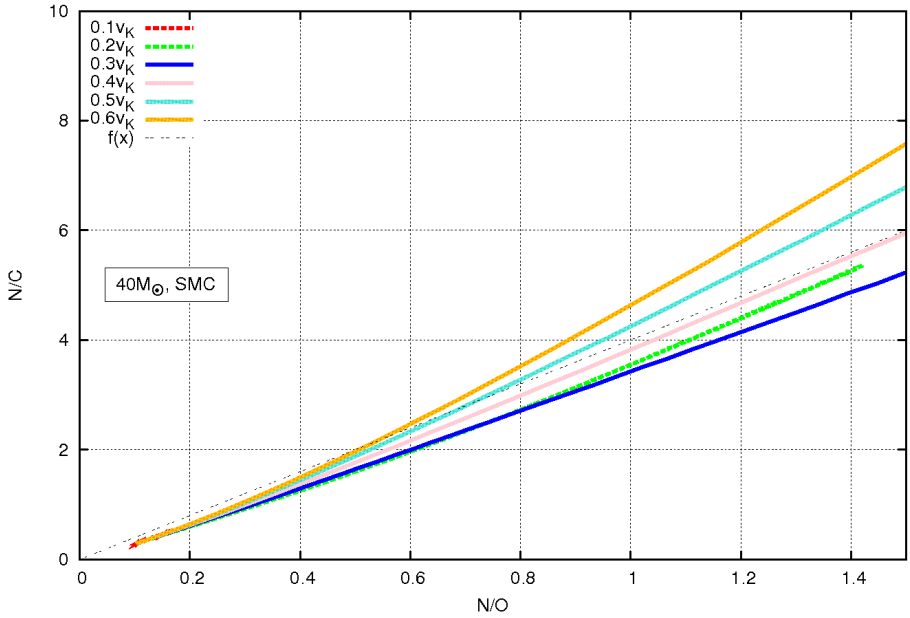

Figure 4.6: Example to the examination of the CNO-abundances in stars with $40M_{\odot}$, $Z = 0.004$ and different f_K as the ratios $\frac{N}{C}$ against $\frac{N}{O}$. The function $f(x)$ is a straight line with slope 4.

4.1.4 Fluorine

In examination of the element fluorine, clear differences for all masses and metallicities between the homogeneous and non-homogeneous evolution in the abundance-time plot are discovered, similar to oxygen. For low rotational velocities, the surface abundance decreases only slightly, whereas for high velocities, existing from an early point in time, an enormous decrease of fluorine is observed. This can be explained by the reactions with oxygen in the CNO-cycle, which quickly transform and therefore "destroy" fluorine in a completely mixed star. In the diagrams, as for example in figure 4.7, it is visible, that the surface abundance of fluorine decreases down to about 10^{-6} times the initial value. The higher the rotation rate, the faster the decrease proceeds. The very low abundance value is very difficult to detect in observations. Thus, it can be assumed that if there is no fluorine present in a star, complete mixing has happened and the star can be identified as chemically homogeneous. In non-homogeneously evolving stars at the surface at low temperatures, at which the CNO-cycle does not proceed, fluorine is able to sort of "survive". The consideration of the "Wolf-Rayet threshold" is not necessary, because at the point in time of the threshold the surface abundance of fluorine mostly already lies below 0.0001 times the initial value, which is comparable low to 10^{-6}.

For the SMC-metallicity, the limit for the recognition of the homogeneous evolution, the abundance value divided by the initial value, results in 0.01. If one examines the stellar models of the masses 12, 16 and 60$M_\odot$, as described for oxygen, via the "dex-criterion" between the partially homogeneous and non-homogeneous evolution tracks, the overall limit results in 0.1.

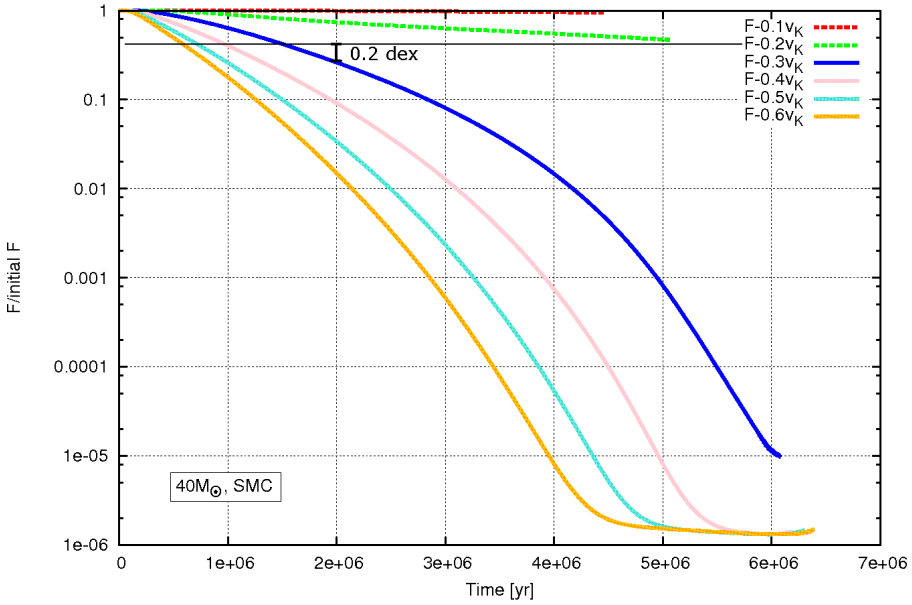

Figure 4.7: Example of an abundance-time diagram of fluorine for stars with 40$M_\odot$, $Z = 0.004$ and different rotation rates, in which the "dex-criterion" is fulfilled already from an abundance value of about 0.3 times the initial value on and at the point of $2 \cdot 10^6$ years.

4.1.5 Sodium

The abundance of sodium at the star's surface behaves differently depending on the metallicity of the star, compare fig. A.144 to A.155 in the appendix A.1. A sample examination of the metallicity dependence is performed for magnesium in section 4.2. In the abundance-time diagrams of the metallicity $Z = 0.004$, see an example in figure 4.8, one sees that the chemically homogeneously evolving stars enrich much more sodium at the surface than non-homogeneously evolving stars. The non-homogeneous stellar models show an increase of the surface abundance up to about 2 times the initial value. From early on, especially for the stellar models with low masses, the enrichment values subsequently do not change for the rest of the main sequence phase. The higher the rotation rate, the higher the value of enrichment. The behaviour can be described directly by the NeNa-cycle, in which neon is effectively transformed to sodium.

In the analysis of the sodium abundance at the stellar surface, the difference in the examination of the "dex-criterion" between partially homogeneous and homogeneous or partially homogeneous and non-homogeneous evolution tracks stands out. If one wants to obtain a distinction between partially and completely homogeneous evolution out of the abundance-time

diagrams, sodium is only eligible for this in the stellar models with 25 and 40$M_\odot$ of the SMC-metallicity. In the remaining models either the "dex-criterion" itself is not fulfilled or it is only fulfilled after the "Wolf-Rayet threshold", because the partially homogeneously evolving stars behave too similarly to the homogeneously evolving ones. If one regards the differentiation between non-homogeneous and partially homogeneous evolution in the abundance-time plots, a completely different result yields. In this case all stellar models of the metallicity $Z = 0.004$ are eligible for the recognition of partially and completely homogeneously evolving stars. Moreover there is no interference by the "Wolf-Rayet threshold".
In figure 4.8 an example is visible, in which the difference between the above described considerations become apparent.

In general, which means also in the special consideration of the partially homogeneous evolution, it results that sodium serves as a recognition method for chemically homogeneous stars between surface abundances of about 3 to 4.5 times the initial value. The upper limit occurs by the "Wolf-Rayet threshold".

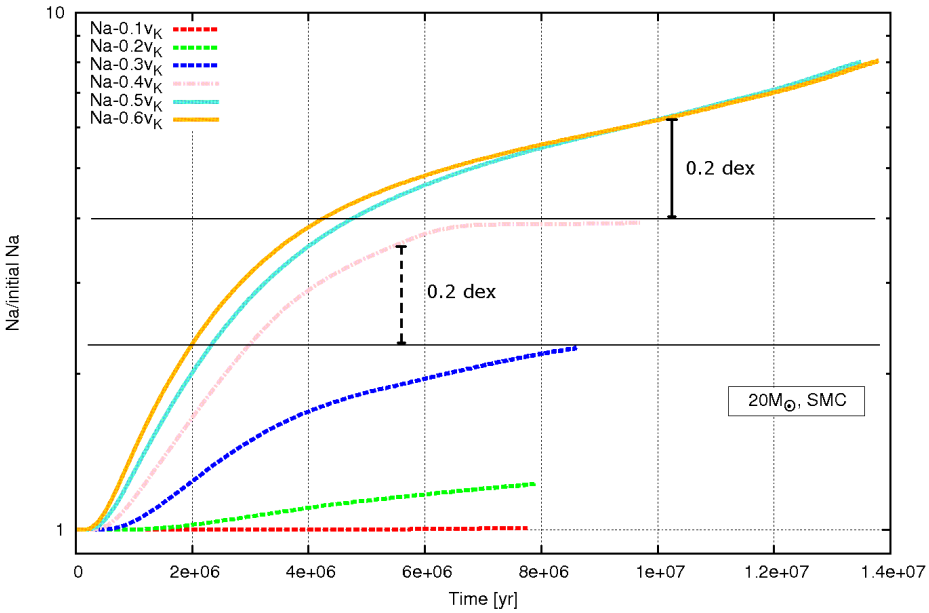

Figure 4.8: Example of an abundance-time diagram of sodium for stars with 20$M_\odot$, $Z = 0.004$ and different rotation rates, in which the "dex-criterion" is fulfilled dependening on the position. In the differentiation between the partially and completely homogeneous evolution tracks the criterion is fulfilled slightly before the point in time of the "Wolf-Rayet threshold" of about $1.1 \cdot 10^7$ years at an abundance value of about 4 times the initial value (continuous dex-bar). In the differentiation between the non-homogeneous and partially homogeneous tracks the criterion is fulfilled at slightly more than about 2 times the initial value and well before the point in time of the "Wolf-Rayet threshold". (dashed dex-bar).

4.1.6 Aluminium

The developing in the abundance-time plot of aluminium looks similar to the one of sodium. Aluminium shows the metallicity dependent behaviour as well, which can be viewed in figures A.175 to A.186 in the appendix A.1. The similar progress to sodium is caused by the equivalent development of the NeNa- and MgAl-cycles, which are visible at the surface in the homogeneous evolution. Here magnesium is transformed into aluminium, so that the relative abundance at the surface of aluminium increases, whereas the one of magnesium decreases. Furthermore, a similar limited eligibility as a recognition method for completely homogeneous evolution, as with sodium, results due to the "Wolf-Rayet threshold". In all abundance-time diagrams the "dex-criterion" is fulfilled shortly before or after the threshold, compare figure 4.9. For aluminium, it further arises that the "dex-criterion" is not fulfilled in the test between partially homogeneous and non-homogeneous evolution tracks.

In general, a chemically homogeneously evolving star with the metallicity $Z = 0.004$ can be badly recognised with the help of the surface abundance of aluminium, because the observed abundance can also be caused by the exposed core of a Wolf-Rayet star.

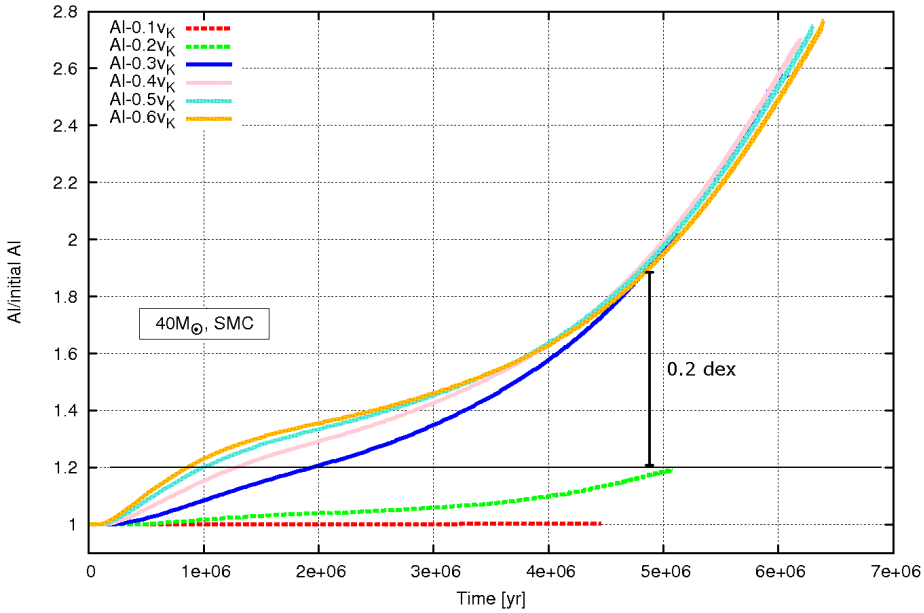

Figure 4.9: Example of an abundance-time diagram of aluminium for stars with $40M_\odot$, $Z = 0.004$ and different rotation rates, in which the "dex-criterion" is fulfilled slightly before the point in time of the "Wolf-Rayet threshold" of about $5 \cdot 10^6$ years from an abundance value of about 1.9 times the initial value on.

4.2 Detailed examination of the metallicity dependence

In this section the metallicity-dependent behaviour of the elements neon, sodium, magnesium and aluminium is further discussed. Generally, one can already note that the different progress of the surface abundances of neon, sodium and aluminium, especially in homogeneously evolving stars, is probably caused by temperature differences at different metallicities. The lower the metallicity, the higher the temperature in the stellar interior where the nucleosynthesis happens, refer to section 1.2 for an explanation. Therefore, the reactions which lead to the creation of sodium and aluminium, proceed faster in stars with the metallicity of $Z = 10^{-5}$ than in ones with $Z = 0.004$ and reach after a short time in the main sequence phase the maximal abundance of the elements at the surface, compare fig. A.151 to A.155 and fig. A.182 to A.186. The abundance of sodium and aluminium reaches the highest values at the lowest metallicity. After the maximum abundance at the surface in stars with $Z = 10^{-5}$ drops in the residue time of the main sequence phase back down to the initial abundance value or lower. In this period of time, one notices a slight increase of the surface abundance in the abundance-time plots of neon, which reach lower values in the stellar models with the lowest metallicities than in those with higher metallicities.

The metallicity-dependent development of the surface abundances of neon, sodium and aluminium thus can be explained by the knowledge of the nuclear reactions in stars. The surface abundance of magnesium presents in the stellar models of the metallicity $Z = 10^{-5}$ and the masses 16 to $40M_{\odot}$ an unexpected behaviour, which has been described in section 3.2 with the help of 3.7. Interestingly, the abundance of magnesium decreases strongly after the maximum, which originates out of the transformation of sodium to magnesium, because the NeNa- and MgAl-cycles interact with each other. In the stellar models with $Z = 10^{-5}$ the magnesium abundance at the surface also decreases a little at the beginning of the main sequence phase and increases strongly after about $2 \cdot 10^6$ years and sinks after a short time down to almost zero. To be able to identify the metallicity at which this behaviour occurs, further abundance-time diagrams of the metallicity $Z = 10^{-3}$ are examined. The classification of the evolutionary tracks in the diagrams shown in appendix A.2 has been created as well as for the other metallicities with the help of the Hertzsprung-Russel diagrams, which are visible in fig. A.13 to A.19 in appendix A.1.

In the following the stellar models with two different masses, $20M_{\odot}$ and $40M_{\odot}$, the metallicities $Z = 0,004$, 10^{-3} and 10^{-5} and different rotation rates are compared.

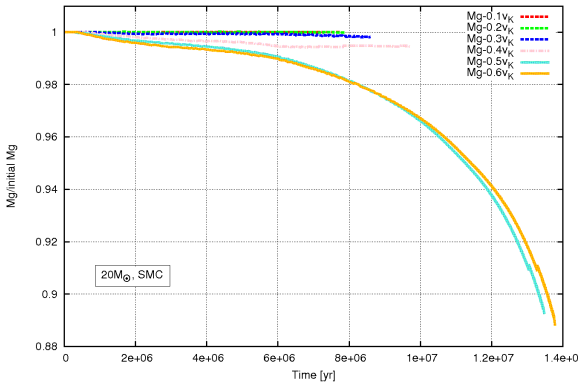

Figure 4.10: Example to the element abundance of magnesium at the surface as a function of time in stars with $20M_\odot$, $Z = 0.004$ and different f_K.

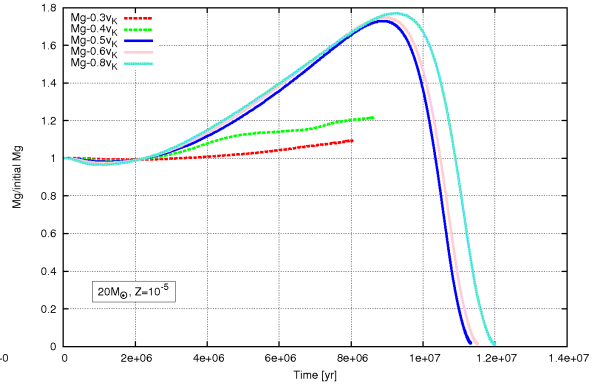

Figure 4.11: Example to the element abundance of magnesium at the surface as a function of time in stars with $20M_\odot$, $Z = 10^{-5}$ and different f_K.

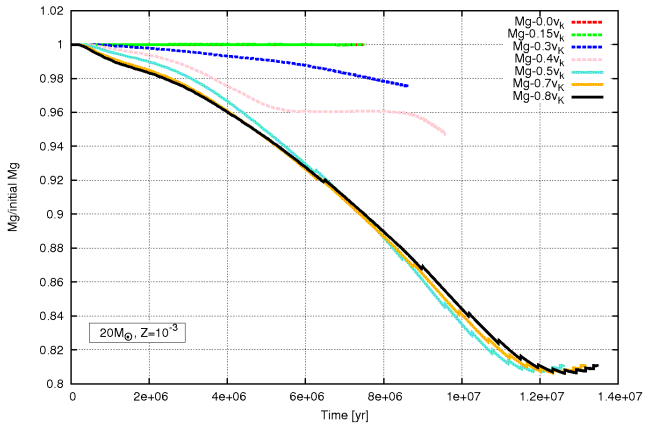

Figure 4.12: Example to the element abundance of magnesium at the surface as a function of time in stars with $20M_\odot$, $Z = 10^{-3}$ and different f_K.

In the above figures 4.10 to 4.12 of the stellar models with $20M_\odot$ one notices that, at the metallicity $Z = 10^{-3}$, there is no increase in magnesium abundance at the surface. The values of which the abundance sinks, are in a similar range as in the abundance-time plots with $Z = 0.004$, up to 0.8 times of the initial value for the homogeneously evolving stars. However, the developing of the curves of the homogeneously evolving stars with $Z = 10^{-3}$ appears slightly different than the ones in the abundance-time plot with $Z = 0.004$. At the end of the main sequence phase, a slight increase of the magnesium abundance arises, similar to the diagrams of neon of the metallicity $Z = 10^{-5}$, compare A.139 bis A.143. This behaviour arises from the stellar models with $16M_\odot$ and $Z = 10^{-3}$.
In the following stellar models of the figures 4.13 to 4.15 with $40M_\odot$, one sees the same behaviour in dependence on the metallicity. The minimal abundance in the abundance-time diagrams with $Z = 10^{-3}$ is reached earlier with higher mass.

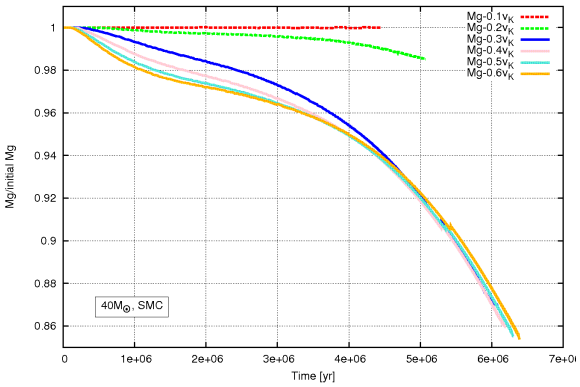

Figure 4.13: Example to the element abundance of magnesium at the surface as a function of time in stars with $40M_\odot$, $Z = 0.004$ and different f_K.

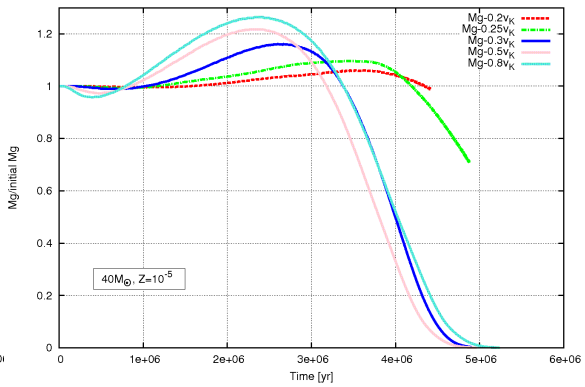

Figure 4.14: Example to the element abundance of magnesium at the surface as a function of time in stars with $40M_\odot$, $Z = 10^{-5}$ and different f_K.

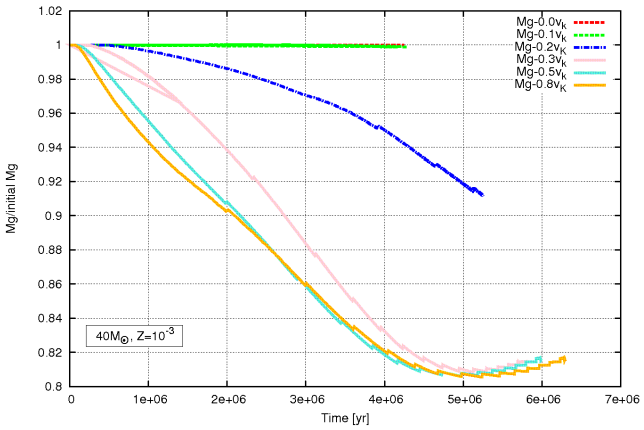

Figure 4.15: Example to the element abundance of magnesium at the surface as a function of time in stars with $40M_\odot$, $Z = 10^{-3}$ and different f_K.

The unexpected behaviour of the magnesium abundance at the stellar surface at the metallicity $Z = 10^{-5}$ thus begins at a metallicity which is lower than $Z = 10^{-3}$. Further investigations are necessary to understand the interaction between time and the progression of magnesium surface abundance in very metal-poor stars.

5 Results

In this bachelor thesis a detailed analysis of the surface abundances of various elements in different stellar models with various masses, metallicities and rotation rates in the main sequence phase has been performed.
In the process it generally resulted, that the behaviour of the element abundances at the surface due to rotationally induced homogeneity for the most part can be well explained by the known nuclear reactions in massive main sequence stars. But, in addition, unexpected and not directly explainable progressions of the element abundances also occurred. This concerns the elements lithium, beryllium, boron and magnesium. Possible explanations for the unusual changes in the surface abundances, especially regarding the metallicity dependence of magnesium are briefly discussed. It is necessary to perform more detailed examinations of these elements in further papers.

The results show that oxygen and fluorine are the best elements for distinguishing the chemical homogeneity in massive main sequence stars. With the help of the surface abundance of those elements in all examined stellar models, partially and completely homogeneous evolution can even be distinguished. The "dex-criterion", described in section 3.1, is fulfilled by oxygen and fluorine in each stellar model, which means, that the results are applicable within a measurement error of 0.2 dex, which mainly occurs in observations. A recognition of chemically homogeneous evolution is possible with the surface abundance of oxygen and fluorine independent of the stellar mass and metallicity, which is important if one does not know the mass or metal content of the observed star.
Section 3.2 described the phenomenon of Wolf-Rayet stars, which can limit the eligibility of an element for the recognition of chemical homogeneity, only needs to be mildly considered for these elements. The "dex-criterion" is fulfilled at a much earlier point in time than the point of the "Wolf-Rayet threshold". This threshold is determined with the help of the point in time at which the hydrogen abundance at the stellar surface is below a mass fraction of 40%.
The analysis also showed, that for oxygen, a star could be clearly identified as chemically homogeneous as soon as the surface abundance lies below 0.05 times the initial value. For fluorine, this is obtained below 0.006 times the initial value. This means, that fluorine, in principle, disappears in chemically homogeneously evolving stars.
In a more detailed analysis regarding the distinction of partially and completely homogeneously evolving stars, see section 4.1.3, slightly different thresholds of the surface abundance for the recognition of chemical homogeneity with the help of oxygen and fluorine were obtained. The main conclusion, how well both elements are suited for the recognition, is not changed by this.

The context of partially homogeneously evolving stars behaves differently in the abundance-time diagrams of sodium and aluminium. In the case of the surface abundance of sodium, a distinction between partially homogeneous and non-homogeneous evolution with the help of the "dex-criterion" works better than between homogeneous and partially homogeneous evolution.

For aluminium as a recognition feature, it is difficult to make the distinction between homogeneous and partially homogeneous evolution and even more difficult to distinguish between partially homogeneous and non-homogeneous evolution. If the “dex-criterion” is fulfilled, the point in time lies too close or even beyond the point of the “Wolf-Rayet threshold”.

The eligibility of the elements examined in this thesis for the recognition of chemical homogeneity is often limited, as already described, due to the similarity of the surface abundances of homogeneously evolving to those of Wolf-Rayet stars. Results show that the “Wolf-Rayet threshold” is of particular concern to the elements hydrogen, helium, sodium and aluminium.

Finally, the analysis of each stellar model shows that the elements carbon, nitrogen, neon and magnesium cannot be recommended in any case as a recognition method for chemically homogeneous stars.

6 Summary

In summary one can say, that out of this bachelor thesis the two elements oxygen and fluorine resulted as the best recognition method for chemical homogeneity, which are eligible for all masses and metallicities and are therefore well applicable for observations. Moreover, there have excelled phenomenons, which challenge the further understanding of the theory of chemically homogeneous evolution. On the one hand, this is the metallicity dependence of the elements neon, sodium, aluminium and especially magnesium and, on the other hand, the detailed examination of partially chemically homogeneously evolving stars. Hence it is now necessary to verify the results of this bachelor thesis by observations and to gain new knowledge regarding the chemically homogeneous evolution of massive main sequence stars.

A Appendix

A.1 Figures

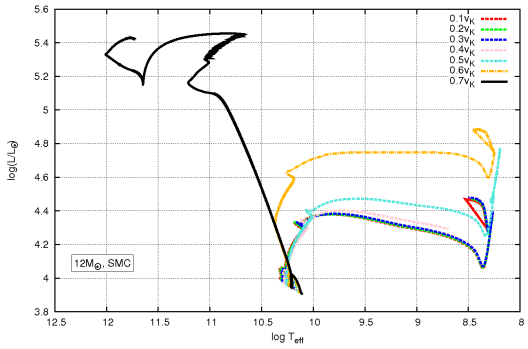

Figure A.1: HRD for stellar models with $M = 12M_{\odot}$, $Z = 0.004$ and different f_K.

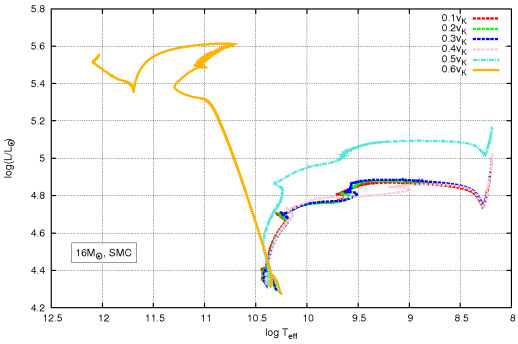

Figure A.2: HRD for stellar models with $M = 16M_{\odot}$, $Z = 0.004$ and different f_K.

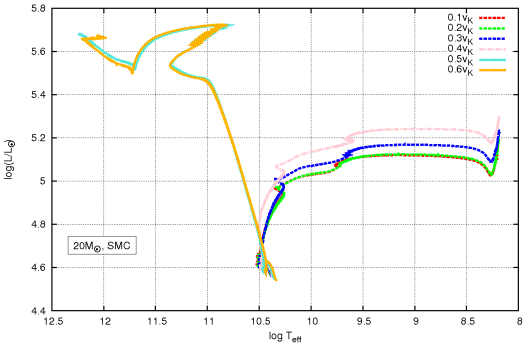

Figure A.3: HRD for stellar models with $M = 20M_{\odot}$, $Z = 0.004$ and different f_K.

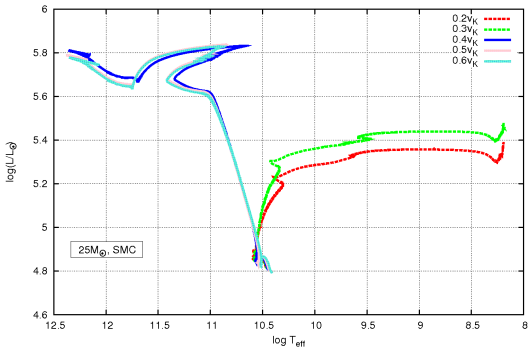

Figure A.4: HRD for stellar models with $M = 25M_{\odot}$, $Z = 0.004$ and different f_K.

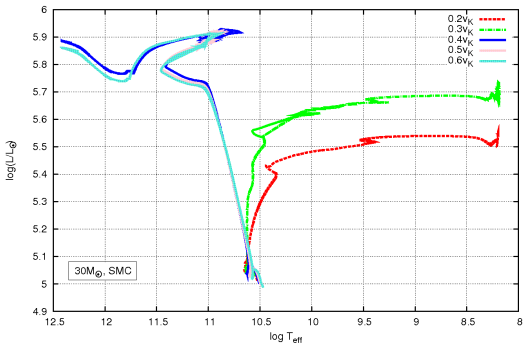

Figure A.5: HRD for stellar models with $M = 30M_{\odot}$, $Z = 0.004$ and different f_K.

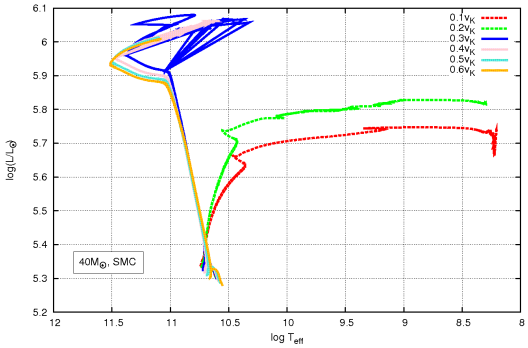

Figure A.6: HRD for stellar models with $M = 40M_{\odot}$, $Z = 0.004$ and different f_K.

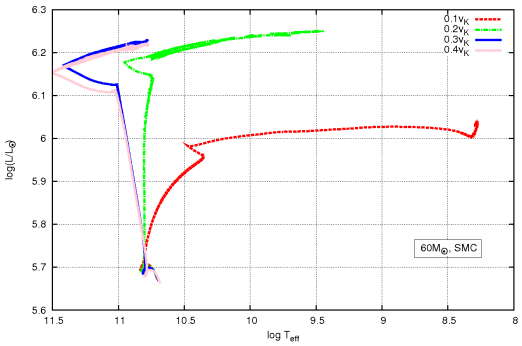

Figure A.7: HRD for stellar models with $M = 60M_{\odot}$, $Z = 0.004$ and different f_K.

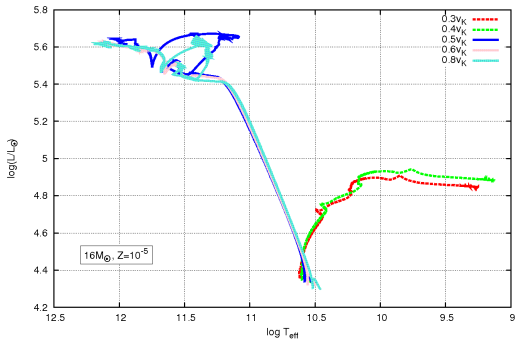

Figure A.8: HRD for stellar models with $M = 16M_{\odot}$, $Z = 10^{-5}$ and different f_K.

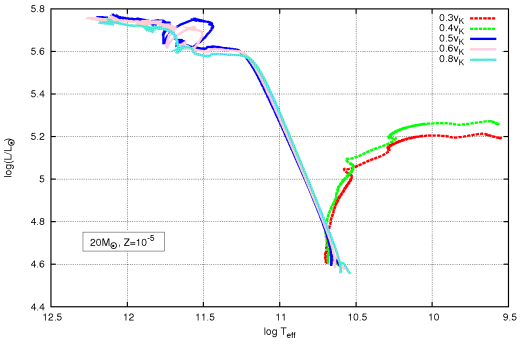

Figure A.9: HRD for stellar models with $M = 20M_{\odot}$, $Z = 10^{-5}$ and different f_K.

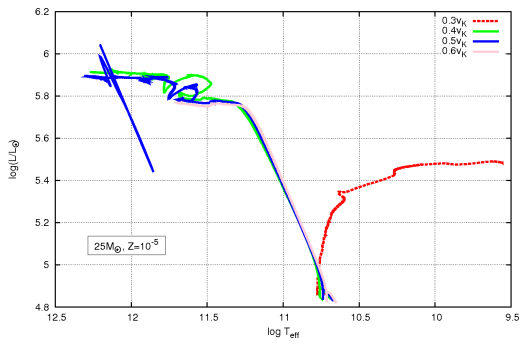

Figure A.10: HRD for stellar models with $M = 25M_{\odot}$, $Z = 10^{-5}$ and different f_K.

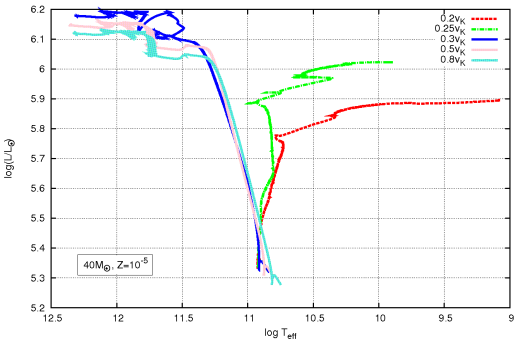

Figure A.11: HRD for stellar models with $M = 40M_{\odot}$, $Z = 10^{-5}$ and different f_K.

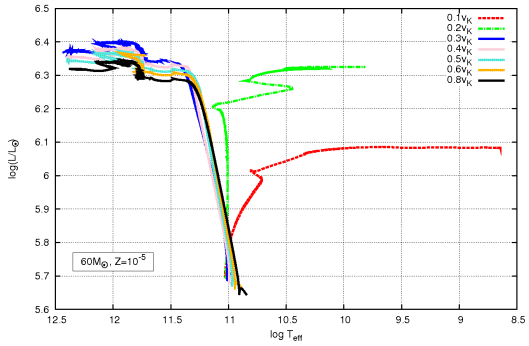

Figure A.12: HRD for stellar models with $M = 60M_{\odot}$, $Z = 10^{-5}$ and different f_K.

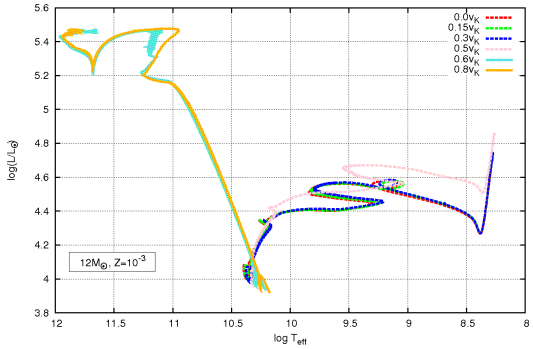

Figure A.13: HRD for stellar models with $M = 12M_{\odot}$, $Z = 10^{-3}$ and different f_K.

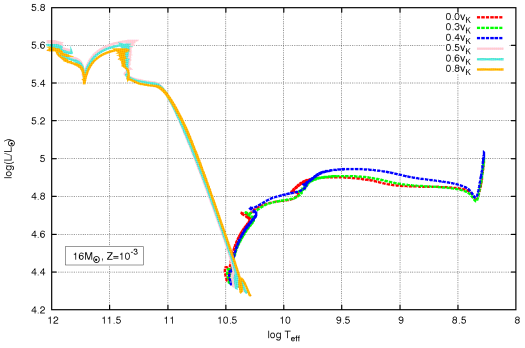

Figure A.14: HRD for stellar models with $M = 16M_{\odot}$, $Z = 10^{-3}$ and different f_K.

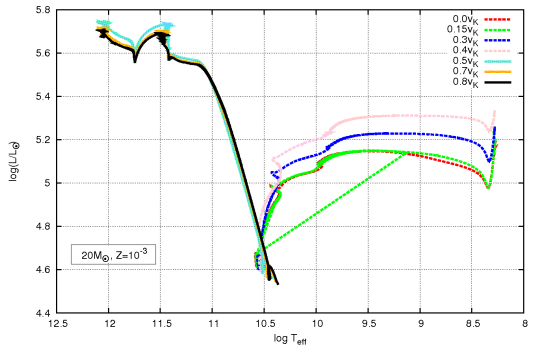

Figure A.15: HRD for stellar models with $M = 20M_{\odot}$, $Z = 10^{-3}$ and different f_K.

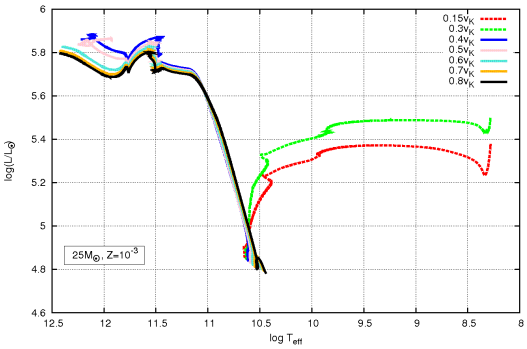

Figure A.16: HRD for stellar models with $M = 25M_{\odot}$, $Z = 10^{-3}$ and different f_K.

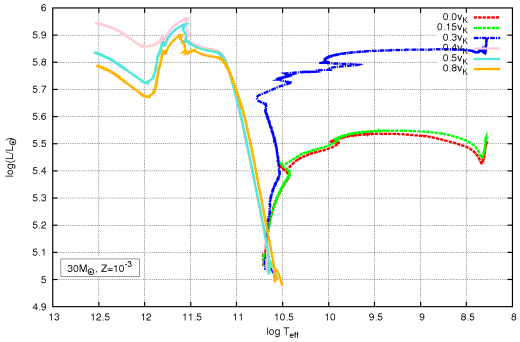

Figure A.17: HRD for stellar models with $\mathrm{M} = 30\mathrm{M}_{\odot}$, $Z = 10^{-3}$ and different f_K.

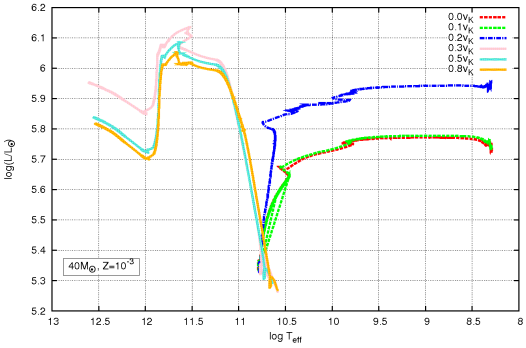

Figure A.18: HRD for stellar models with $\mathrm{M} = 40\mathrm{M}_{\odot}$, $Z = 10^{-3}$ and different f_K.

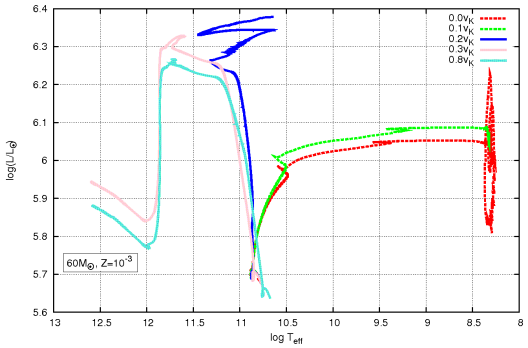

Figure A.19: HRD for stellar models with $\mathrm{M} = 60\mathrm{M}_{\odot}$, $Z = 10^{-3}$ and different f_K.

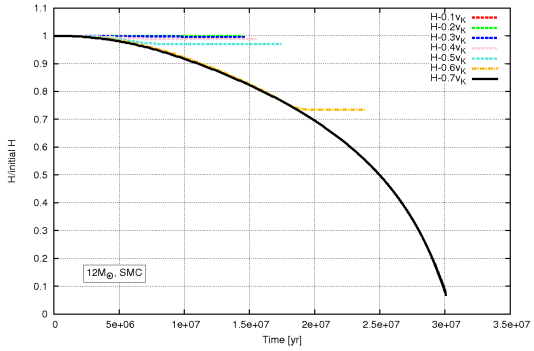

Figure A.20: Mass fraction divided by the initial value of hydrogen as a function of time for stars with $M = 12M_\odot$, $Z = 0.004$ and different f_K.

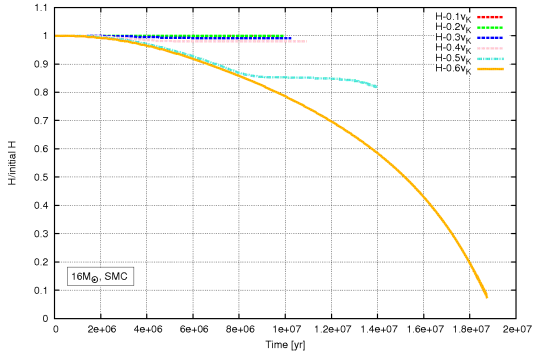

Figure A.21: Mass fraction divided by the initial value of hydrogen as a function of time for stars with $M = 16M_\odot$, $Z = 0.004$ and different f_K.

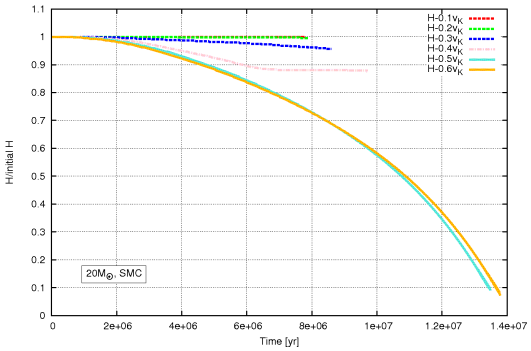

Figure A.22: Mass fraction divided by the initial value of hydrogen as a function of time for stars with $M = 20M_\odot$, $Z = 0.004$ and different f_K.

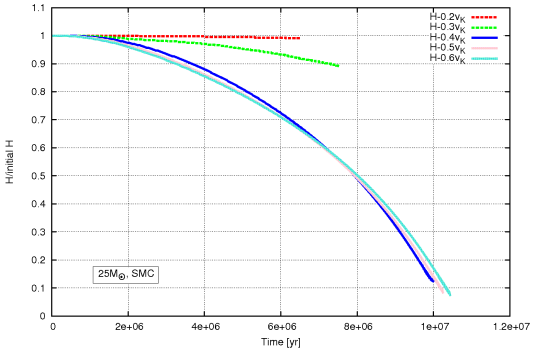

Figure A.23: Mass fraction divided by the initial value of hydrogen as a function of time for stars with $M = 25M_\odot$, $Z = 0.004$ and different f_K.

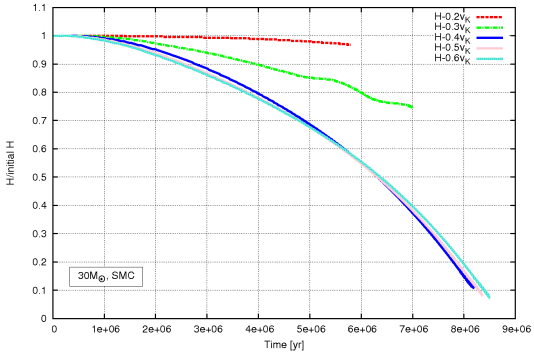

Figure A.24: Mass fraction divided by the initial value of hydrogen as a function of time for stars with $M = 30M_\odot$, $Z = 0.004$ and different f_K.

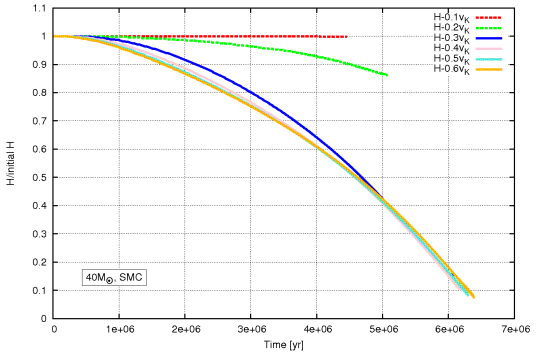

Figure A.25: Mass fraction divided by the initial value of hydrogen as a function of time for stars with $M = 40M_\odot$, $Z = 0.004$ and different f_K.

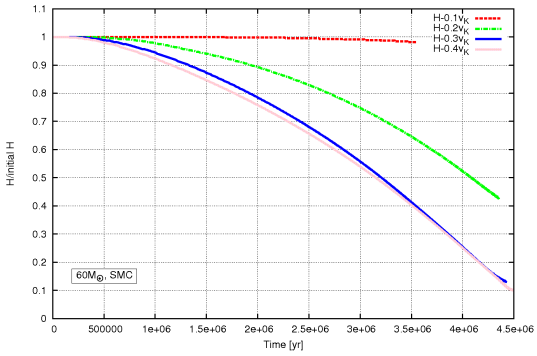

Figure A.26: Mass fraction divided by the initial value of hydrogen as a function of time for stars with $M = 60M_{\odot}$, $Z = 0.004$ and different f_K.

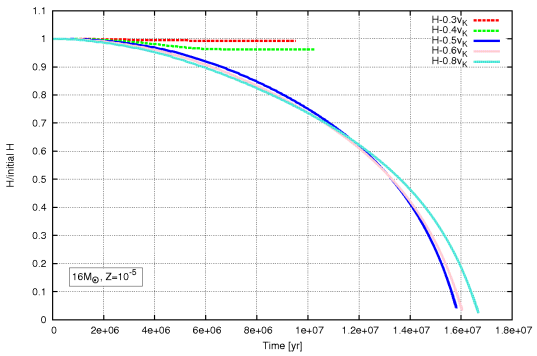

Figure A.27: Mass fraction divided by the initial value of hydrogen as a function of time for stars with $M = 16M_{\odot}$, $Z = 10^{-5}$ and different f_K.

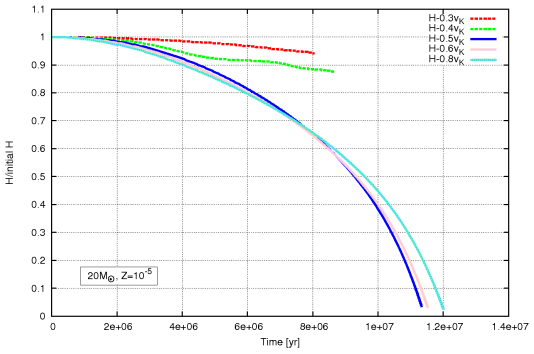

Figure A.28: Mass fraction divided by the initial value of hydrogen as a function of time for stars with $M = 20M_{\odot}$, $Z = 10^{-5}$ and different f_K.

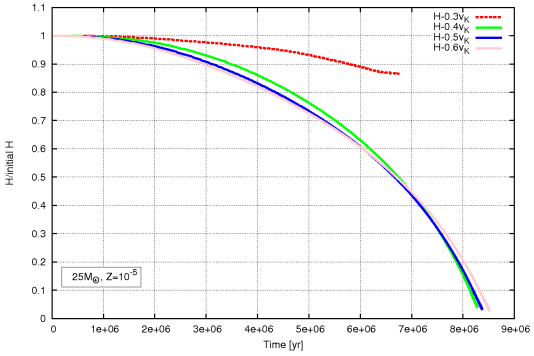

Figure A.29: Mass fraction divided by the initial value of hydrogen as a function of time for stars with $M = 25M_{\odot}$, $Z = 10^{-5}$ and different f_K.

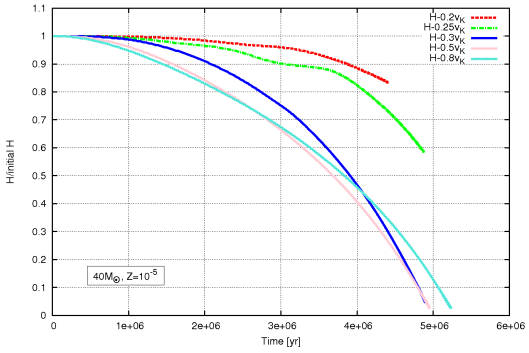

Figure A.30: Mass fraction divided by the initial value of hydrogen as a function of time for stars with $M = 40M_{\odot}$, $Z = 10^{-5}$ and different f_K.

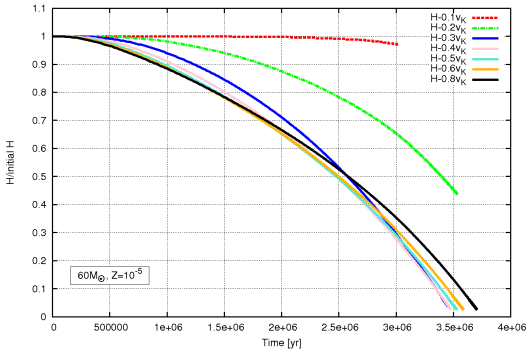

Figure A.31: Mass fraction divided by the initial value of hydrogen as a function of time for stars with $M = 60M_{\odot}$, $Z = 10^{-5}$ and different f_K.

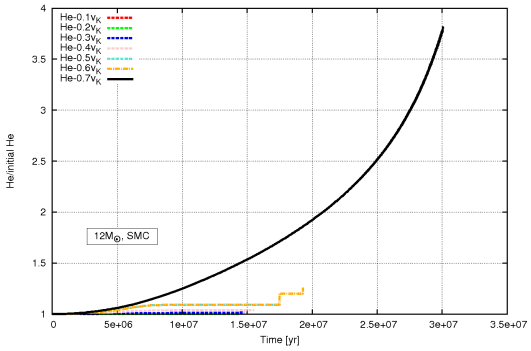

Figure A.32: Mass fraction divided by the initial value of helium as a function of time for stars with $M = 12M_{\odot}$, $Z = 0.004$ and different f_K.

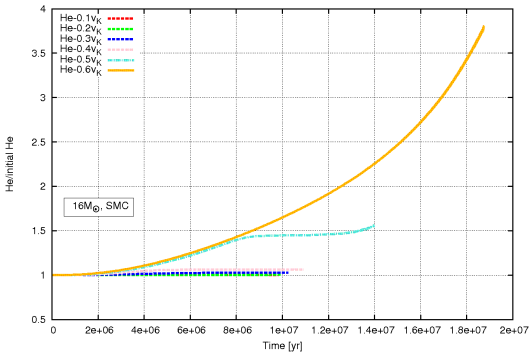

Figure A.33: Mass fraction divided by the initial value of helium as a function of time for stars with $M = 16M_{\odot}$, $Z = 0.004$ and different f_K.

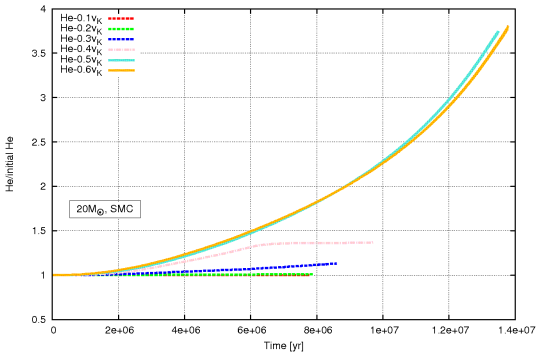

Figure A.34: Mass fraction divided by the initial value of helium as a function of time for stars with $M = 20M_{\odot}$, $Z = 0.004$ and different f_K.

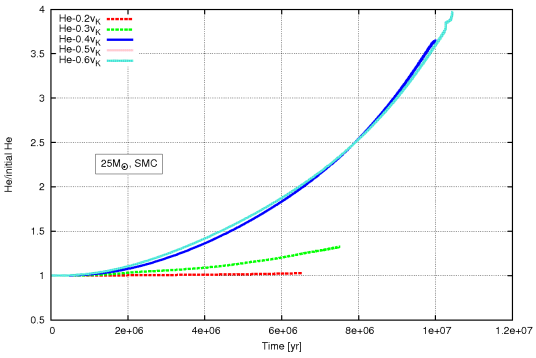

Figure A.35: Mass fraction divided by the initial value of helium as a function of time for stars with $M = 25M_{\odot}$, $Z = 0.004$ and different f_K.

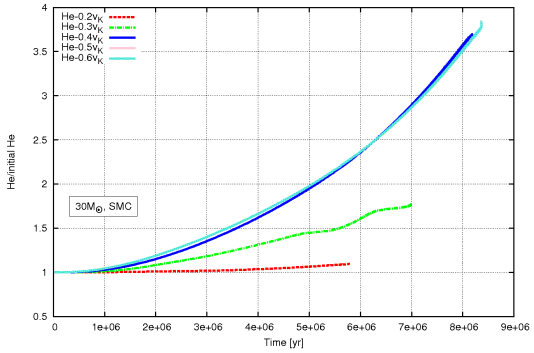

Figure A.36: Mass fraction divided by the initial value of helium as a function of time for stars with $M = 30M_{\odot}$, $Z = 0.004$ and different f_K.

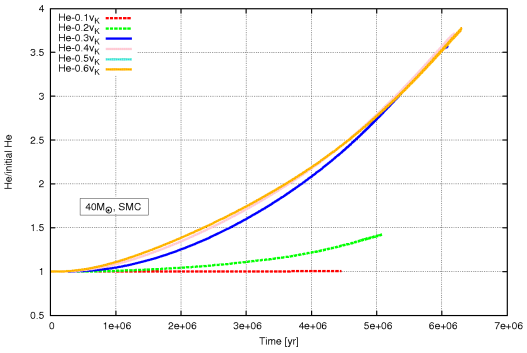

Figure A.37: Mass fraction divided by the initial value of helium as a function of time for stars with $M = 40M_{\odot}$, $Z = 0.004$ and different f_K.

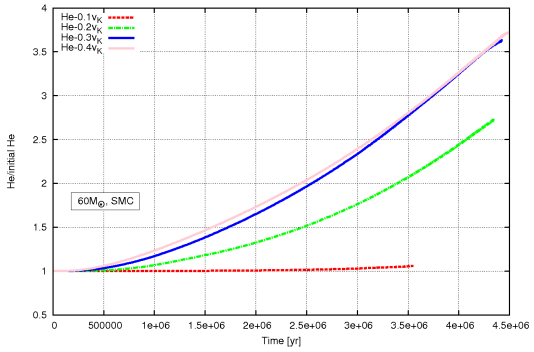

Figure A.38: Mass fraction divided by the initial value of helium as a function of time for stars with $M = 60M_{\odot}$, $Z = 0.004$ and different f_K.

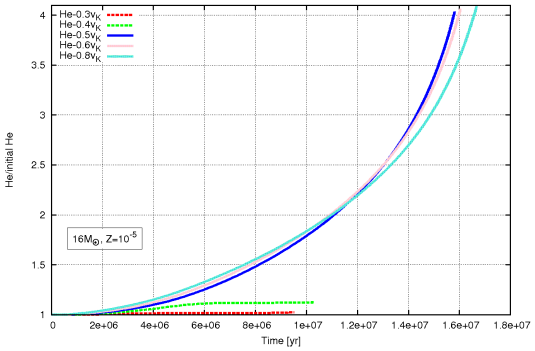

Figure A.39: Mass fraction divided by the initial value of helium as a function of time for stars with $M = 16M_{\odot}$, $Z = 10^{-5}$ and different f_K.

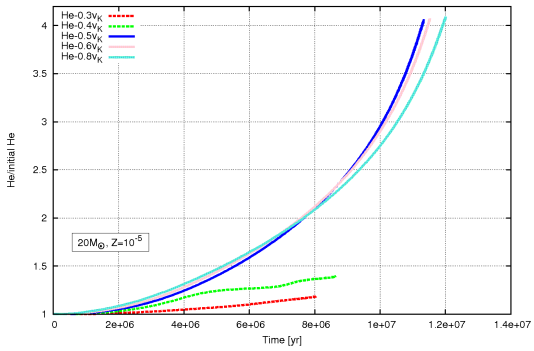

Figure A.40: Mass fraction divided by the initial value of helium as a function of time for stars with $M = 20M_{\odot}$, $Z = 10^{-5}$ and different f_K.

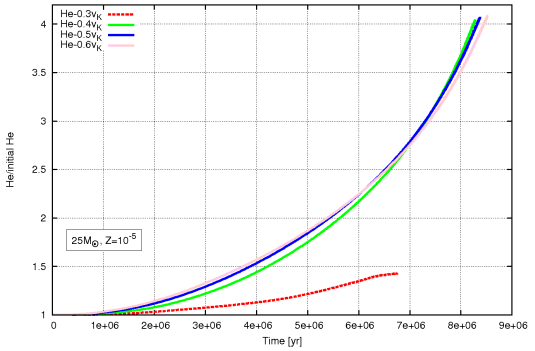

Figure A.41: Mass fraction divided by the initial value of helium as a function of time for stars with $M = 25M_{\odot}$, $Z = 10^{-5}$ and different f_K.

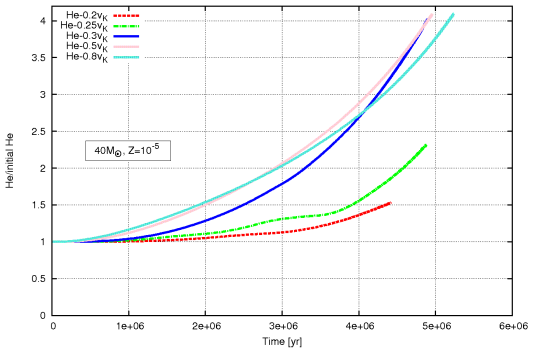

Figure A.42: Mass fraction divided by the initial value of helium as a function of time for stars with $M = 40M_{\odot}$, $Z = 10^{-5}$ and different f_K.

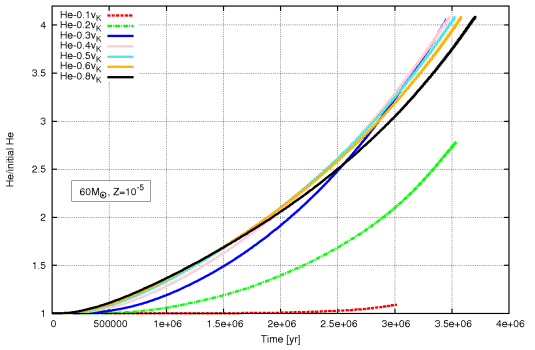

Figure A.43: Mass fraction divided by the initial value of helium as a function of time for stars with $M = 60M_{\odot}$, $Z = 10^{-5}$ and different f_K.

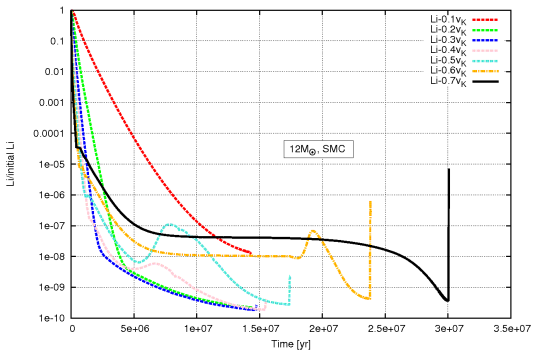

Figure A.44: Mass fraction divided by the initial value of lithium as a function of time for stars with $M = 12M_{\odot}$, $Z = 0.004$ and different f_K.

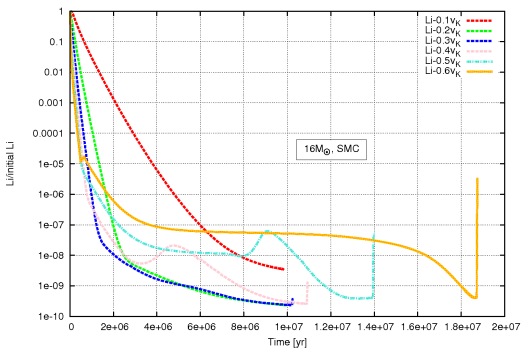

Figure A.45: Mass fraction divided by the initial value of lithium as a function of time for stars with $M = 16M_{\odot}$, $Z = 0.004$ and different f_K.

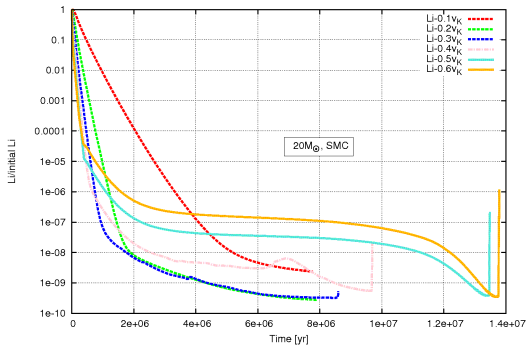

Figure A.46: Mass fraction divided by the initial value of lithium as a function of time for stars with $M = 20M_{\odot}$, $Z = 0.004$ and different f_K.

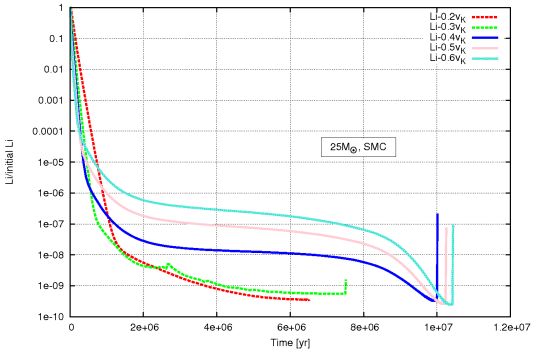

Figure A.47: Mass fraction divided by the initial value of lithium as a function of time for stars with $M = 25M_{\odot}$, $Z = 0.004$ and different f_K.

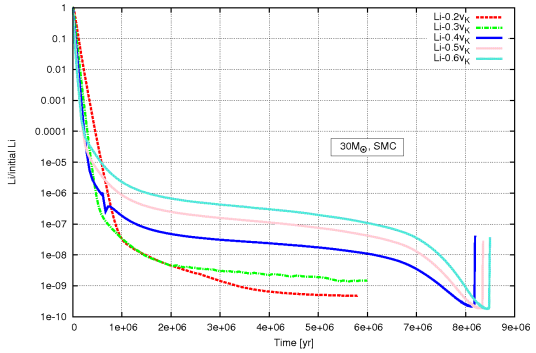

Figure A.48: Mass fraction divided by the initial value of lithium as a function of time for stars with $M = 30M_{\odot}$, $Z = 0.004$ and different f_K.

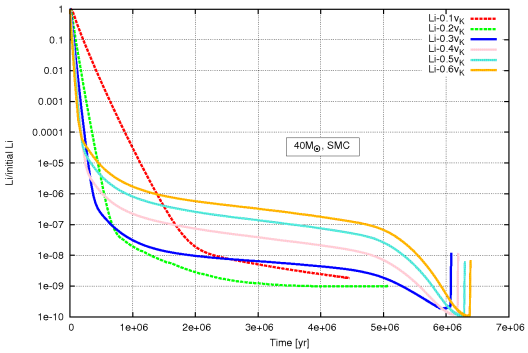

Figure A.49: Mass fraction divided by the initial value of lithium as a function of time for stars with $M = 40M_{\odot}$, $Z = 0.004$ and different f_K.

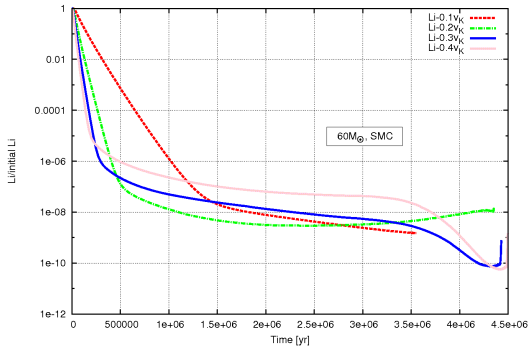

Figure A.50: Mass fraction divided by the initial value of lithium as a function of time for stars with $M = 60M_{\odot}$, $Z = 0.004$ and different f_K.

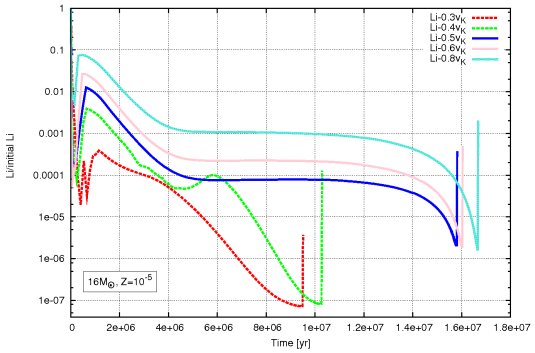

Figure A.51: Mass fraction divided by the initial value of lithium as a function of time for stars with $M = 16M_{\odot}$, $Z = 10^{-5}$ and different f_K.

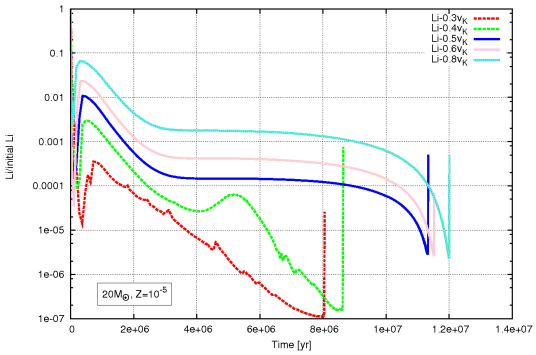

Figure A.52: Mass fraction divided by the initial value of lithium as a function of time for stars with $M = 20M_{\odot}$, $Z = 10^{-5}$ and different f_K.

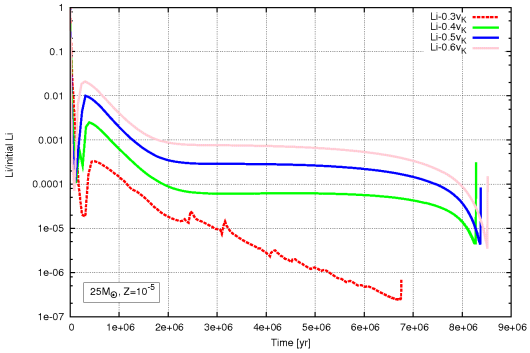

Figure A.53: Mass fraction divided by the initial value of lithium as a function of time for stars with $M = 25M_{\odot}$, $Z = 10^{-5}$ and different f_K.

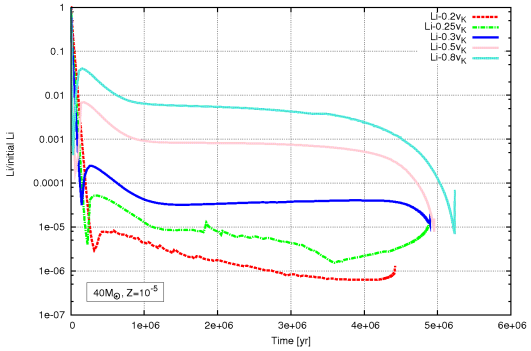

Figure A.54: Mass fraction divided by the initial value of lithium as a function of time for stars with $M = 40M_{\odot}$, $Z = 10^{-5}$ and different f_K.

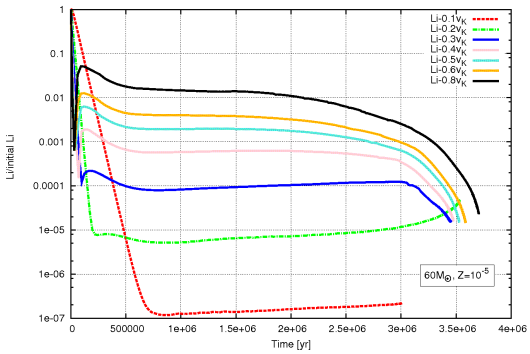

Figure A.55: Mass fraction divided by the initial value of lithium as a function of time for stars with $M = 60M_{\odot}$, $Z = 10^{-5}$ and different f_K.

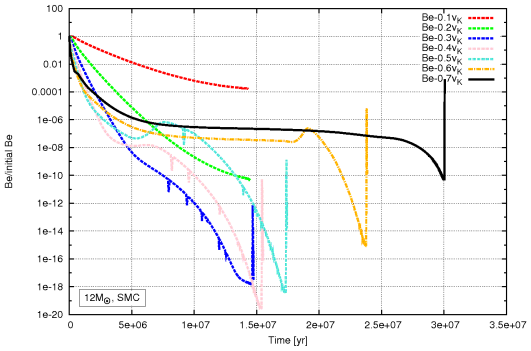

Figure A.56: Mass fraction divided by the initial value of beryllium as a function of time for stars with $M = 12M_{\odot}$, $Z = 0.004$ and different f_K.

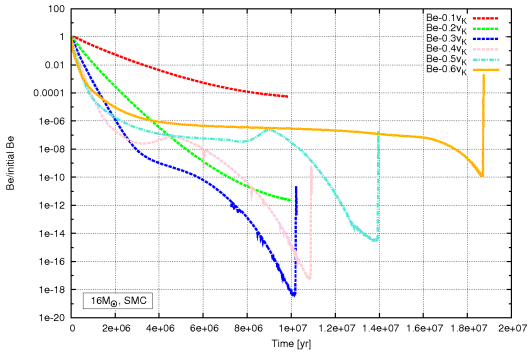

Figure A.57: Mass fraction divided by the initial value of beryllium as a function of time for stars with $M = 16M_{\odot}$, $Z = 0.004$ and different f_K.

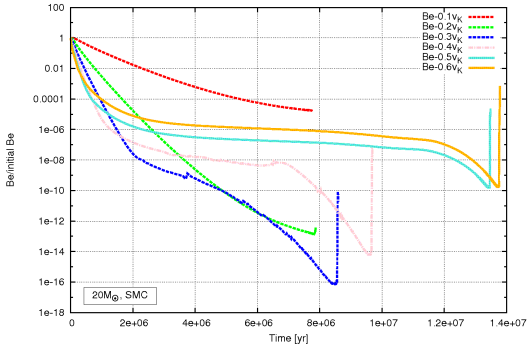

Figure A.58: Mass fraction divided by the initial value of beryllium as a function of time for stars with $M = 20M_{\odot}$, $Z = 0.004$ and different f_K.

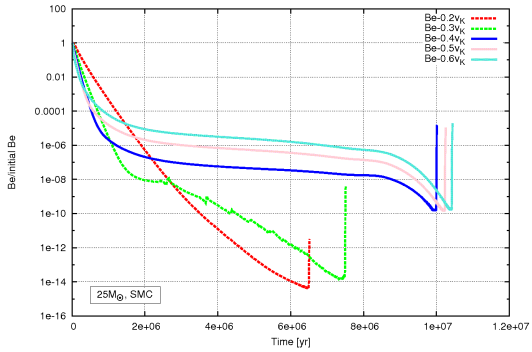

Figure A.59: Mass fraction divided by the initial value of beryllium as a function of time for stars with $M = 25M_{\odot}$, $Z = 0.004$ and different f_K.

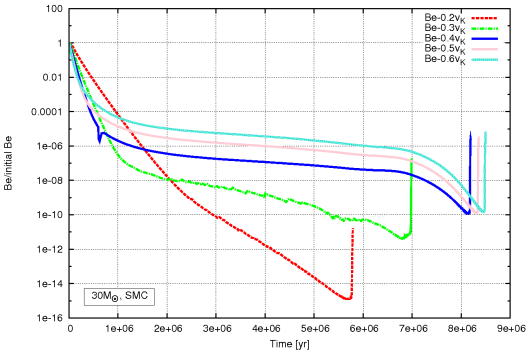

Figure A.60: Mass fraction divided by the initial value of beryllium as a function of time for stars with $M = 30M_{\odot}$, $Z = 0.004$ and different f_K.

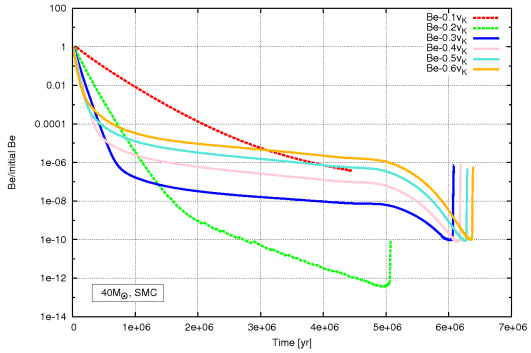

Figure A.61: Mass fraction divided by the initial value of beryllium as a function of time for stars with $M = 40M_{\odot}$, $Z = 0.004$ and different f_K.

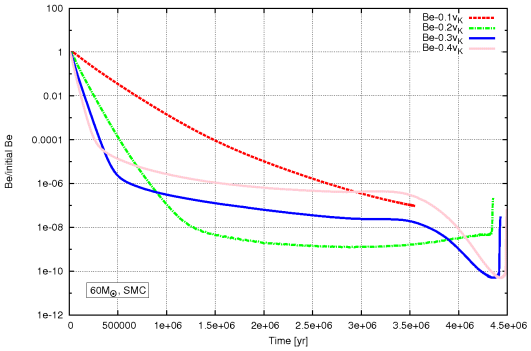

Figure A.62: Mass fraction divided by the initial value of beryllium as a function of time for stars with $M = 60M_\odot$, $Z = 0.004$ and different f_K.

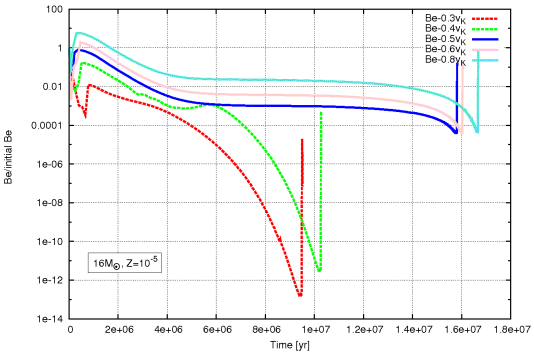

Figure A.63: Mass fraction divided by the initial value of beryllium as a function of time for stars with $M = 16M_\odot$, $Z = 10^{-5}$ and different f_K.

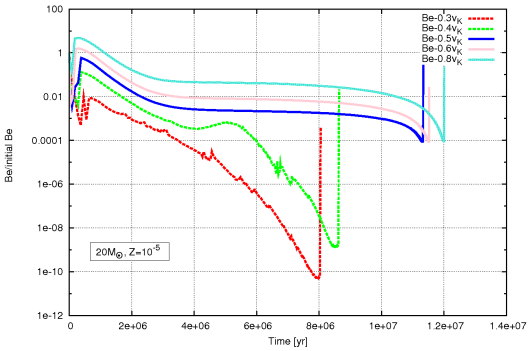

Figure A.64: Mass fraction divided by the initial value of beryllium as a function of time for stars with $M = 20M_\odot$, $Z = 10^{-5}$ and different f_K.

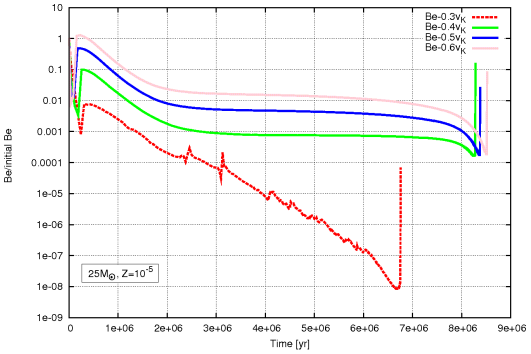

Figure A.65: Mass fraction divided by the initial value of beryllium as a function of time for stars with $M = 25M_\odot$, $Z = 10^{-5}$ and different f_K.

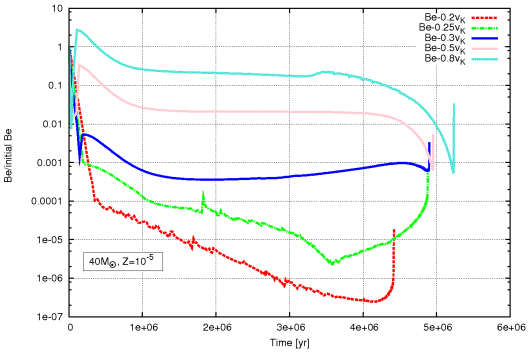

Figure A.66: Mass fraction divided by the initial value of beryllium as a function of time for stars with $M = 40M_\odot$, $Z = 10^{-5}$ and different f_K.

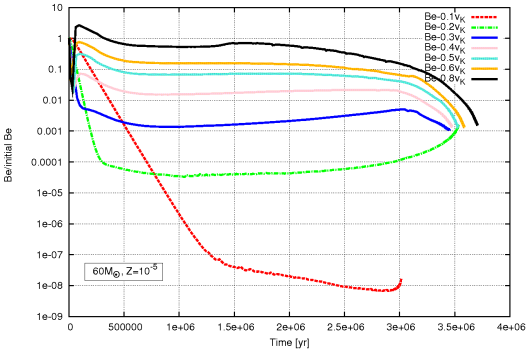

Figure A.67: Mass fraction divided by the initial value of beryllium as a function of time for stars with $M = 60M_\odot$, $Z = 10^{-5}$ and different f_K.

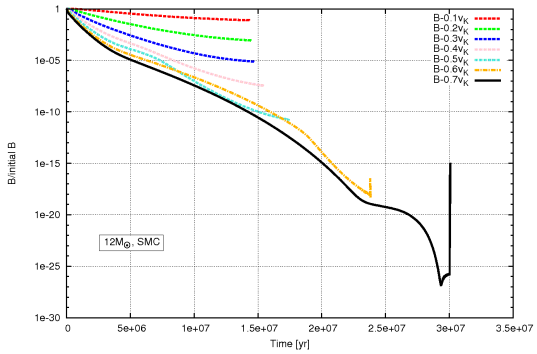

Figure A.68: Mass fraction divided by the initial value of boron as a function of time for stars with $M = 12M_{\odot}$, $Z = 0.004$ and different f_K.

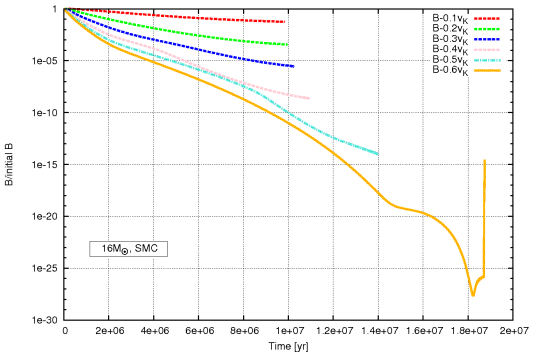

Figure A.69: Mass fraction divided by the initial value of boron as a function of time for stars with $M = 16M_{\odot}$, $Z = 0.004$ and different f_K.

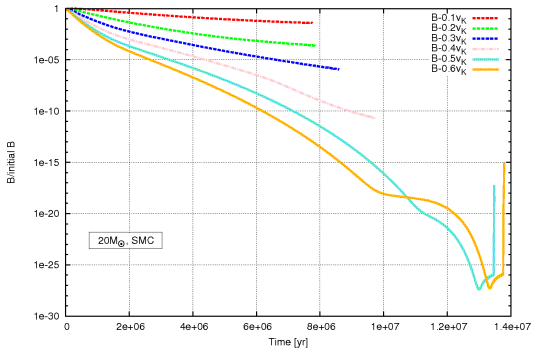

Figure A.70: Mass fraction divided by the initial value of boron as a function of time for stars with $M = 20M_{\odot}$, $Z = 0.004$ and different f_K.

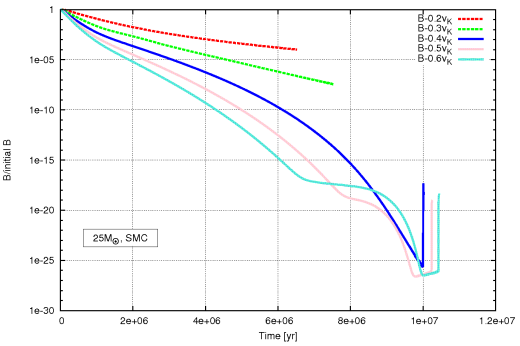

Figure A.71: Mass fraction divided by the initial value of boron as a function of time for stars with $M = 25M_{\odot}$, $Z = 0.004$ and different f_K.

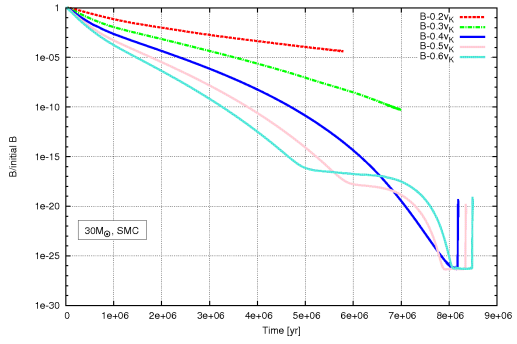

Figure A.72: Mass fraction divided by the initial value of boron as a function of time for stars with $M = 30M_{\odot}$, $Z = 0.004$ and different f_K.

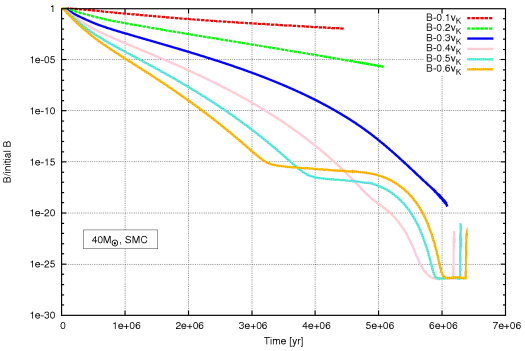

Figure A.73: Mass fraction divided by the initial value of boron as a function of time for stars with $M = 40M_{\odot}$, $Z = 0.004$ and different f_K.

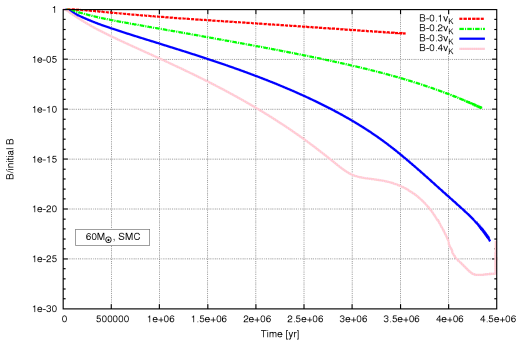

Figure A.74: Mass fraction divided by the initial value of boron as a function of time for stars with M = 60M$_\odot$, $Z = 0.004$ and different f_K.

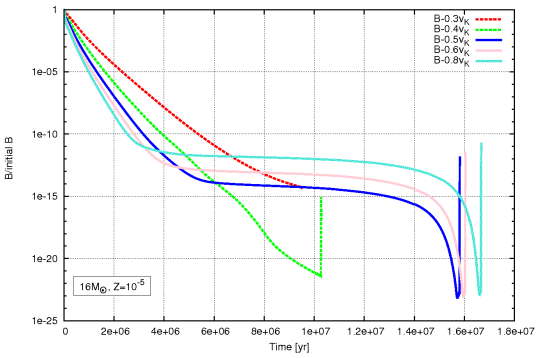

Figure A.75: Mass fraction divided by the initial value of boron as a function of time for stars with M = 16M$_\odot$, $Z = 10^{-5}$ and different f_K.

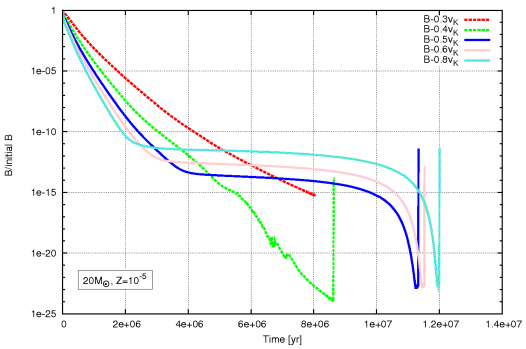

Figure A.76: Mass fraction divided by the initial value of boron as a function of time for stars with M = 20M$_\odot$, $Z = 10^{-5}$ and different f_K.

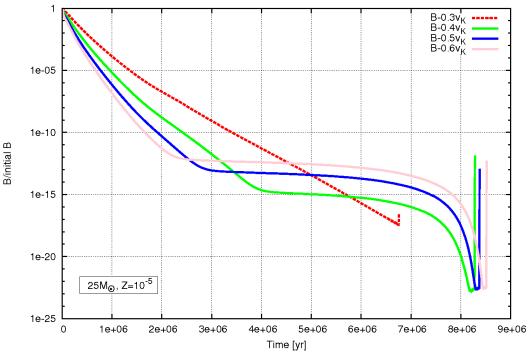

Figure A.77: Mass fraction divided by the initial value of boron as a function of time for stars with M = 25M$_\odot$, $Z = 10^{-5}$ and different f_K.

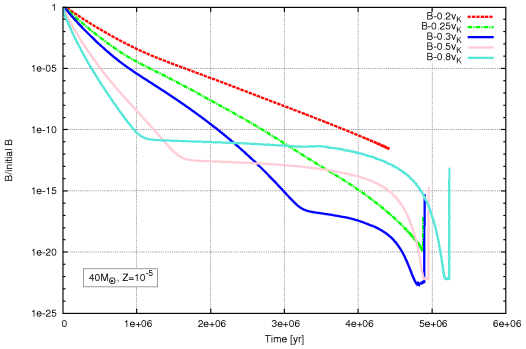

Figure A.78: Mass fraction divided by the initial value of boron as a function of time for stars with M = 40M$_\odot$, $Z = 10^{-5}$ and different f_K.

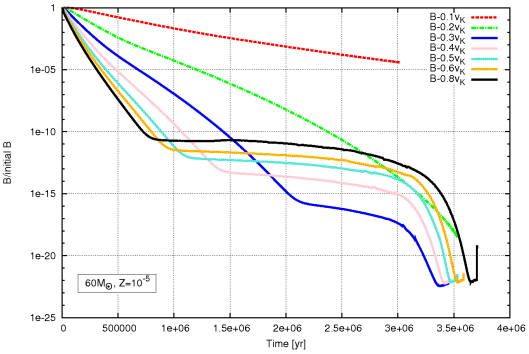

Figure A.79: Mass fraction divided by the initial value of boron as a function of time for stars with M = 60M$_\odot$, $Z = 10^{-5}$ and different f_K.

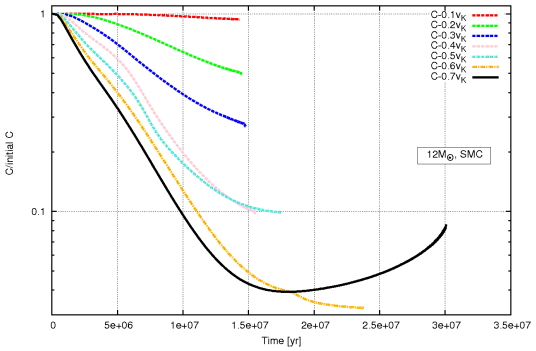

Figure A.80: Mass fraction divided by the initial value of carbon as a function of time for stars with $M = 12M_{\odot}$, $Z = 0.004$ and different f_K.

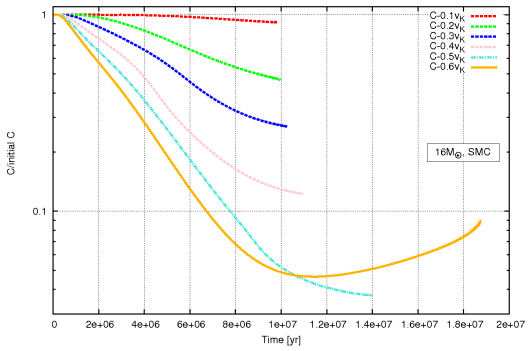

Figure A.81: Mass fraction divided by the initial value of carbon as a function of time for stars with $M = 16M_{\odot}$, $Z = 0.004$ and different f_K.

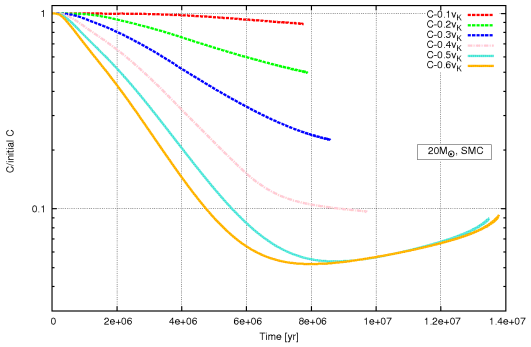

Figure A.82: Mass fraction divided by the initial value of carbon as a function of time for stars with $M = 20M_{\odot}$, $Z = 0.004$ and different f_K.

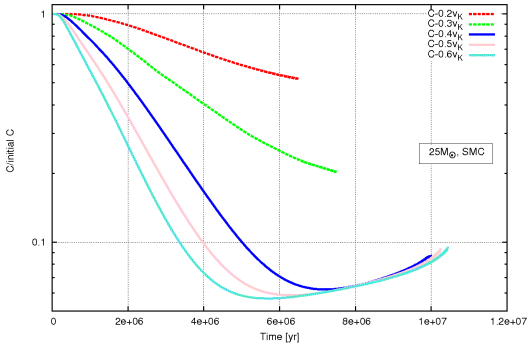

Figure A.83: Mass fraction divided by the initial value of carbon as a function of time for stars with $M = 25M_{\odot}$, $Z = 0.004$ and different f_K.

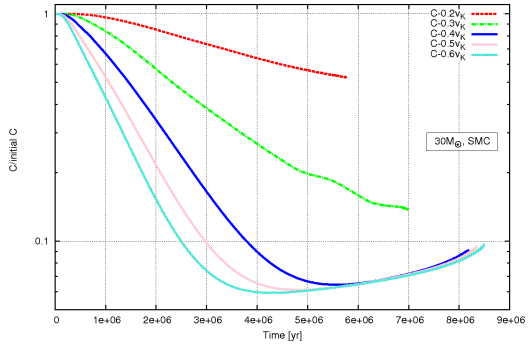

Figure A.84: Mass fraction divided by the initial value of carbon as a function of time for stars with $M = 30M_{\odot}$, $Z = 0.004$ and different f_K.

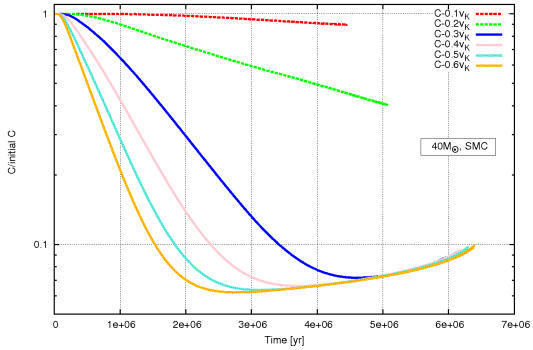

Figure A.85: Mass fraction divided by the initial value of carbon as a function of time for stars with $M = 40M_{\odot}$, $Z = 0.004$ and different f_K.

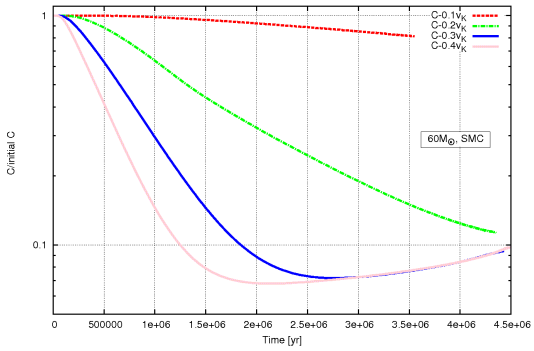

Figure A.86: Mass fraction divided by the initial value of carbon as a function of time for stars with $M = 60M_{\odot}$, $Z = 0.004$ and different f_K.

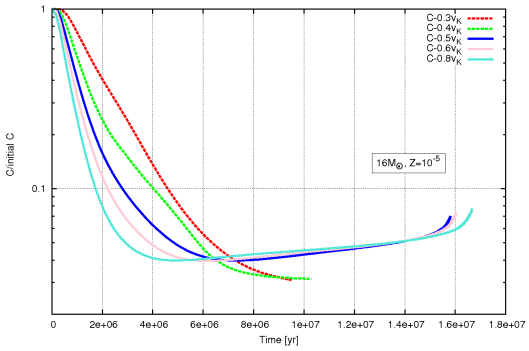

Figure A.87: Mass fraction divided by the initial value of carbon as a function of time for stars with $M = 16M_{\odot}$, $Z = 10^{-5}$ and different f_K.

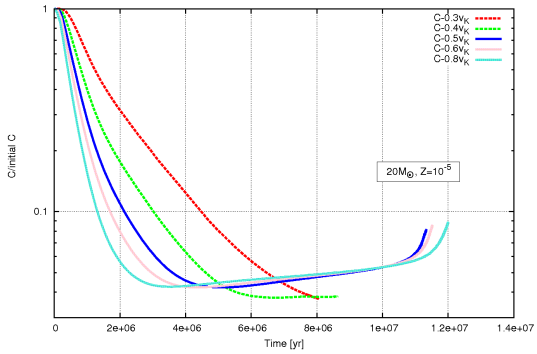

Figure A.88: Mass fraction divided by the initial value of carbon as a function of time for stars with $M = 20M_{\odot}$, $Z = 10^{-5}$ and different f_K.

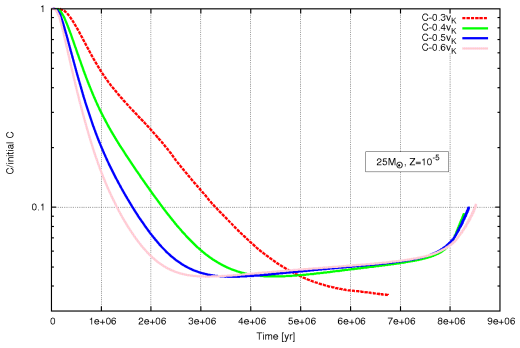

Figure A.89: Mass fraction divided by the initial value of carbon as a function of time for stars with $M = 25M_{\odot}$, $Z = 10^{-5}$ and different f_K.

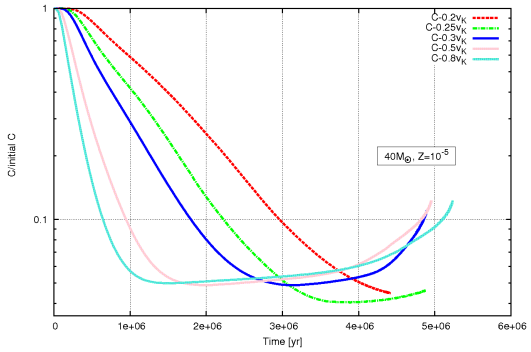

Figure A.90: Mass fraction divided by the initial value of carbon as a function of time for stars with $M = 40M_{\odot}$, $Z = 10^{-5}$ and different f_K.

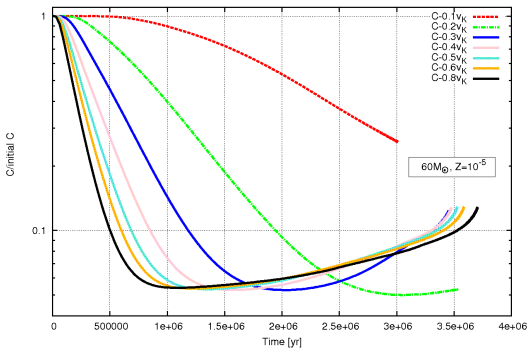

Figure A.91: Mass fraction divided by the initial value of carbon as a function of time for stars with $M = 60M_{\odot}$, $Z = 10^{-5}$ and different f_K.

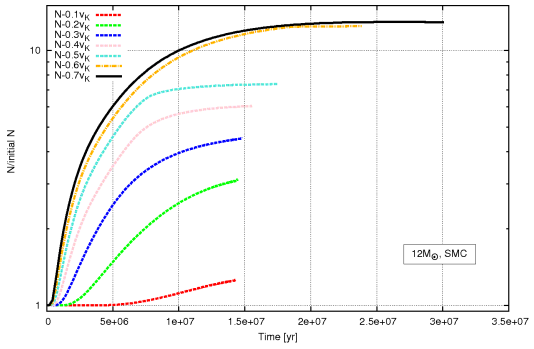

Figure A.92: Mass fraction divided by the initial value of nitrogen as a function of time for stars with $M = 12M_{\odot}$, $Z = 0.004$ and different f_K.

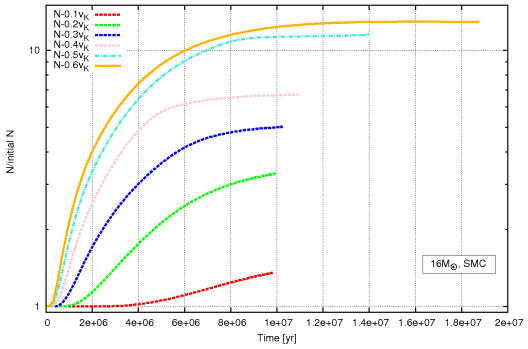

Figure A.93: Mass fraction divided by the initial value of nitrogen as a function of time for stars with $M = 16M_{\odot}$, $Z = 0.004$ and different f_K.

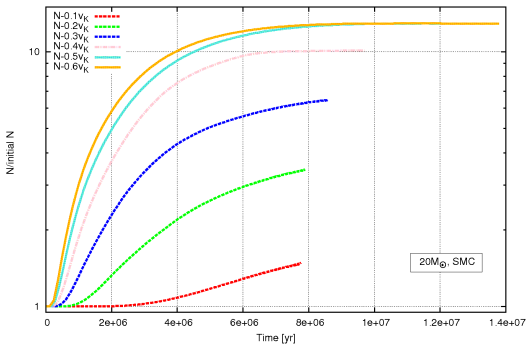

Figure A.94: Mass fraction divided by the initial value of nitrogen as a function of time for stars with $M = 20M_{\odot}$, $Z = 0.004$ and different f_K.

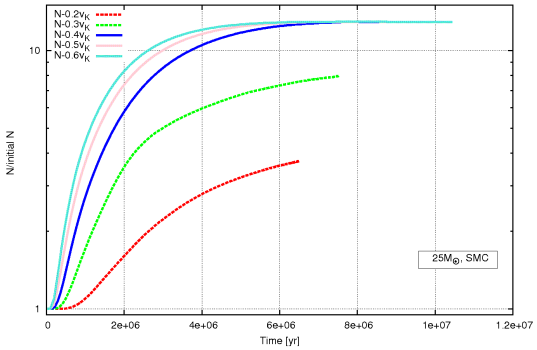

Figure A.95: Mass fraction divided by the initial value of nitrogen as a function of time for stars with $M = 25M_{\odot}$, $Z = 0.004$ and different f_K.

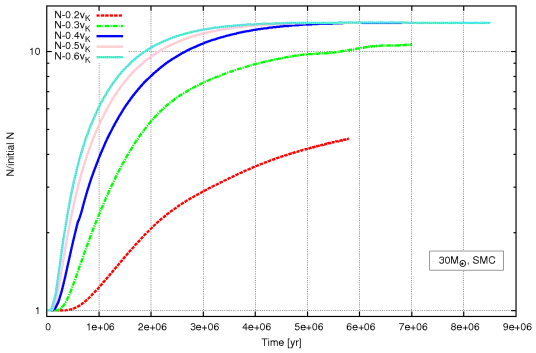

Figure A.96: Mass fraction divided by the initial value of nitrogen as a function of time for stars with $M = 30M_{\odot}$, $Z = 0.004$ and different f_K.

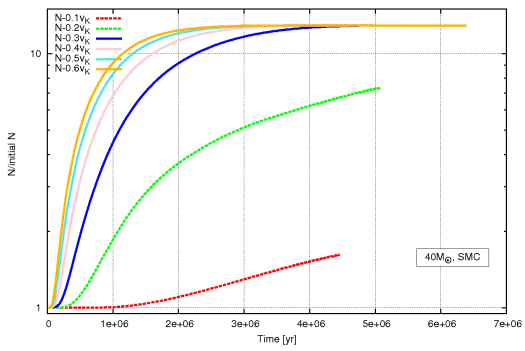

Figure A.97: Mass fraction divided by the initial value of nitrogen as a function of time for stars with $M = 40M_{\odot}$, $Z = 0.004$ and different f_K.

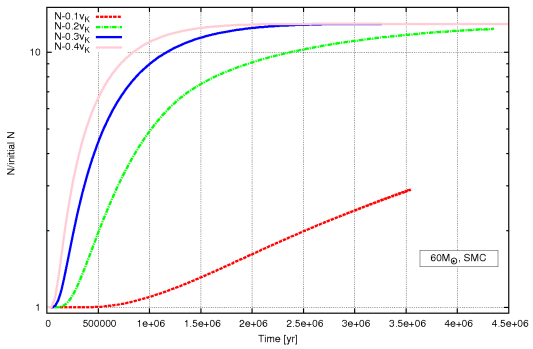

Figure A.98: Mass fraction divided by the initial value of nitrogen as a function of time for stars with $M = 60M_{\odot}$, $Z = 0.004$ and different f_K.

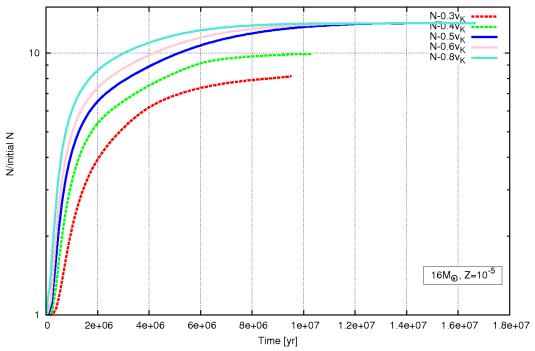

Figure A.99: Mass fraction divided by the initial value of nitrogen as a function of time for stars with $M = 16M_{\odot}$, $Z = 10^{-5}$ and different f_K.

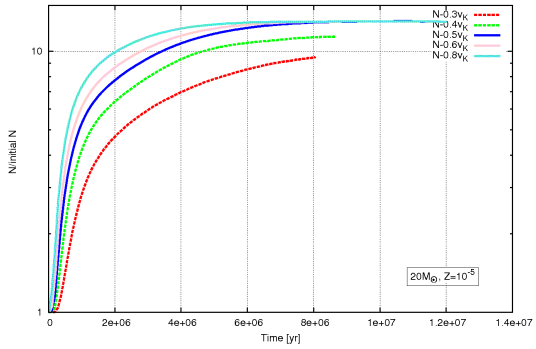

Figure A.100: Mass fraction divided by the initial value of nitrogen as a function of time for stars with $M = 20M_{\odot}$, $Z = 10^{-5}$ and different f_K.

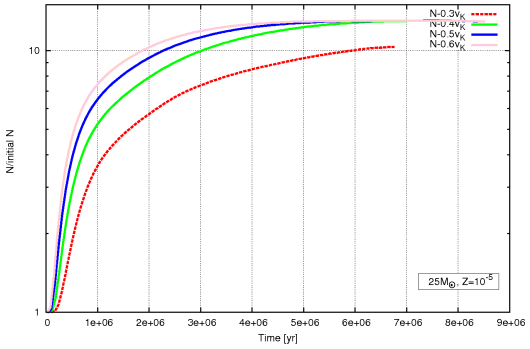

Figure A.101: Mass fraction divided by the initial value of nitrogen as a function of time for stars with $M = 25M_{\odot}$, $Z = 10^{-5}$ and different f_K.

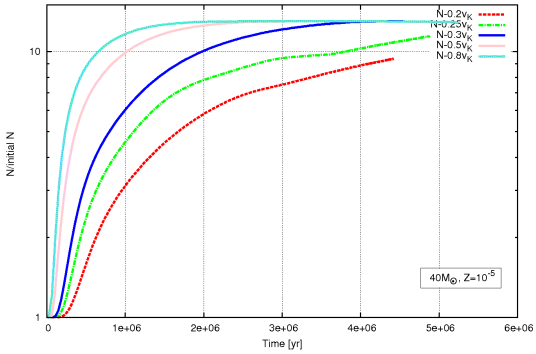

Figure A.102: Mass fraction divided by the initial value of nitrogen as a function of time for stars with $M = 40M_{\odot}$, $Z = 10^{-5}$ and different f_K.

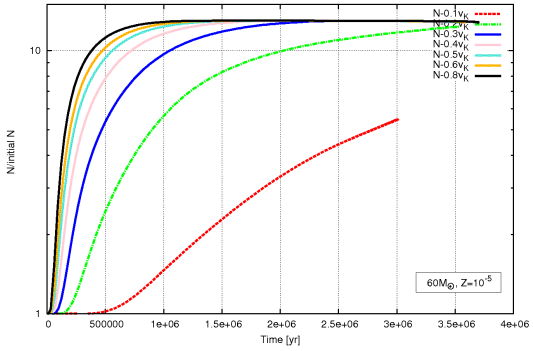

Figure A.103: Mass fraction divided by the initial value of nitrogen as a function of time for stars with $M = 60M_{\odot}$, $Z = 10^{-5}$ and different f_K.

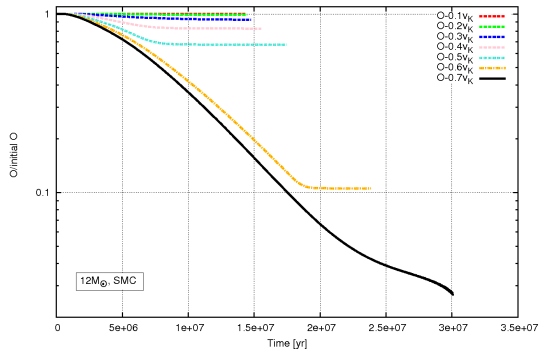

Figure A.104: Mass fraction divided by the initial value of oxygen as a function of time for stars with $M = 12M_{\odot}$, $Z = 0.004$ and different f_K.

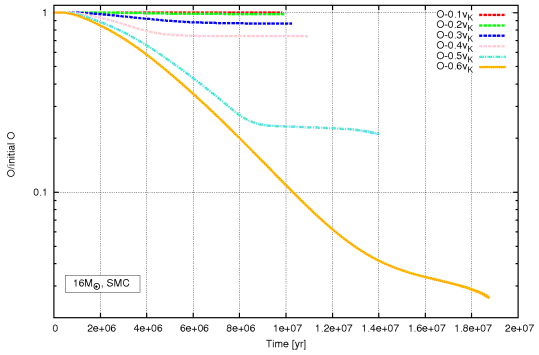

Figure A.105: Mass fraction divided by the initial value of oxygen as a function of time for stars with $M = 16M_{\odot}$, $Z = 0.004$ and different f_K.

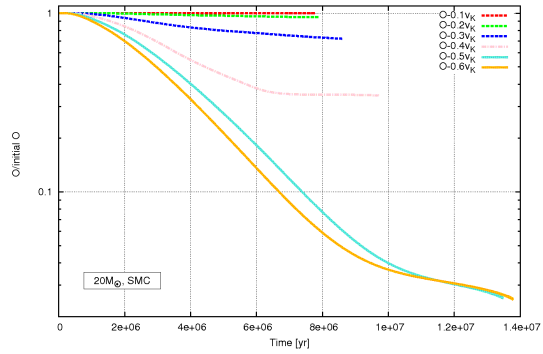

Figure A.106: Mass fraction divided by the initial value of oxygen as a function of time for stars with $M = 20M_{\odot}$, $Z = 0.004$ and different f_K.

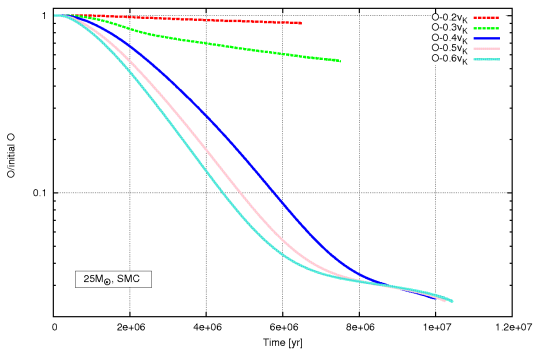

Figure A.107: Mass fraction divided by the initial value of oxygen as a function of time for stars with $M = 25M_{\odot}$, $Z = 0.004$ and different f_K.

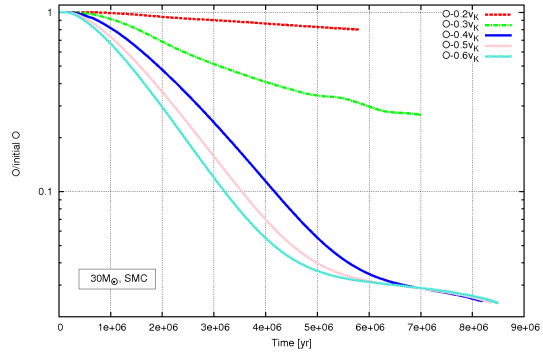

Figure A.108: Mass fraction divided by the initial value of oxygen as a function of time for stars with $M = 30M_{\odot}$, $Z = 0.004$ and different f_K.

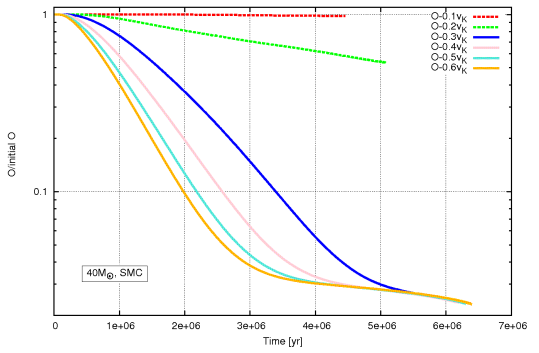

Figure A.109: Mass fraction divided by the initial value of oxygen as a function of time for stars with $M = 40M_{\odot}$, $Z = 0.004$ and different f_K.

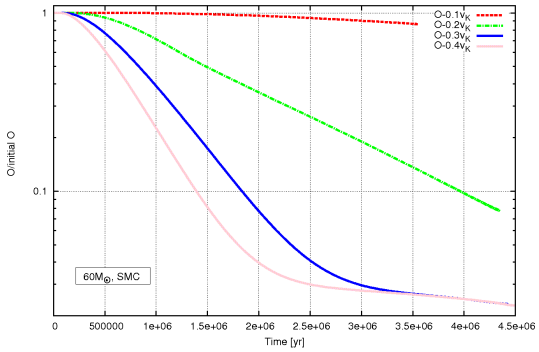

Figure A.110: Mass fraction divided by the initial value of oxygen as a function of time for stars with $M = 60M_{\odot}$, $Z = 0.004$ and different f_K.

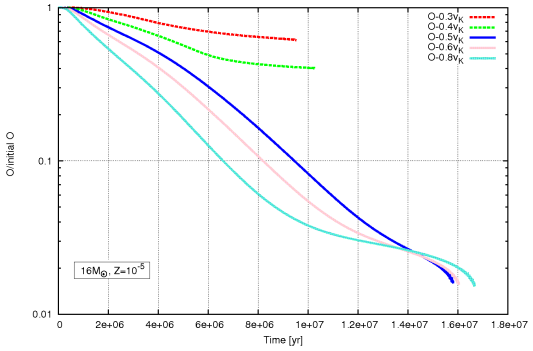

Figure A.111: Mass fraction divided by the initial value of oxygen as a function of time for stars with $M = 16M_{\odot}$, $Z = 10^{-5}$ and different f_K.

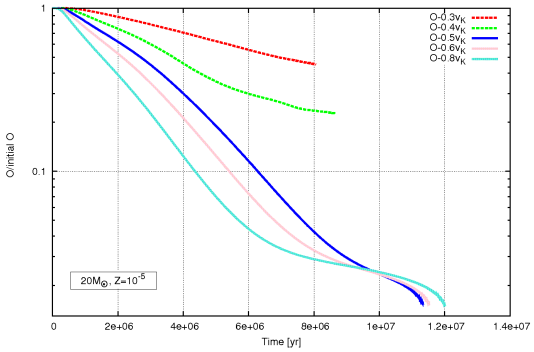

Figure A.112: Mass fraction divided by the initial value of oxygen as a function of time for stars with $M = 20M_{\odot}$, $Z = 10^{-5}$ and different f_K.

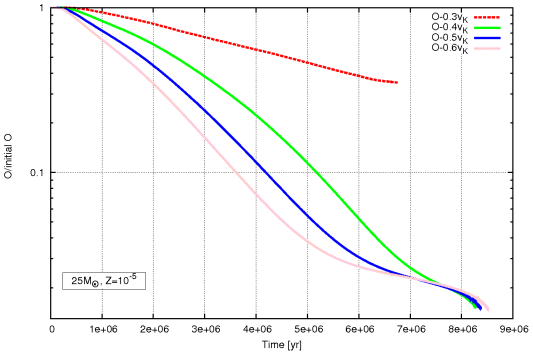

Figure A.113: Mass fraction divided by the initial value of oxygen as a function of time for stars with $M = 25M_{\odot}$, $Z = 10^{-5}$ and different f_K.

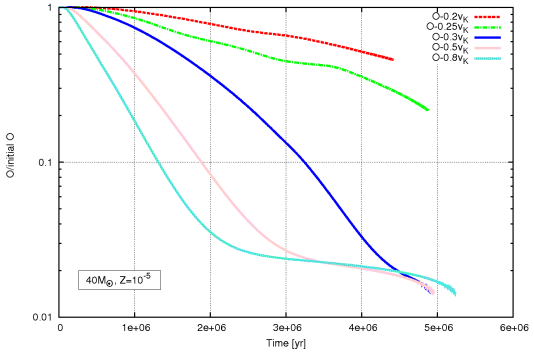

Figure A.114: Mass fraction divided by the initial value of oxygen as a function of time for stars with $M = 40M_{\odot}$, $Z = 10^{-5}$ and different f_K.

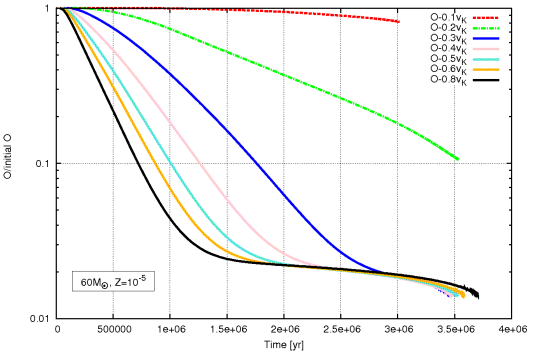

Figure A.115: Mass fraction divided by the initial value of oxygen as a function of time for stars with $M = 60M_{\odot}$, $Z = 10^{-5}$ and different f_K.

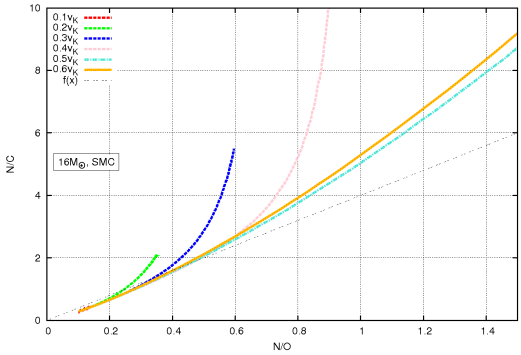

Figure A.116: Variation of the CNO-abundance as a function of time for stars with $M = 16M_{\odot}$, $Z = 0.004$ and different f_K.

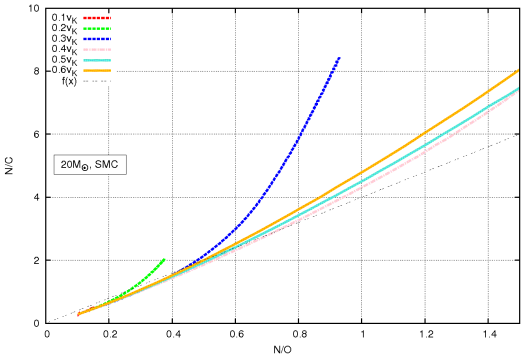

Figure A.117: Variation of the CNO-abundance as a function of time for stars with $M = 20M_{\odot}$, $Z = 0.004$ and different f_K.

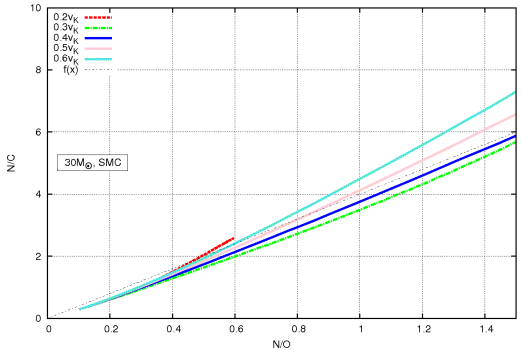

Figure A.118: Variation of the CNO-abundance as a function of time for stars with $M = 30M_{\odot}$, $Z = 0.004$ and different f_K.

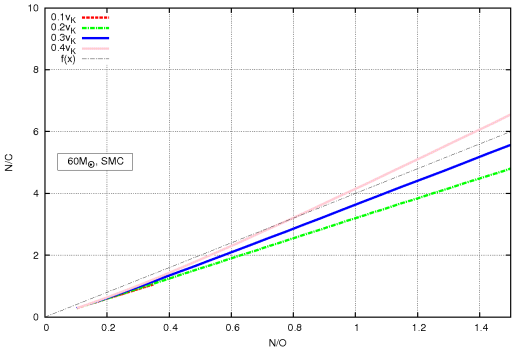

Figure A.119: Variation of the CNO-abundance as a function of time for stars with $M = 60M_{\odot}$, $Z = 0.004$ and different f_K.

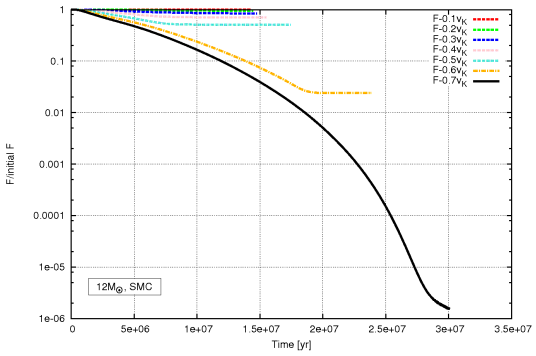

Figure A.120: Mass fraction divided by the initial value of fluorine as a function of time for stars with $M = 12M_\odot$, $Z = 0.004$ and different f_K.

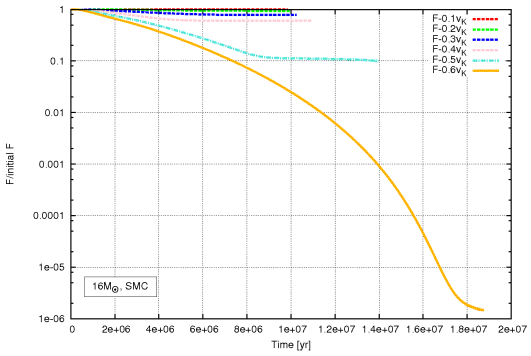

Figure A.121: Mass fraction divided by the initial value of fluorine as a function of time for stars with $M = 16M_\odot$, $Z = 0.004$ and different f_K.

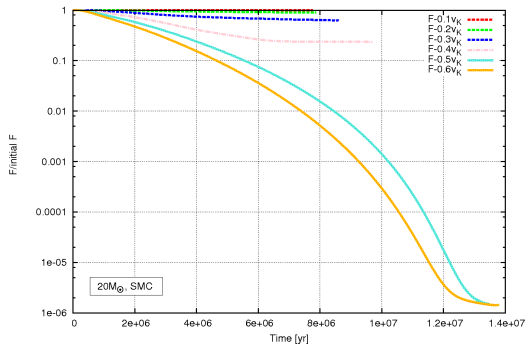

Figure A.122: Mass fraction divided by the initial value of fluorine as a function of time for stars with $M = 20M_\odot$, $Z = 0.004$ and different f_K.

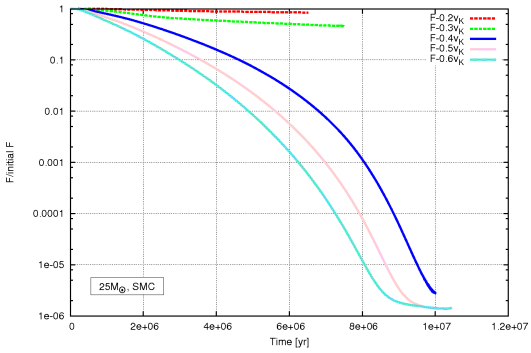

Figure A.123: Mass fraction divided by the initial value of fluorine as a function of time for stars with $M = 25M_\odot$, $Z = 0.004$ and different f_K.

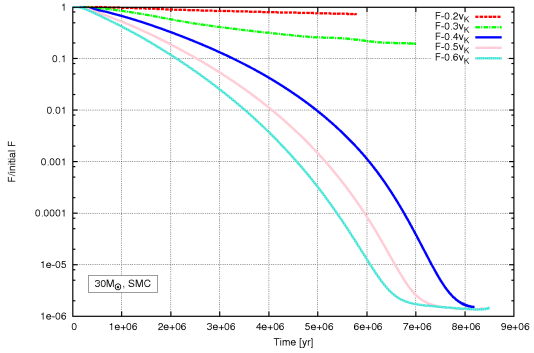

Figure A.124: Mass fraction divided by the initial value of fluorine as a function of time for stars with $M = 30M_\odot$, $Z = 0.004$ and different f_K.

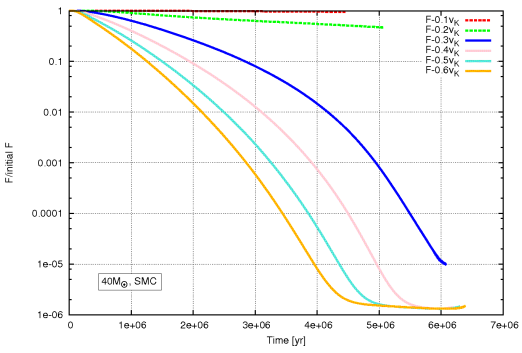

Figure A.125: Mass fraction divided by the initial value of fluorine as a function of time for stars with $M = 40M_\odot$, $Z = 0.004$ and different f_K.

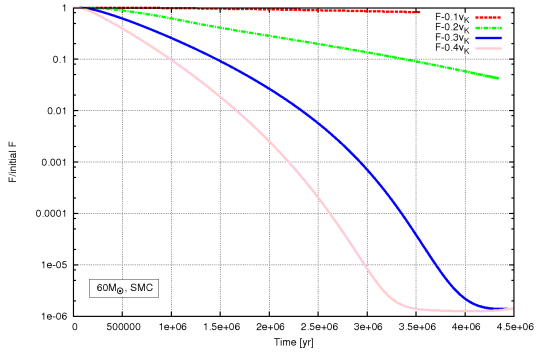

Figure A.126: Mass fraction divided by the initial value of fluorine as a function of time for stars with $\mathrm{M} = 60\mathrm{M}_{\odot}$, $Z = 0.004$ and different f_K.

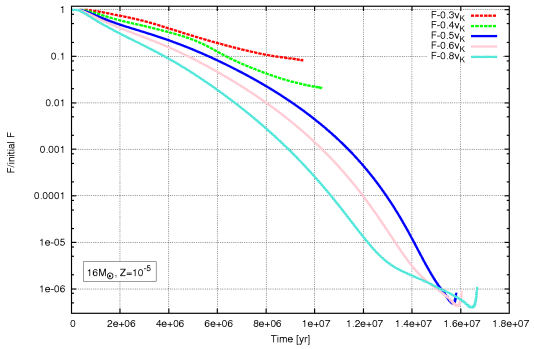

Figure A.127: Mass fraction divided by the initial value of fluorine as a function of time for stars with $\mathrm{M} = 16\mathrm{M}_{\odot}$, $Z = 10^{-5}$ and different f_K.

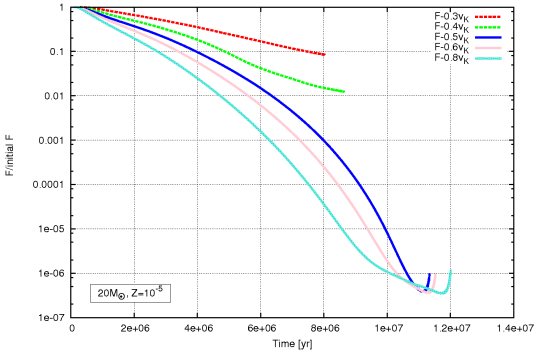

Figure A.128: Mass fraction divided by the initial value of fluorine as a function of time for stars with $\mathrm{M} = 20\mathrm{M}_{\odot}$, $Z = 10^{-5}$ and different f_K.

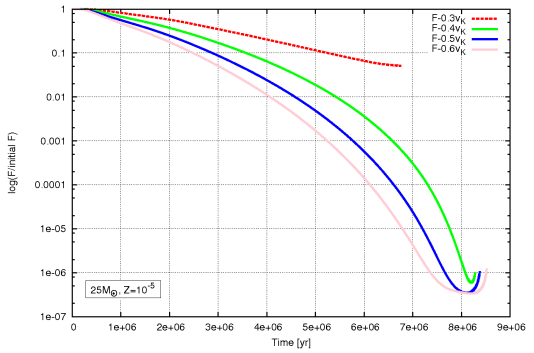

Figure A.129: Mass fraction divided by the initial value of fluorine as a function of time for stars with $\mathrm{M} = 25\mathrm{M}_{\odot}$, $Z = 10^{-5}$ and different f_K.

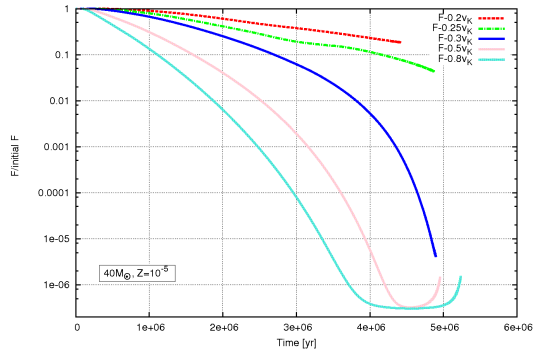

Figure A.130: Mass fraction divided by the initial value of fluorine as a function of time for stars with $\mathrm{M} = 40\mathrm{M}_{\odot}$, $Z = 10^{-5}$ and different f_K.

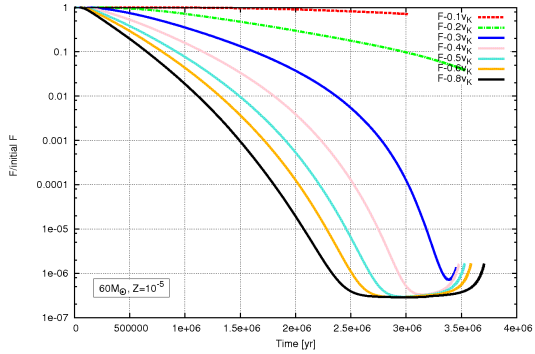

Figure A.131: Mass fraction divided by the initial value of fluorine as a function of time for stars with $\mathrm{M} = 60\mathrm{M}_{\odot}$, $Z = 10^{-5}$ and different f_K.

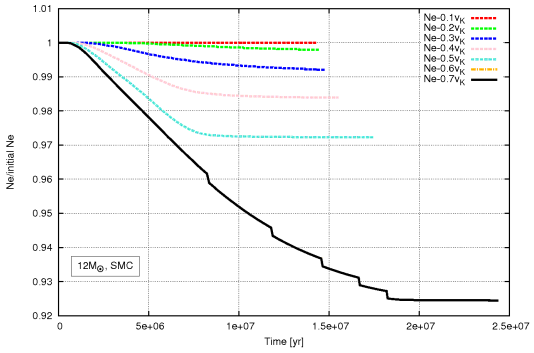

Figure A.132: Mass fraction divided by the initial value of neon as a function of time for stars with M = 12M$_\odot$, $Z = 0.004$ and different f_K.

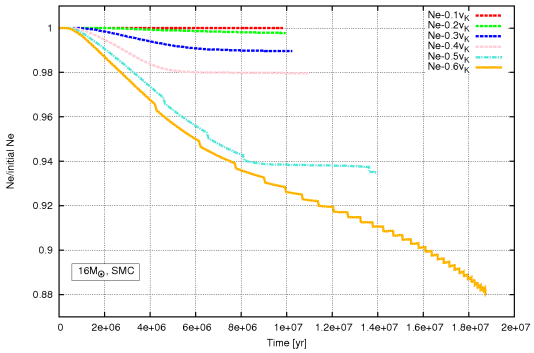

Figure A.133: Mass fraction divided by the initial value of neon as a function of time for stars with M = 16M$_\odot$, $Z = 0.004$ and different f_K.

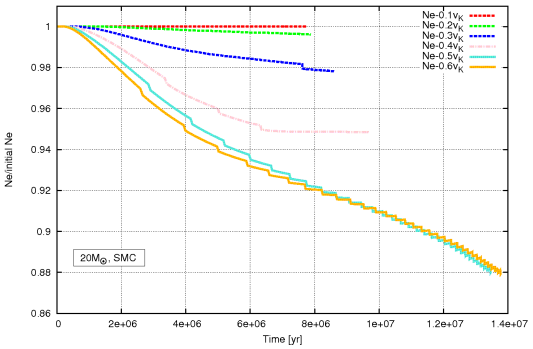

Figure A.134: Mass fraction divided by the initial value of neon as a function of time for stars with M = 20M$_\odot$, $Z = 0.004$ and different f_K.

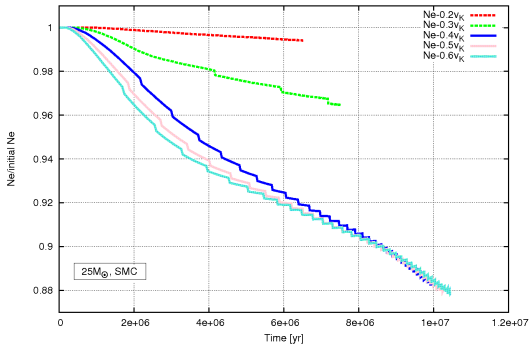

Figure A.135: Mass fraction divided by the initial value of neon as a function of time for stars with M = 25M$_\odot$, $Z = 0.004$ and different f_K.

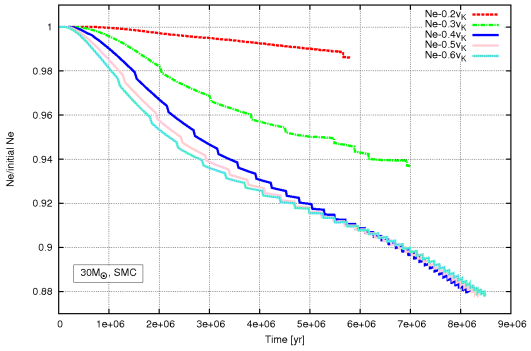

Figure A.136: Mass fraction divided by the initial value of neon as a function of time for stars with M = 30M$_\odot$, $Z = 0.004$ and different f_K.

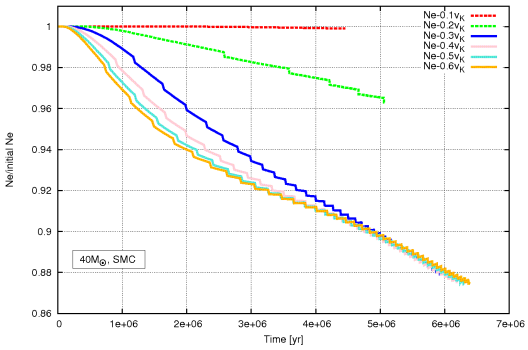

Figure A.137: Mass fraction divided by the initial value of neon as a function of time for stars with M = 40M$_\odot$, $Z = 0.004$ and different f_K.

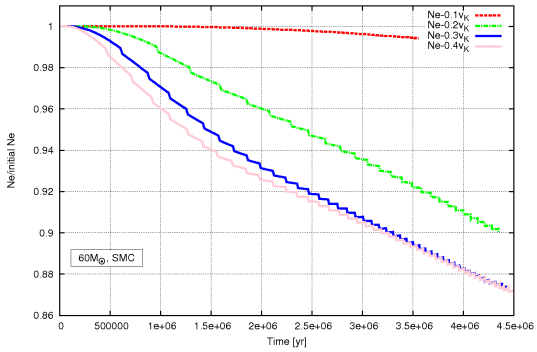

Figure A.138: Mass fraction divided by the initial value of neon as a function of time for stars with $M = 60M_{\odot}$, $Z = 0.004$ and different f_K.

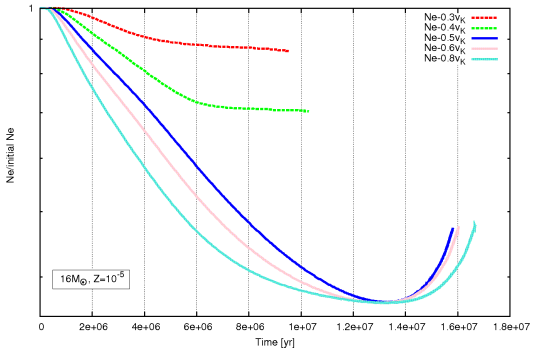

Figure A.139: Mass fraction divided by the initial value of neon as a function of time for stars with $M = 16M_{\odot}$, $Z = 10^{-5}$ and different f_K.

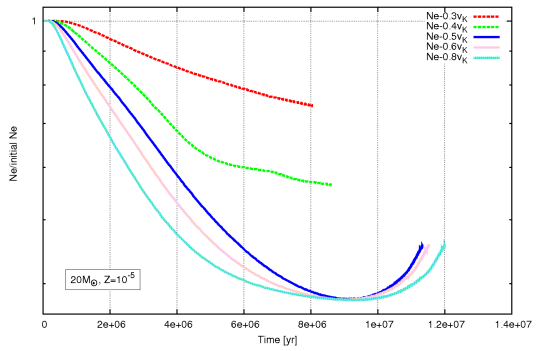

Figure A.140: Mass fraction divided by the initial value of neon as a function of time for stars with $M = 20M_{\odot}$, $Z = 10^{-5}$ and different f_K.

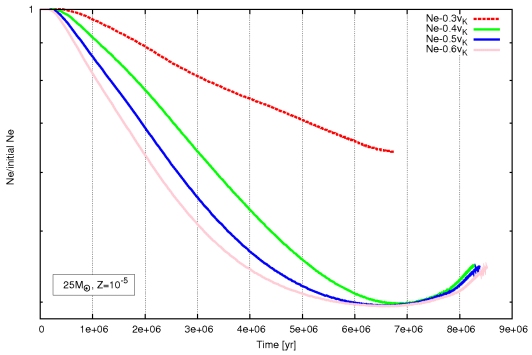

Figure A.141: Mass fraction divided by the initial value of neon as a function of time for stars with $M = 25M_{\odot}$, $Z = 10^{-5}$ and different f_K.

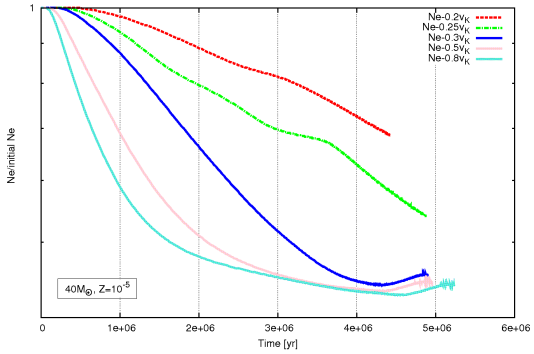

Figure A.142: Mass fraction divided by the initial value of neon as a function of time for stars with $M = 40M_{\odot}$, $Z = 10^{-5}$ and different f_K.

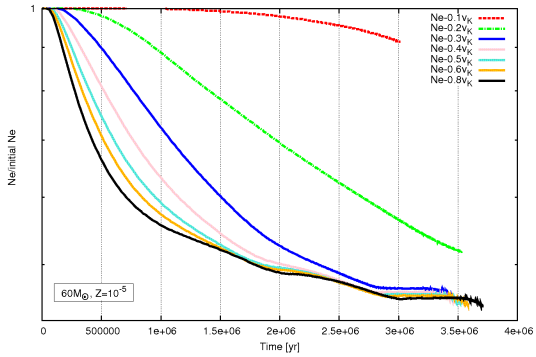

Figure A.143: Mass fraction divided by the initial value of neon as a function of time for stars with $M = 60M_{\odot}$, $Z = 10^{-5}$ and different f_K.

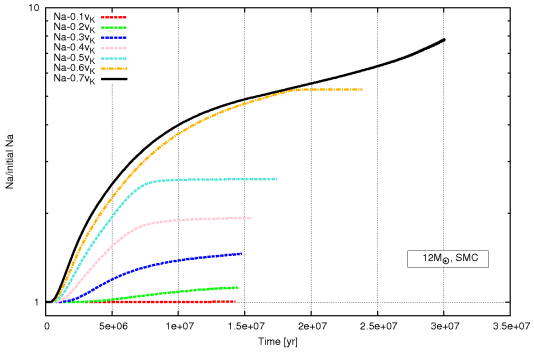

Figure A.144: Mass fraction divided by the initial value of sodium as a function of time for stars with M = 12M$_\odot$, $Z = 0.004$ and different f_K.

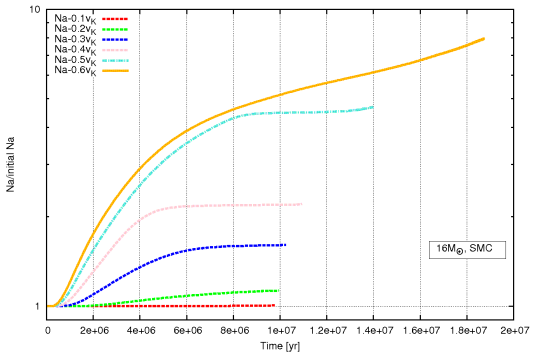

Figure A.145: Mass fraction divided by the initial value of sodium as a function of time for stars with M = 16M$_\odot$, $Z = 0.004$ and different f_K.

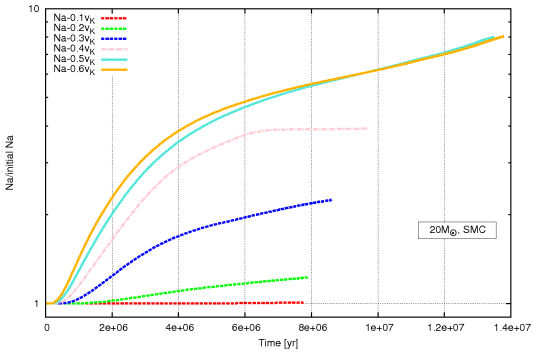

Figure A.146: Mass fraction divided by the initial value of sodium as a function of time for stars with M = 20M$_\odot$, $Z = 0.004$ and different f_K.

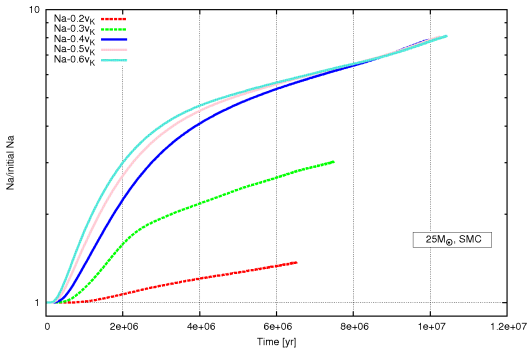

Figure A.147: Mass fraction divided by the initial value of sodium as a function of time for stars with M = 25M$_\odot$, $Z = 0.004$ and different f_K.

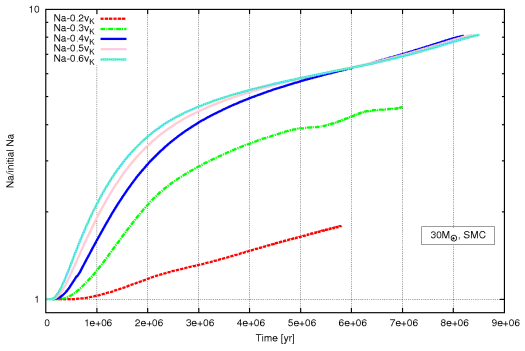

Figure A.148: Mass fraction divided by the initial value of sodium as a function of time for stars with M = 30M$_\odot$, $Z = 0.004$ and different f_K.

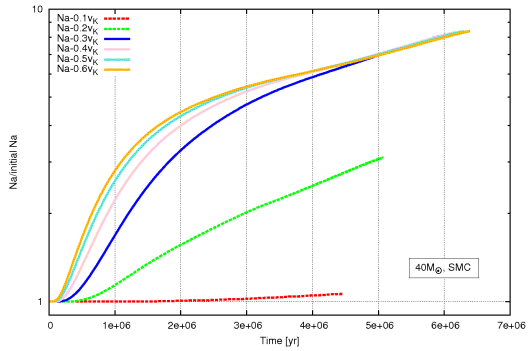

Figure A.149: Mass fraction divided by the initial value of sodium as a function of time for stars with M = 40M$_\odot$, $Z = 0.004$ and different f_K.

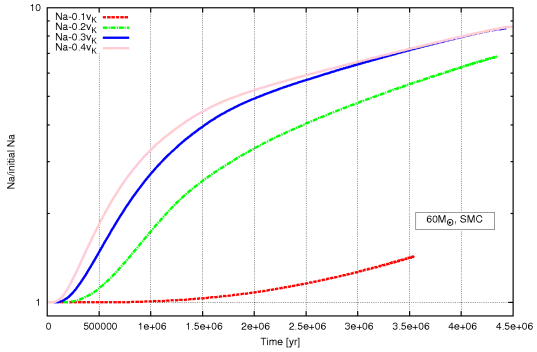

Figure A.150: Mass fraction divided by the initial value of sodium as a function of time for stars with $M = 60M_\odot$, $Z = 0.004$ and different f_K.

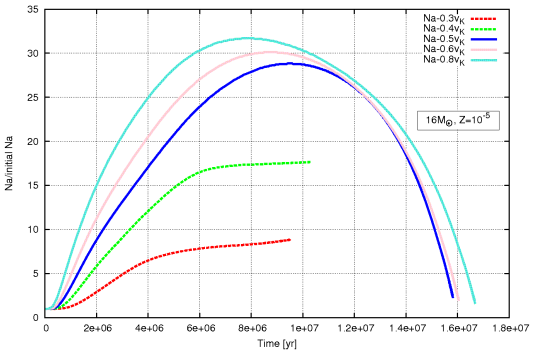

Figure A.151: Mass fraction divided by the initial value of sodium as a function of time for stars with $M = 16M_\odot$, $Z = 10^{-5}$ and different f_K.

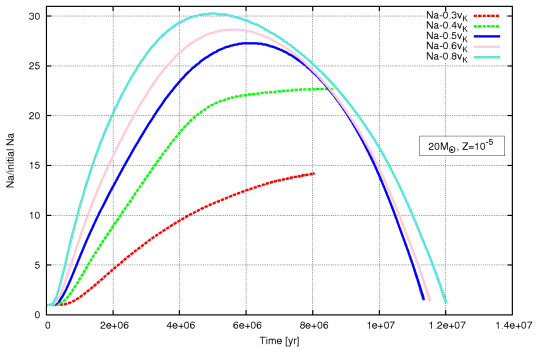

Figure A.152: Mass fraction divided by the initial value of sodium as a function of time for stars with $M = 20M_\odot$, $Z = 10^{-5}$ and different f_K.

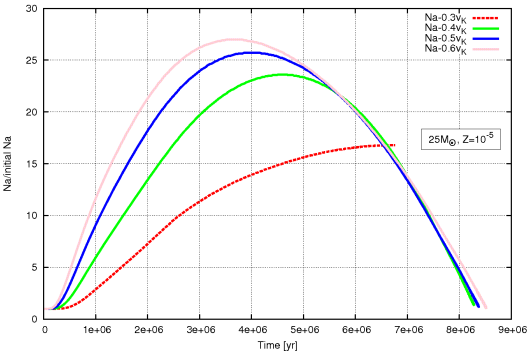

Figure A.153: Mass fraction divided by the initial value of sodium as a function of time for stars with $M = 25M_\odot$, $Z = 10^{-5}$ and different f_K.

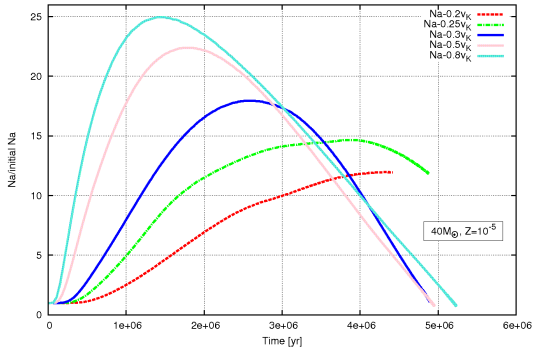

Figure A.154: Mass fraction divided by the initial value of sodium as a function of time for stars with $M = 40M_\odot$, $Z = 10^{-5}$ and different f_K.

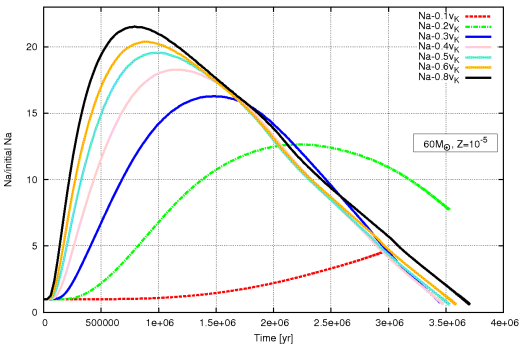

Figure A.155: Mass fraction divided by the initial value of sodium as a function of time for stars with $M = 60M_\odot$, $Z = 10^{-5}$ and different f_K.

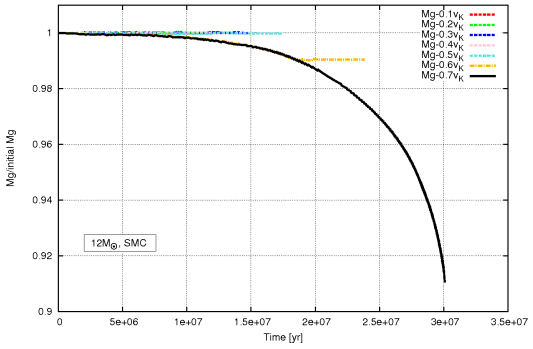

Figure A.156: Mass fraction divided by the initial value of magnesium as a function of time for stars with M = 12M$_\odot$, $Z = 0.004$ and different f_K.

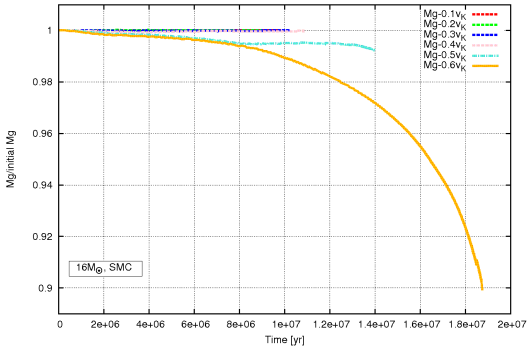

Figure A.157: Mass fraction divided by the initial value of magnesium as a function of time for stars with M = 16M$_\odot$, $Z = 0.004$ and different f_K.

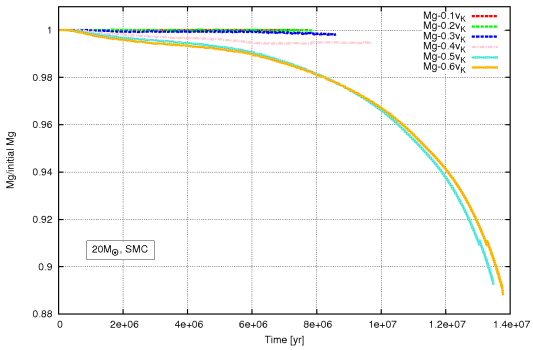

Figure A.158: Mass fraction divided by the initial value of magnesium as a function of time for stars with M = 20M$_\odot$, $Z = 0.004$ and different f_K.

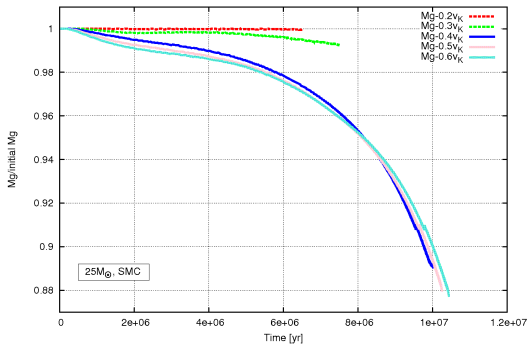

Figure A.159: Mass fraction divided by the initial value of magnesium as a function of time for stars with M = 25M$_\odot$, $Z = 0.004$ and different f_K.

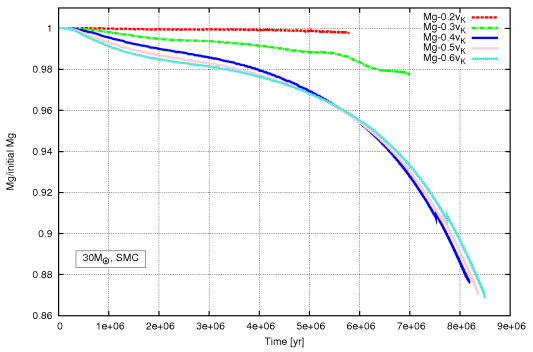

Figure A.160: Mass fraction divided by the initial value of magnesium as a function of time for stars with M = 30M$_\odot$, $Z = 0.004$ and different f_K.

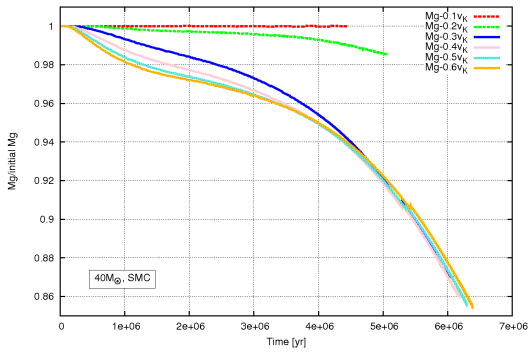

Figure A.161: Mass fraction divided by the initial value of magnesium as a function of time for stars with M = 40M$_\odot$, $Z = 0.004$ and different f_K.

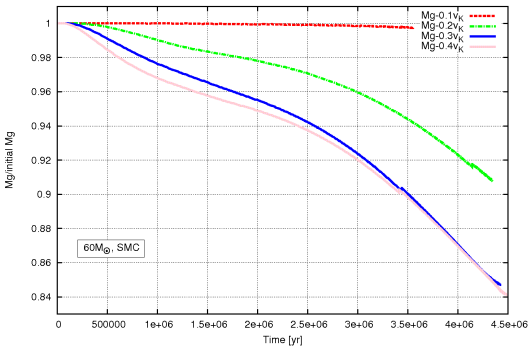

Figure A.162: Mass fraction divided by the initial value of magnesium as a function of time for stars with $M = 60M_{\odot}$, $Z = 0.004$ and different f_K.

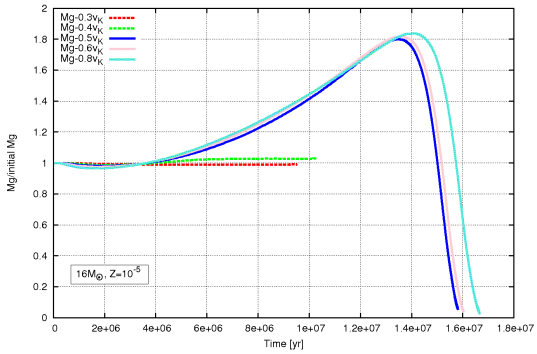

Figure A.163: Mass fraction divided by the initial value of magnesium as a function of time for stars with $M = 16M_{\odot}$, $Z = 10^{-5}$ and different f_K.

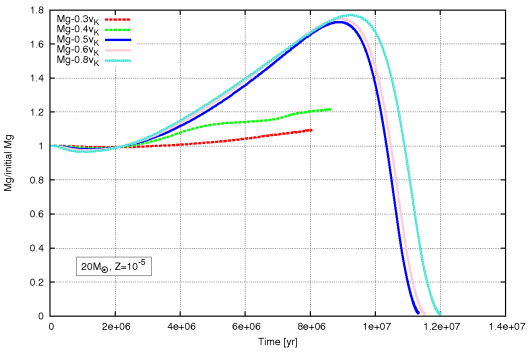

Figure A.164: Mass fraction divided by the initial value of magnesium as a function of time for stars with $M = 20M_{\odot}$, $Z = 10^{-5}$ and different f_K.

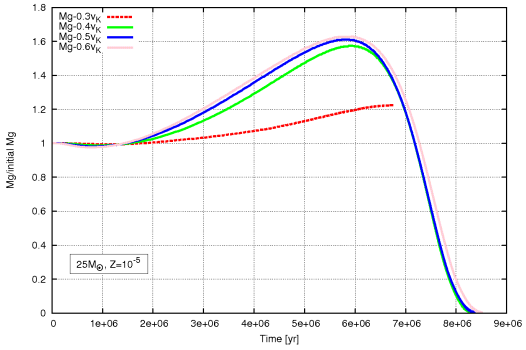

Figure A.165: Mass fraction divided by the initial value of magnesium as a function of time for stars with $M = 25M_{\odot}$, $Z = 10^{-5}$ and different f_K.

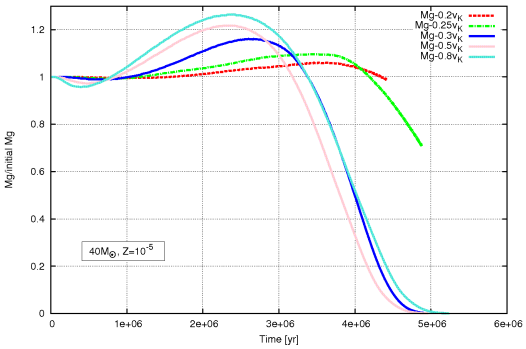

Figure A.166: Mass fraction divided by the initial value of magnesium as a function of time for stars with $M = 40M_{\odot}$, $Z = 10^{-5}$ and different f_K.

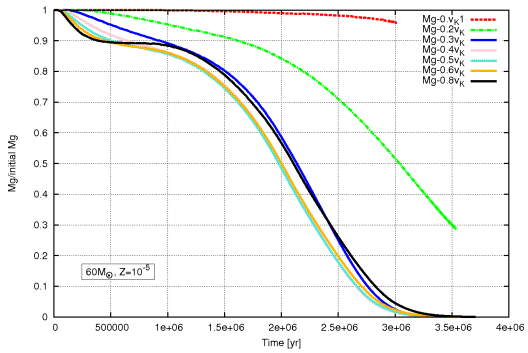

Figure A.167: Mass fraction divided by the initial value of magnesium as a function of time for stars with $M = 60M_{\odot}$, $Z = 10^{-5}$ and different f_K.

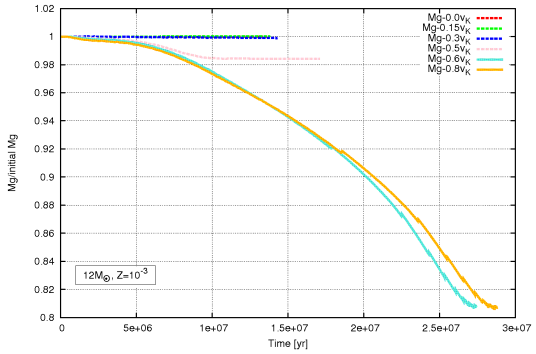

Figure A.168: Mass fraction divided by the initial value of magnesium as a function of time for stars with $M = 12M_{\odot}$, $Z = 10^{-3}$ and different f_K.

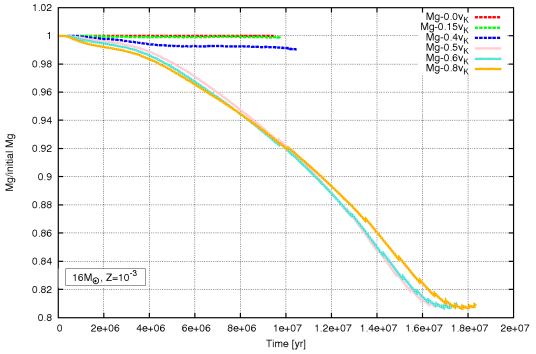

Figure A.169: Mass fraction divided by the initial value of magnesium as a function of time for stars with $M = 16M_{\odot}$, $Z = 10^{-3}$ and different f_K.

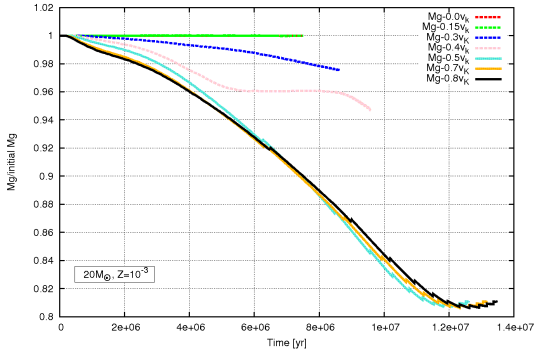

Figure A.170: Mass fraction divided by the initial value of magnesium as a function of time for stars with $M = 20M_{\odot}$, $Z = 10^{-3}$ and different f_K.

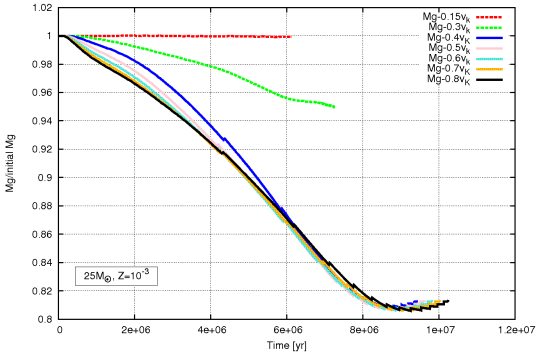

Figure A.171: Mass fraction divided by the initial value of magnesium as a function of time for stars with $M = 25M_{\odot}$, $Z = 10^{-3}$ and different f_K.

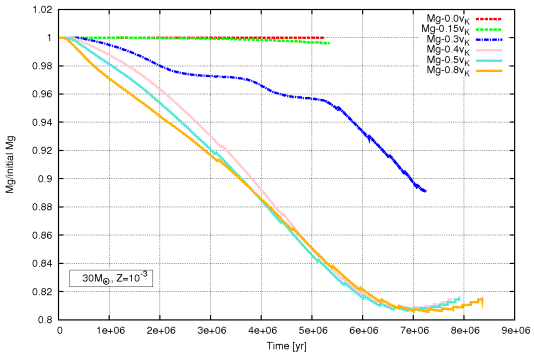

Figure A.172: Mass fraction divided by the initial value of magnesium as a function of time for stars with $M = 30M_{\odot}$, $Z = 10^{-3}$ and different f_K.

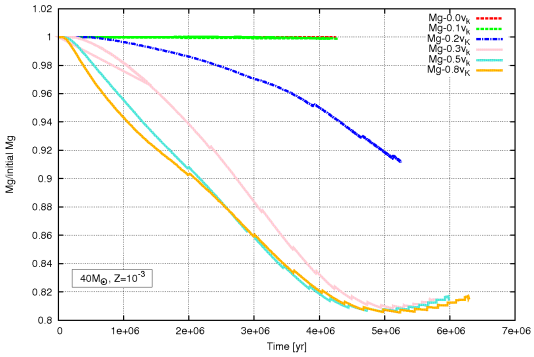

Figure A.173: Mass fraction divided by the initial value of magnesium as a function of time for stars with $M = 40M_{\odot}$, $Z = 10^{-3}$ and different f_K.

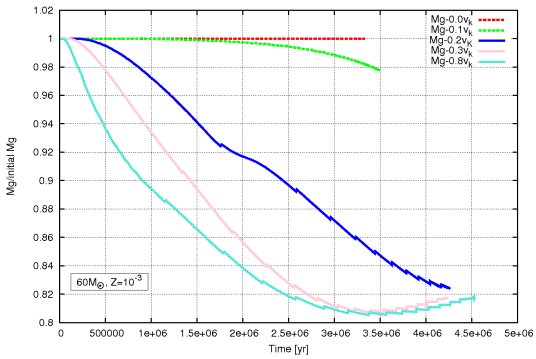

Figure A.174: Mass fraction divided by the initial value of magnesium as a function of time for stars with $M = 60M_{\odot}$, $Z = 10^{-3}$ and different f_K.

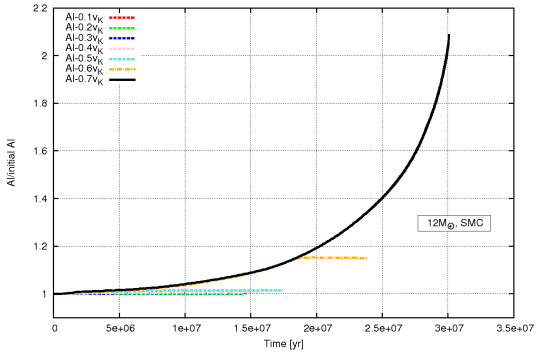

Figure A.175: Mass fraction divided by the initial value of aluminium as a function of time for stars with $M = 12M_\odot$, $Z = 0.004$ and different f_K.

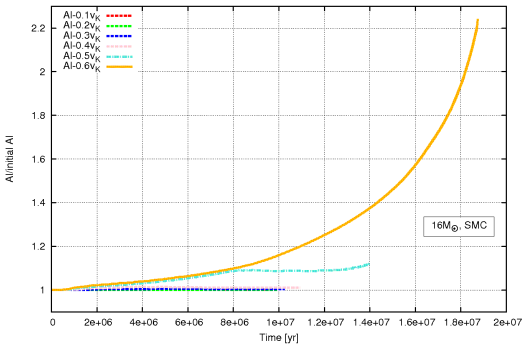

Figure A.176: Mass fraction divided by the initial value of aluminium as a function of time for stars with $M = 16M_\odot$, $Z = 0.004$ and different f_K.

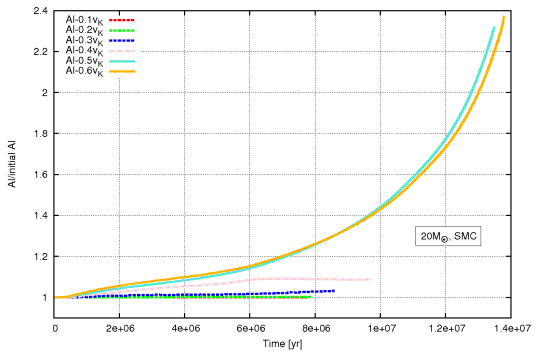

Figure A.177: Mass fraction divided by the initial value of aluminium as a function of time for stars with $M = 20M_\odot$, $Z = 0.004$ and different f_K.

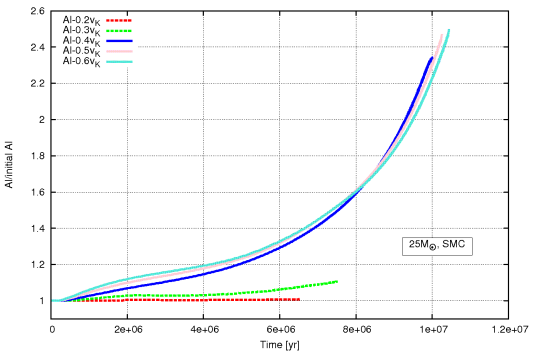

Figure A.178: Mass fraction divided by the initial value of aluminium as a function of time for stars with $M = 25M_\odot$, $Z = 0.004$ and different f_K.

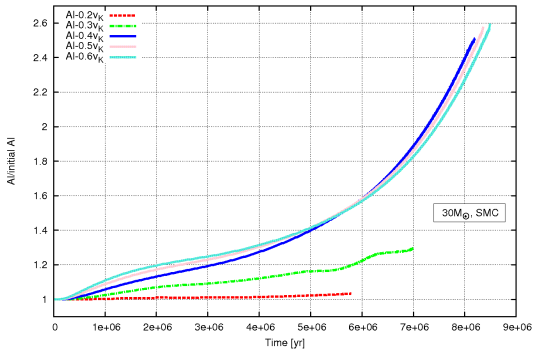

Figure A.179: Mass fraction divided by the initial value of aluminium as a function of time for stars with $M = 30M_\odot$, $Z = 0.004$ and different f_K.

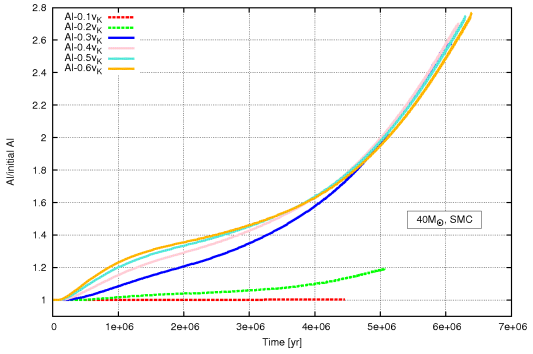

Figure A.180: Mass fraction divided by the initial value of aluminium as a function of time for stars with $M = 40M_\odot$, $Z = 0.004$ and different f_K.

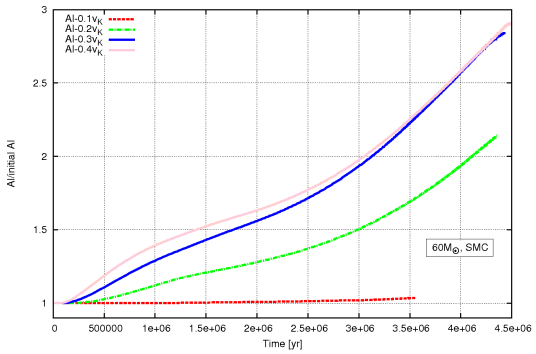

Figure A.181: Mass fraction divided by the initial value of aluminium as a function of time for stars with $M = 60M_\odot$, $Z = 0.004$ and different f_K.

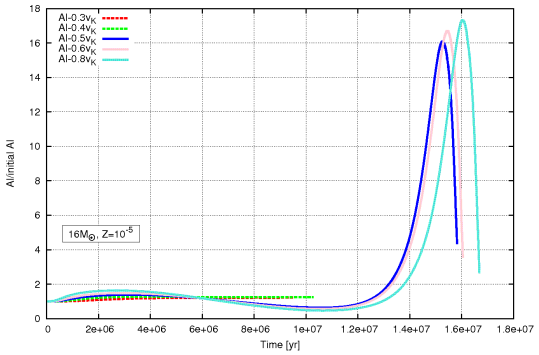

Figure A.182: Mass fraction divided by the initial value of aluminium as a function of time for stars with $M = 16M_\odot$, $Z = 10^{-5}$ and different f_K.

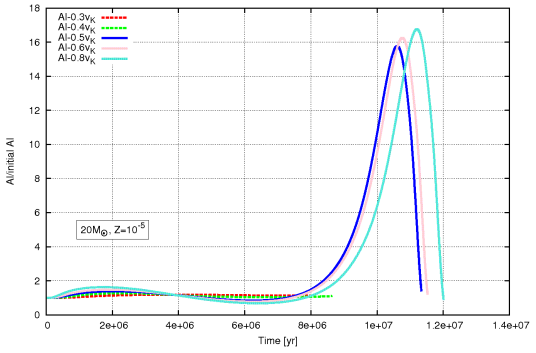

Figure A.183: Mass fraction divided by the initial value of aluminium as a function of time for stars with $M = 20M_\odot$, $Z = 10^{-5}$ and different f_K.

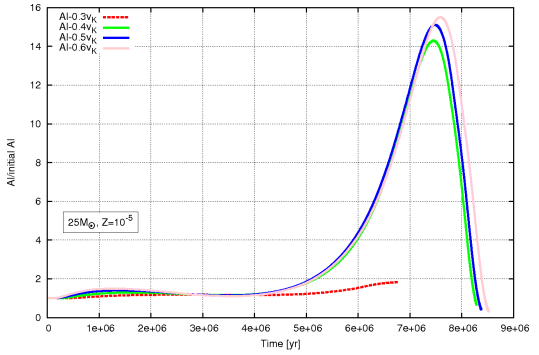

Figure A.184: Mass fraction divided by the initial value of aluminium as a function of time for stars with $M = 25M_\odot$, $Z = 10^{-5}$ and different f_K.

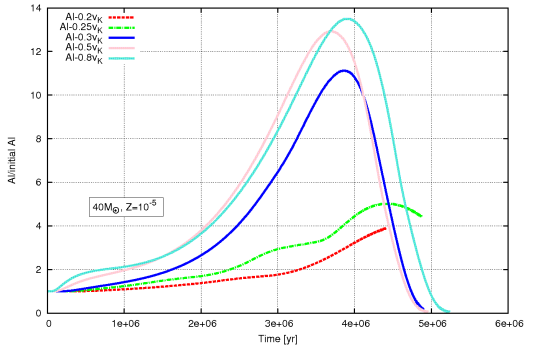

Figure A.185: Mass fraction divided by the initial value of aluminium as a function of time for stars with $M = 40M_\odot$, $Z = 10^{-5}$ and different f_K.

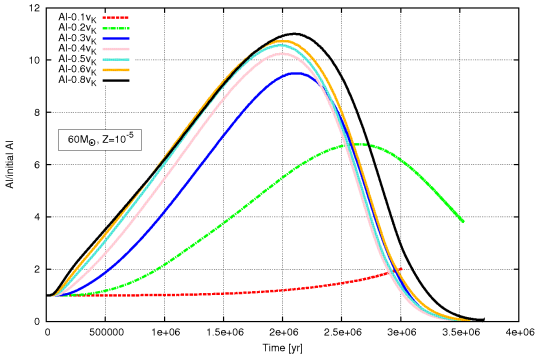

Figure A.186: Mass fraction divided by the initial value of aluminium as a function of time for stars with $M = 60M_\odot$, $Z = 10^{-5}$ and different f_K.

A.2 Data

Mass ‖ $\mathbf{f}_K$	0.1	0.2	0.3	0.4
12 $M_\odot$	non-homogeneous	non-homogeneous	non-homogeneous	non-homogeneous
16 $M_\odot$	non-homogeneous	non-homogeneous	non-homogeneous	non-homogeneous
20 $M_\odot$	non-homogeneous	non-homogeneous	non-homogeneous	part. homogeneous
25 $M_\odot$	-	non-homogeneous	non-homogeneous	homogeneous
30 $M_\odot$	-	non-homogeneous	part. homogeneous	homogeneous
40 $M_\odot$	non-homogeneous	non-homogeneous	homogeneous	homogeneous
60 $M_\odot$	non-homogeneous	part. homogeneous	homogeneous	homogeneous

Table A.1: Classification of the evolutionary tracks for $Z = 0.004$ (Part 1)

Mass ‖ $\mathbf{f}_K$	0.5	0.6	0.7	0.8
12 $M_\odot$	non-homogeneous	part. homogeneous	homogeneous	-
16 $M_\odot$	part. homogeneous	homogeneous	-	-
20 $M_\odot$	homogeneous	homogeneous	-	-
25 $M_\odot$	homogeneous	homogeneous	-	-
30 $M_\odot$	homogeneous	homogeneous	-	-
40 $M_\odot$	homogeneous	homogeneous	-	-
60 $M_\odot$	-	-	-	-

Table A.2: Classification of the evolutionary tracks for $Z = 0.004$ (Part 2)

Mass ‖ $\mathbf{f}_K$	0.1	0.2	0.25	0.3
12 $M_\odot$	-	-	-	-
16 $M_\odot$	-	-	-	non-homogeneous
20 $M_\odot$	-	-	-	non-homogeneous
25 $M_\odot$	-	-	-	non-homogeneous
30 $M_\odot$	-	-	-	-
40 $M_\odot$	-	non-homogeneous	part. homogeneous	homogeneous
60 $M_\odot$	non-homogeneous	part. homogeneous	-	homogeneous

Table A.3: Classification of the evolutionary tracks for $Z = 10^{-5}$ (Part 1)

Mass ‖ $\mathbf{f}_K$	0.4	0.5	0.6	0.7	0.8
12 $M_\odot$	-	-	-	-	-
16 $M_\odot$	non-homogeneous	homogeneous	homogeneous	-	homogeneous
20 $M_\odot$	non-homogeneous	homogeneous	homogeneous	-	homogeneous
25 $M_\odot$	homogeneous	homogeneous	homogeneous	-	-
30 $M_\odot$	-	-	-	-	-
40 $M_\odot$	-	homogeneous	-	-	homogeneous
60 $M_\odot$	homogeneous	homogeneous	homogeneous	-	homogeneous

Table A.4: Classification of the evolutionary tracks for $Z = 10^{-5}$ (Part 2)

Mass ‖ $\mathbf{f}_K$	0.0	0.1	0.15	0.2	0.3
12	non-homogeneous	-	non-homogeneous	-	non-homogeneous
16	non-homogeneous	-	-	-	non-homogeneous
20	non-homogeneous	-	non-homogeneous	-	non-homogeneous
25	-	-	non-homogeneous	-	non-homogeneous
30	non-homogeneous	-	non-homogeneous	-	part. homogeneous
40	non-homogeneous	non-homogeneous	-	part. homogeneous	homogeneous
60	non-homogeneous	non-homogeneous	-	homogeneous	homogeneous

Table A.5: Classification of the evolutionary tracks for $Z = 10^{-3}$ (Part 1)

Mass ‖ $\mathbf{f}_K$	0.4	0.5	0.6	0.7	0.8
12	-	non-homogeneous	homogeneous	-	homogeneous
16	non-homogeneous	homogeneous	homogeneous	-	homogeneous
20	non-homogeneous	homogeneous	-	homogeneous	homogeneous
25	homogeneous	homogeneous	homogeneous	homogeneous	homogeneous
30	homogeneous	homogeneous	-	-	homogeneous
40	-	homogeneous	-	-	homogeneous
60	-	-	-	-	homogeneous

Table A.6: Classification of the evolutionary tracks for $Z = 10^{-3}$ (Part 2)

Mass ‖ **Element**	H	He	C	N	O	F	Ne	Na	Mg	Al
12 $M_\odot$	$(\surd)$	$\surd$	X	X	$\surd$	$\surd$	X	X	X	X
16 $M_\odot$	$\surd$	X	X	X	$\surd$	$\surd$	X	X	X	X
20 $M_\odot$	$\surd$	$\surd$	X	X	$\surd$	$\surd$	X	$(\surd)$	X	X
25 $M_\odot$	$\surd$	$(\surd)$	$(\surd)$	X	$\surd$	$\surd$	X	$\surd$	X	X
30 $M_\odot$	$(\surd)$	$(\surd)$	X	X	$\surd$	$\surd$	X	X	X	$(\surd)$
40 $M_\odot$	$\surd$	$\surd$	$\surd$	$(\surd)$	$\surd$	$\surd$	X	$\surd$	X	$(\surd)$
60 $M_\odot$	X	X	X	X	$\surd$	$\surd$	X	X	X	X

Table A.7: Eligibility of the elements with the help of the "dex-criterion" for $Z = 0.004$, whereby $\surd$ means eligible, $(\surd)$ hardly eligible and X ineligible.

Mass ‖ **Element**	H	He	C	N	O	F	Ne	Na	Mg	Al
12 $M_\odot$	-	-	-	-	-	-	-	-	-	-
16 $M_\odot$	$\surd$	$\surd$	X	X	$\surd$	$\surd$	X	$(\surd)$	$(\surd)$	$\surd$
20 $M_\odot$	$\surd$	$\surd$	X	X	$\surd$	$\surd$	X	X	X	$\surd$
25 $M_\odot$	$\surd$	$\surd$	X	X	$\surd$	$\surd$	X	$(\surd)$	X	$\surd$
30 $M_\odot$	-	-	-	-	-	-	-	-	-	-
40 $M_\odot$	$(\surd)$	$(\surd)$	X	X	$\surd$	$\surd$	X	$(\surd)$	X	$\surd$
60 $M_\odot$	$(\surd)$	X	X	X	$\surd$	$\surd$	X	$(\surd)$	$\surd$	$(\surd)$

Table A.8: Eligibility of the elements with the help of the "dex-criterion" for $Z = 10^{-5}$, whereby $\surd$ means eligible, $(\surd)$ hardly eligible and X ineligible.

References

[Bethe (1939)] H.A. Bethe: *Energy Production in Stars*, Physical Review 55, 1939, 434-456

[Burbidge et al. (1957)] E.M. Burbidge, G.R. Burbidge, W.A Fowler, F. Hoyle *Synthesis of the Elements in Stars*, 1957, Reviews of Modern Physics 29, 547-647

[de Mink (2010)] S.E. de Mink: *Stellar evolution at low metallicity under the influence of binary interaction and rotation*, 2010, Doctoral Thesis, 7-118

[Frebel (2008)] A. Frebel: *Auf der Spur der Sterngreise*, Spektrum der Wissenschaft, September 2008, 24-32

[Heger, Langer (2000)] A. Heger, N. Langer: *Presupernova evolution of rotating massive stars. II. Evolution of the surface properties*, 2000, APJ 544, 1016-1035

[Heger et al. (2000)] A. Heger, N. Langer, S.E. Woosley: *Presupernova evolution of rotating massive stars. I. Numerical method and evolution of the internal stellar structure*, 2000, APJ 528, 368-396

[Kippenhahn, Weigert (1991)] R. Kippenhahn, A. Weigert: *Stellar Structure and Evolution*, 1991, A&A Library, Springer Verlag, 1-468

[Langer (2009)] N. Langer: *Nucleosynthesis*, 2009, Bonn University, Lecture Notes, 51-60

[Pols (2009)] O.R. Pols: *Stellar Structure and Evolution*, 2009, Lecture Notes, 65-76

[Przybilla et al. (2010)] N. Przybilla, M. Firnstein, M.F. Nieva, G. Maynet, A. Maeder: *Mixing of CNO-cycled matter in massive stars*, 2010, A&A, in press

[Yoon, Langer (2005)] S.-C. Yoon, N. Langer: *Evolution of rapidly rotating metal-poor massive stars towards gamma-ray bursts*, 2005, A&A 443, 643-648

[Yoon et al. (2006)] S.-C. Yoon, N. Langer, C. Norman: *Single star progenitors of long gamma-ray bursts. I. Model grids and redshift dependent GRB rate*, 2006, A&A 460, 199-208